Analysis of the interplay between protein quality control pathways in aging and neurodegenerative diseases

Inaugural-Dissertation

to obtain the academic degree

Doctor rerum naturalium (Dr. rer. nat.)

submitted to the Department of Biology, Chemistry and Pharmacy

of Freie Universität Berlin

by

Diogo Alexandre Rodrigues Feleciano

from Portugal

2018

The doctoral studies were conducted from the 2nd of February 2015 until the 21st of September 2018, under the supervision of Dr. Janine Kirstein at the Leibniz Institute for Molecular Pharmacology (FMP Berlin).

1st Reviewer:

Janine Kirstein

Institute: Leibniz Institute for Molecular Pharmacology (FMP Berlin)

2nd Reviewer:

Hartmut Oschkinat

Institute: Leibniz Institute for Molecular Pharmacology (FMP Berlin)

Date of defense: 20.12.2018

1 Table of Contents

2   Summary

A functional protein quality control machinery is crucial to maintaining cellular and organismal physiology. Perturbation in the protein homeostasis network can lead to the formation of misfolded and aggregated proteins that are a hallmark of protein conformational disorders and aging. Protein aggregation is counteracted by the action of chaperones that can resolubilize aggregated proteins. An alternative protein clearance strategy is the elimination by proteolysis employing the ubiquitin-proteasome system (UPS) or autophagy. Little is known how these three protein aggregate clearance strategies are regulated and coordinated in an organismal level with the progression of aging or upon expression of disease-associated proteins.

In this study, I aimed to unravel the crosstalk between the different clearance options. To address this, I investigated how autophagy and UPS respond to the expression of disease-associated proteins and during aging when the chaperone capacity is compromised in *C. elegans* and HEK293 cells. Here, I demonstrate that wild-type animals display a reduced autophagic flux with the progression of aging whereas the UPS activity is altered in a tissue-specific manner (reduced activity in the neuronal cells and increased activity in the muscle cells). A knockdown of chaperones that constitute the HSP110/70/J disaggregation complex leads to an activation of autophagy that probably serves as a compensatory mechanism to rebalance proteostasis. Notably, the compensatory effect of autophagy in response to a depletion of chaperones is diminished with the progression of aging in *C. elegans*. Interestingly, the proteasomal activity and 20S levels are reduced in response to chaperone depletion, in particular upon knockdown of *hsp-110/hspa4*.

Moreover, the capacity of the clearance machinery was analyzed in neurodegenerative disease models. The expression of aggregation-prone and disease-associated Aβ and polyglutamine (Q_{40}) proteins leads to an impairment of both proteolytic pathways. Notably, the expression of Aβ perturbs the proteasome system also in a distal tissue demonstrating a trans-tissue communication. Lastly, in order to better understand how amyloid aggregates affect the cellular environment, correlative light and electron microscopy studies were performed in *C. elegans*. The Q_{40} aggregates display an amyloid structure

and are not enclosed by any membrane. The lack of a surrounding membrane exposes the aggregate to all cellular components, which allows it to sequester numerous cellular components.

The results obtained in this thesis, further elucidate the tight coordination between the different nodes of the proteostasis network with the progression of aging and disease on a cellular and organismal level.

Keywords: *C. elegans*, Proteostasis, Chaperones, Autophagy, Ubiquitin-Proteasome System, Aging, Protein aggregation, Neurodegeneration

2.1 Zusammenfassung

Eine funktionelle Proteinqualitätskontrolle ist essentiell, um die Funktionstüchtigkeit jeder einzelnen Zelle und des gesamten Organismus aufrecht zu halten. Beeinträchtigungen der Proteinhomöostase können zu Proteinmisfaltungen und schließlich auch zur Bildung von Proteinaggregaten führen. Proteinaggregate treten vermehrt im Alter auf und sind auch ein Charakteristikum von neurodegenerativen Erkrankungen. Molekulare Chaperone können die Bildung von Proteinaggregaten unterdrücken und bestehende Aggregate auch resolubilisieren. Eine alternative Strategie, Proteinaggregate zu eliminieren ist der proteolytische Abbau durch das Proteasom oder über Autophagie. Unser Wissen, wie diese Strategien zum Abbau oder der Auflösung der Aggregate mit dem Alter oder nach Expression von krankheitsassoziierten Proteinen koordiniert werden, ist sehr limitiert.

An dieser Fragestellung setzte meine Arbeit an und ich untersuchte, wie die verschiedenen Proteinabbaumechanismen koordiniert werden. Dazu analysierte ich die Aktivität der Autophagie und auch des Proteasoms nach Depletion disaggregierender Chaperone, nach Expression von amyloiden krankheitsassoziierten Proteinen und mit fortschreitendem Alter im Nematoden *C. elegans* und in HEK293 Zellen. Ich konnte zeigen, dass die Aktivität der Autophagie mit dem Alter abnimmt, das Proteasom jedoch gewebsspezifisch reguliert wird und in alternden Neuronen an Aktivität abnimmt, im Muskel jedoch aktiver wird. Eine Depletion der Chaperone, die für die Disaggregation von

Proteinaggregaten verantwortlich sind, führt zu einer Aktivierung der Autophagie. Der kompensatorische Effekt der Autophagie nach Beeinträchtigung der Disaggregation ist jedoch auf die reproduktive Phase des Tiers beschränkt. Mit fortschreitendem Alter, nimmt die Aktivierung der Autophagie in *C. elegans* ab. Interessanterweise kommt es nach Depletion der disaggregierenden Chaperone zu einer Reduktion der 20S Untereinheiten und damit einhergehenden verminderten Aktivität des Proteasoms. Dieser Effekt ist besonders nach Depletion von *hsp-110/hspa4* ausgeprägt.

Die Expression von amyloiden krankheitsassoziierten Proteinen wie beispielsweise Aβ und polyQ führt zu einer Beeinträchtigung von beiden proteolytischen Abbaumechanismen. Ich konnte zudem beobachten, dass Aβ das Proteasom auch in benachbarten Geweben, in denen Aβ nicht exprimiert wird, inhibiert. Dieser gewebsübergreifende proteotoxische Effekt deutet auf systemische Beeinträchtigungen nach Aβ Expression hin. Um einen Einblick zu gewinnen wie amyloide Proteinaggregate zelluläre Funktionen beeinflussen, habe ich die Ultrastruktur von Q_{40} Proteinaggregaten elektronenmikroskopisch im Nematoden untersucht. Mittels korrelativer Licht und Elektronenmikroskopie (CLEM) und Elektronenmikroskopie (EM) konnte ich die Ultrastruktur der Amyloidfibrillen von Q_{40} Proteinaggregaten erstmalig im Tiermodell darstellen und auch zeigen, dass die Aggregate *in vivo* nicht membranumschlossen sind. Die amyloiden Proteinaggregate können so leicht zelluläre Komponenten wie beispielsweise endogene Proteine sequestrieren und so deren physiologische Funktion in der Zelle beeinträchtigen.

Die Ergebnisse dieser Arbeit ermöglichen mechanistische Einblicke in die Regulation der verschiedenen Strategien zum Abbau von Proteinaggregaten mit fortschreitendem Alter und nach Expression krankheitsassoziierter amyloider Proteine.

Stichworte: *C. elegans*, Proteostase, Chaperone, Autophagie, Ubiquitin-Proteasom-System, Altern, Proteinaggregation, Neurodegeneration

3 Introduction

3.1 Proteostasis Network

The maintenance of a functional proteome is critical for the cellular and organismal physiology. Mammalian cells are composed of around 20.000 distinct proteins that support protein homeostasis (proteostasis) by playing key roles in the immune system, signaling pathways, metabolism and cellular structures (Reszka et al. 1995, Miners et al. 1998, Schlessinger 2000, Lemmon et al. 2010, Balchin et al. 2016). Proteins are synthesized by the ribosome and to be fully functional they must achieve its three-dimensional structure (Figure 1.1) (Balchin et al. 2016). Despite the specific protein folding being determined by the amino acid sequence, proteins need to overcome many challenges to achieve the correct folding (Anfinsen et al. 1961). Cellular crowding is one of the major barriers that proteins face in order to achieve a correct folding (Ellis 2001). The high cellular protein concentration (200-300 g/l) is known to perturb protein folding, and consequently promotes protein misfolding and aggregation (Ellis et al. 2006, Kim et al. 2013).

To preserve a healthy cellular environment, cells must achieve a balance between protein synthesis and degradation (Figure 1.1) (Kim et al. 2013). Proteins can misfold and aggregate due to many factors, but this occurs mainly in response to acute stress such as oxidative and heat stress, or protein mutations (Lindquist 1986, Ellis et al. 2006). Protein aggregates may exhibit different structures depending on the type of stress. While the aggregates generated after heat stress display an amorphous structure, mutations in specific proteins can lead to the formation of amyloid aggregates (Stranks et al. 2009, Tyedmers et al. 2010). The latter is the hallmark of many neurodegenerative diseases like Alzheimer, Parkinson, and Huntington's disease (Nozaki et al. 2001, Carnini et al. 2012, Gao et al. 2015). In each of these neurodegenerative diseases, specific proteins are mutated and form amyloid fibrils that are defined by the extension of many beta-sheet structures (Balchin et al. 2016).

Cells are equipped with a proteostasis network (PN) that safeguards the proteome and regulates the correct fold and function of all proteins (Morimoto et al. 2014). The PN is composed of molecular chaperones that ensure the native

state of proteins by assisting *de novo* folding, protein refolding and disaggregation, and also proteolytic clearance pathways such as the autophagy and the ubiquitin-proteasome system (UPS) that eliminate non-functional cellular components (Figure 1.1). A tight regulation between the different proteostasis members is critical to the preservation of a balanced protein homeostasis both on a cellular and organismal level (Wolff et al. 2014, Kaushik et al. 2015).
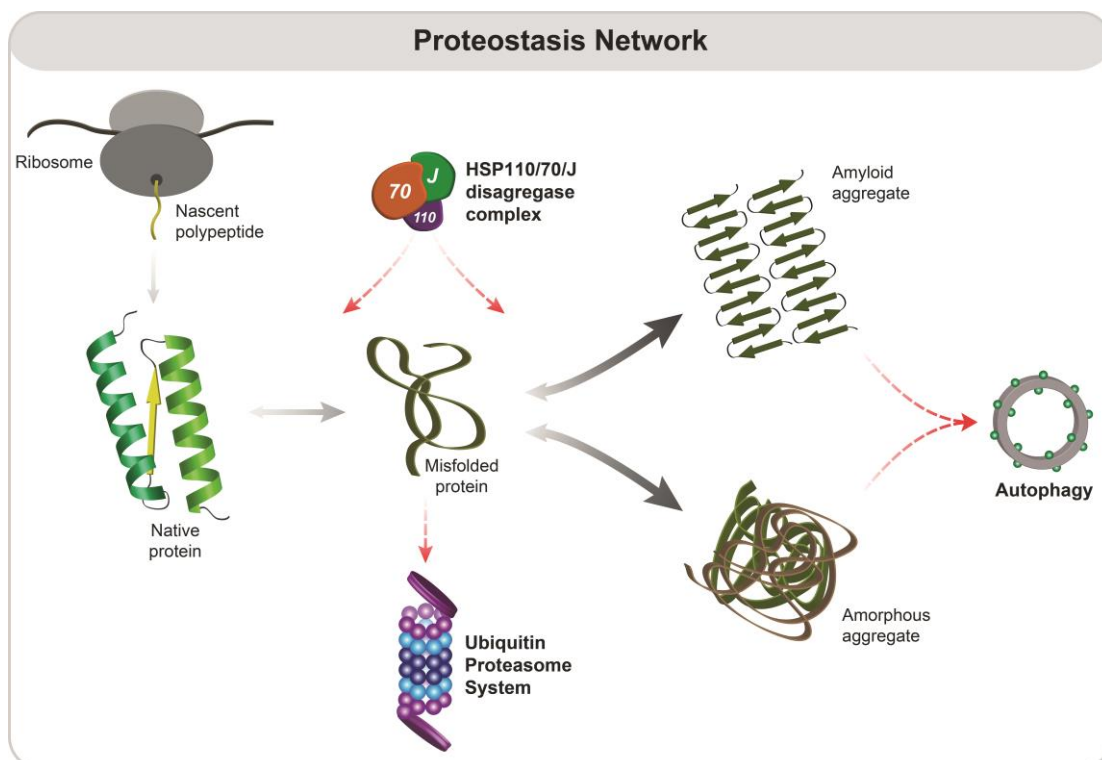
Figure 1. 1 - Proteostasis overview.
Proteins are synthesized at the ribosome and fold into its native state. However, proteins may misfold due to various factors (e.g. heat stress). Chaperones assist not only in the initial folding events, but also in the refolding of misfolded proteins. In particular cases, the misfolded proteins accumulate and form amorphous or amyloid aggregates. Disaggregating chaperones (e.g. HSP110/70/J complex) can prevent and also revert protein aggregation (amorphous and amyloid aggregates). Protein aggregates can also be eliminated by proteolytic clearance pathways such as autophagy or UPS.

3.1.1 Molecular Chaperones

Molecular chaperones were found to be critical in protein folding events as they support *de novo* folding and stabilize the structure of other proteins, without participating in the final protein structure (Ellis 1987, Hartl 1996). Molecular chaperones already assist the folding of nascent chains that emerge from the exit tunnel of the ribosome (Hoffmann et al. 2012). The crowded cellular environment however favors non-native interactions of the nascent chain, which potentially leads to protein misfolding (Anfinsen 1973, Zhou 2008, Zhou et al. 2009).

Molecular chaperones are known as Heat-shock proteins (Hsp), and were historically categorized based on their molecular weight into distinct families e.g. small heat-shock proteins (sHsp), Hsp60, Hsp70, Hsp90 and Hsp100s (Hartl 1996, Hartl et al. 2011, Kim et al. 2013). sHsps are known to function as holdases (ATP-independent), and Hsp60, Hsp70, Hsp90 and Hsp110 as foldases (ATP-dependent) (Taipale et al. 2010, Mayer 2013, Treweek et al. 2015). Despite the nomenclature, heat-shock proteins are not only induced upon heat shock. For instance, the important cytosolic Hsc70 is constitutively expressed under physiological conditions (Kim et al. 2013). Moreover, virus infection or oxidative stress can also induce chaperone expression (Tardif et al. 2002, Park et al. 2009).

Chaperones are a highly diverse family encoding for more than 300 and 200 different proteins in humans and nematodes, respectively. As a consequence of the diversity of the heat-shock protein family, multiple biological processes require the action of Hsps, such as protein folding, refolding, degradation or disaggregation (Agarraberes et al. 2001, Demand et al. 2001, Otto et al. 2005, Rampelt et al. 2012).

3.1.1.1 Chaperone-mediated protein disaggregation

Disaggregation of protein aggregates facilitates the recovery from proteotoxic conditions such as heat stress that lead to an accumulation of misfolded and aggregated proteins (Glover et al. 1998, Mogk et al. 1999, Weibezahn et al. 2004). Many organisms are reported to display a coordinated chaperone-

mediated protein disaggregation. The work developed in Lindquist laboratory shed light into this mechanism in yeast, by demonstrating the critical role of Hsp104 disaggregase in developing tolerance and recovering cells from severe heat stress (Sanchez et al. 1990, Lindquist et al. 1996). Hsp104 (ClpB in *E. Coli*) is an Hsp100 member of the triple ATPase complex protein family (AAA+), and remodel protein substrates by using the energy derived from ATP hydrolysis (Parsell et al. 1994, Mogk et al. 1999).

Humans and *C. elegans* do not have homologs of Hsp104/ClpB in their cytosol. Instead, disaggregation events are coordinated by a trimeric chaperone complex, which is composed of members of the Hsp70, J-protein and Hsp110 chaperone families (Figure 1.2) (Shorter 2011, Rampelt et al. 2012). HSP110/70/J chaperone complex can suppress aggregation and promote disaggregation of amorphous (e.g. luciferase), as well as disease-associated amyloid aggregates (e.g. α-synuclein, α-syn, or huntingtin with abnormal polyglutamine repetitions, mHtt) (Rampelt et al. 2012, Gao et al. 2015, Nillegoda et al. 2015, Kirstein et al. 2017, Scior et al. 2018).

3.1.1.2 HSP110/70/J chaperone disaggregation complex

The Hsp70 family protein members play a central role in cellular protein homeostasis as they are involved in the folding and assembly of newly synthesized proteins, protein transport, prevention of protein misfolding, disaggregation of aggregated proteins, and targeting of misfolded proteins for degradation (Mayer et al. 2005). Humans and *C. elegans* encode for 13 and 9 different Hsp70 family members, respectively (Heschl et al. 1989, Hageman et al. 2009). The Hsp70 chaperones are composed of two domains, the N-terminal nucleotide-binding domain and the C-terminal substrate-binding domain that are connected by a hydrophobic linker (Kumar et al. 2011, Mayer 2013). Hsp70s bind hydrophobic regions of five amino acids (aa) with adjacent positively charged aa that are exposed in misfolded proteins (Fourie et al. 1994, Rudiger et al. 1997). The chaperone activity of Hsp70 is enabled by the hydrolysis of ATP in the N-terminal domain that causes a conformational change in the C-terminal substrate binding domain, leading to an increased substrate affinity of

Hsp70 in the ADP-bound state (Mayer et al. 2005, Zhuravleva et al. 2012, Kityk et al. 2015). Initial substrate recruitment and binding are facilitated by a co-chaperone (J-protein) that accelerates the ATP hydrolysis (more than 100-fold), and consequently changes the Hsp70 substrate binding state from an open to a closed conformation, keeping the substrate bound to Hsp70 (Figure 1.2) (Laufen et al. 1999, Kampinga et al. 2010).

The release of substrates is mediated by nucleotide exchange factors (NEF) such as proteins with a Bcl-2 associated anthanogene (BAG) domain, HSPBP1 and Hsp110s (HSPA4 in humans or HSP-110 in *C. elegans*) that dissociate ADP and allow subsequent rebinding of ATP, resetting the Hsp70 chaperone to the open conformation (Laufen et al. 1999, Raviol et al. 2006, Rampelt et al. 2012). The role of NEFs is essential in the disaggregation process as it regulates the substrate release from the Hsp70 complex and consequently enables the substrates to enter another folding cycle (Figure 1.2) (Bracher et al. 2015).

As mentioned above the Hsp70 chaperone activity is facilitated by the co-chaperones, J-proteins, that recognize and deliver substrates to Hsp70. Previously known as Hsp40s, they are a highly diverse family, composed of 32 and 49 members in nematodes and humans, respectively (Hageman et al. 2009, Craig et al. 2017). J-protein family members are divided into classes due to the presence of specific domains (class A, B, C or type-I, II, III). While type-I members contain a glycine-phenylalanine-rich motif, a zinc finger domain and a C-terminal domain that is important for dimerization and substrate binding, type-II members lack the zinc-finger domain. J-proteins that do not share similarities in the C- and N-terminal domains with type-I/II are classified as type-III (Nillegoda et al. 2017). All classes display a highly conserved J-domain, composed of 70 aa that contains a Histidine-Proline-Aspartate (HPD) motif, essential for the acceleration of the ATP hydrolysis of Hsp70s (Tsai et al. 1996, Greene et al. 1998).
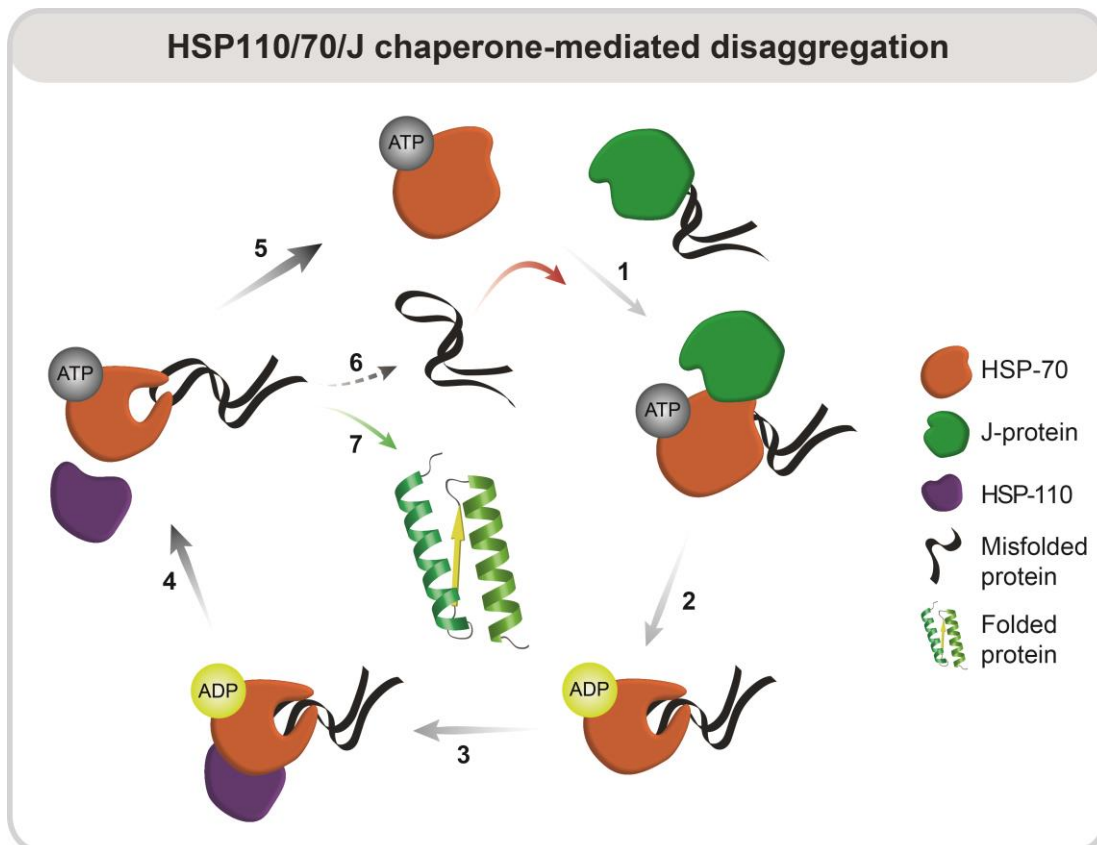
Figure 1. 2 - HSP110/70/J disaggregation cycle.

J-proteins bind and deliver client proteins to Hsp70 (1). The binding of the J-domain stimulates the HSP-70 ATPase hydrolysis leading to a conformational change (closed state) of HSP-70 (2). Upon binding of HSP-110 (3), ADP is replaced by ATP (4), which again alters the conformation (open state) of HSP-70 (5). If the client protein is correctly folded it is released (7) or if the folding was not successful it can enter a new folding cycle (6).

J-proteins exhibit substrate preferences and can also cooperate with other members of the J-protein family and thereby regulate the activity of Hsp70 for respective substrates and also chaperone activity (Table 1). Amorphous aggregates, such as malate dehydrogenase and luciferase aggregates can be re-solubilized by DNJ-12 (DNAJA1 in humans, type-I) or by DNJ-13 (DNAJB1 in humans, type-II) together with HSP-70/HSP-110 (HSPA8/HSPA4 in humans). However, when DNJ-12 and DNJ-13 are combined with HSP-70/HSP-110, a more powerful disaggregation beyond an additive yield is accomplished (Rampelt et al. 2012, Nillegoda et al. 2015, Kirstein et al. 2017). This shows that

type-I and type-II J-proteins act synergistically when disaggregating amorphous aggregates. The HSP110/70/J chaperone complex can also disaggregate amyloid-like aggregates associated with neurodegenerative diseases. In this case, the action of HSP-70, HSP-110 together with a single type II J-protein, DNJ-13/DNAJB1, is sufficient to disaggregate aggregates formed by α-syn and mHtt (Gao et al. 2015, Scior et al. 2018). The addition of a type I J-protein to an Hsp70/type II J-protein mixture reduces the efficiency of the disaggregation activity probably due to competition for Hsp70 binding. Furthermore, it has been reported that early onset spinocerebellar ataxia 3 patients exhibit decreased levels of DNJAB1, pointing to an important biological role of DNAJB1 in neurodegenerative diseases (Zijlstra et al. 2010).

3.1.2 Autophagy System

Autophagy is a crucial multi-step pathway that allows the cell to eliminate misfolded and aggregated proteins, dysfunctional organelles or pathogens (Dunn 1990, Noda et al. 2002, Shintani et al. 2004, Yu et al. 2018). Autophagy is responsible for the degradation of multiple cargos, such as protein aggregates (aggrephagy), mitochondria (mitophagy), lipid droplets (lipophagy), ER (ERphagy), ribosomes (ribophagy), proteasomes (proteophagy) or bacteria (xenophagy) (Rogov et al. 2014).

The initial observations of autophagic events were detected in morphological studies in rat liver cells (De Duve et al. 1955). The autophagy genes were identified in yeast, and it was demonstrated that autophagy is a conserved pathway across various organisms (Tsukada et al. 1993, Klionsky et al. 2003, Meijer et al. 2007). It was found that this multi-step pathway involves the degradation of cytoplasmic material by the lysosome.

There are three major types of autophagy that have distinct cargo delivery mechanisms to the lysosome: chaperone-mediated autophagy (CMA), micro-autophagy and macro-autophagy. While in CMA (only in mammalians) the import of misfolded proteins into the lysosome is assisted by lysosomal membrane proteins (including chaperones) (Agarraberes et al. 2001, Cuervo et

al. 2014), in micro-autophagy, the lysosome membrane directly engulfs a part of the cytoplasm (Li et al. 2012).

The macro-autophagy (thereafter "autophagy") is the main autophagic pathway (Figure 1.3). It is regulated by mTOR and AMPK signaling and can be triggered e.g. by amino acid starvation (induction) promoting the formation of a double vesicle (nucleation) that surrounds a fraction of the cytosol (Figure 1.3) (Kim et al. 2011). Next, the vesicle elongates and forms an autophagosome (elongation). The autophagosome then fuses with a lysosome (maturation) leading to the degradation of all sequestered components (substrate breakdown) (Lawrence et al. 1992, Mizushima et al. 1998, Yu et al. 2018). Autophagy relies on the recognition of cargos by an autophagic adaptor, SQST-1/p62 or NBR-1 that binds to LC3-II (LGG-1 in *C. elegans*), which allows the engulfment of the non-functional cellular components (Figure 1.3) (Kabeya et al. 2000, Johansen et al. 2011).

The autophagy pathway is an essential cell survival mechanism, and an impaired autophagic flux is associated with diverse diseases such as cancer, infectious diseases or neurodegeneration (Shintani et al. 2004, Codogno et al. 2005, Wong et al. 2010, Jiang et al. 2014, Mizumura et al. 2014). It has been shown that neurodegenerative disease models display a dysfunctional autophagic process, despite the fact that disease-associated proteins such as amyloid-beta (Aβ, Alzheimer's disease) or mutant Huntingtin (mHtt, Huntington's disease) can be eliminated by autophagy (Ravikumar et al. 2002, Webb et al. 2003, Yu et al. 2004, Iwata et al. 2005), (Winslow et al. 2010, Nixon 2013, Menzies et al. 2015).
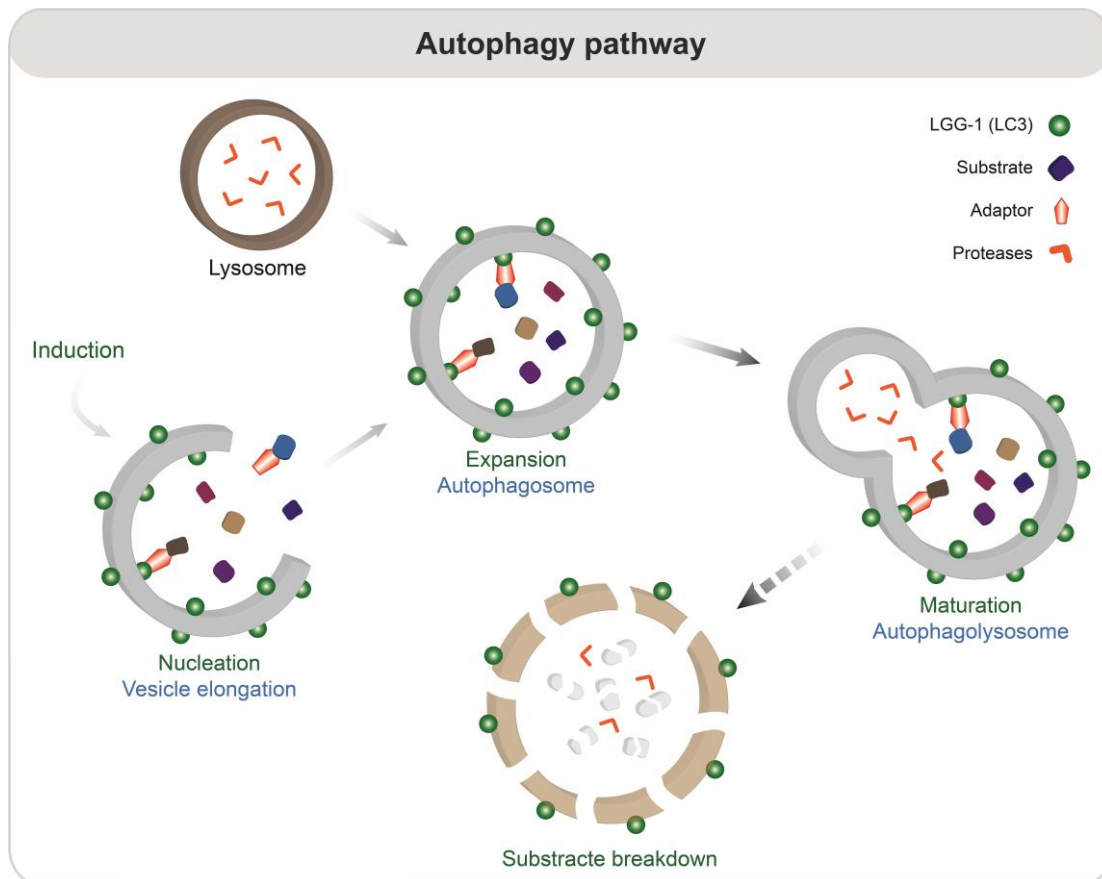
Figure 1. 3 - The multi-step autophagy pathway.

Upon autophagy induction, a double membrane vesicle elongates and engulfs non-functional cellular cargos. The formed vesicle, autophagosome, fuses with the lysosome, leading to the degradation of all encapsulated material. Autophagy adaptors such as the SQST-1/p62 assist the elimination of ubiquitinated cargos, due to its binding to LC3/LGG-1, which is an essential autophagic membrane protein.

3.1.3 Ubiquitin-Proteasome System

The Ubiquitin-Proteasome System (UPS) is the main responsible pathway for the degradation of misfolded proteins (Goldberg 2003, Amm et al. 2014). Substrates for the UPS are poly-ubiquitinated via a cascade reaction conducted by E1, E2 and E3 ligases (Figure 1.4). Subsequently, the ubiquitinated proteins are targeted, unfolded and degraded by the 26S proteasome in an energy-dependent process (Hershko et al. 1980). The formation of specific poly-ubiquitin linkages allows the substrate recognition by the 19S regulatory particle

(RP) and subsequent degradation by the 20S core particle (CP) into small peptides (Figure 1.4).

The UPS is a key component of the proteostasis network, and its function is indispensable for the efficient removal of toxic proteins (Bhattacharyya et al. 2014, Collins et al. 2017). Proteasome dysfunctions have been linked to many diseases such as cancer, autoimmune, and neurodegenerative diseases (Paul 2008, Schmidt et al. 2014). It has been shown that proteins associated with neurodegenerative diseases can impair proteasome function (Ciechanover et al. 2003, Paul 2008, Zheng et al. 2016). Interestingly, proteasomes have the ability to degrade disease-related proteins such as the N-terminal fragment of mHtt (Juenemann et al. 2013). Despite this observation, the poly-ubiquitin tagging and the degradation rates are not sufficient to prevent an accumulation of aggregated mHtt that ultimately leads to proteasome dysfunction (Bence et al. 2001, Ciechanover et al. 2003, Holmberg et al. 2004, Bhat et al. 2014).
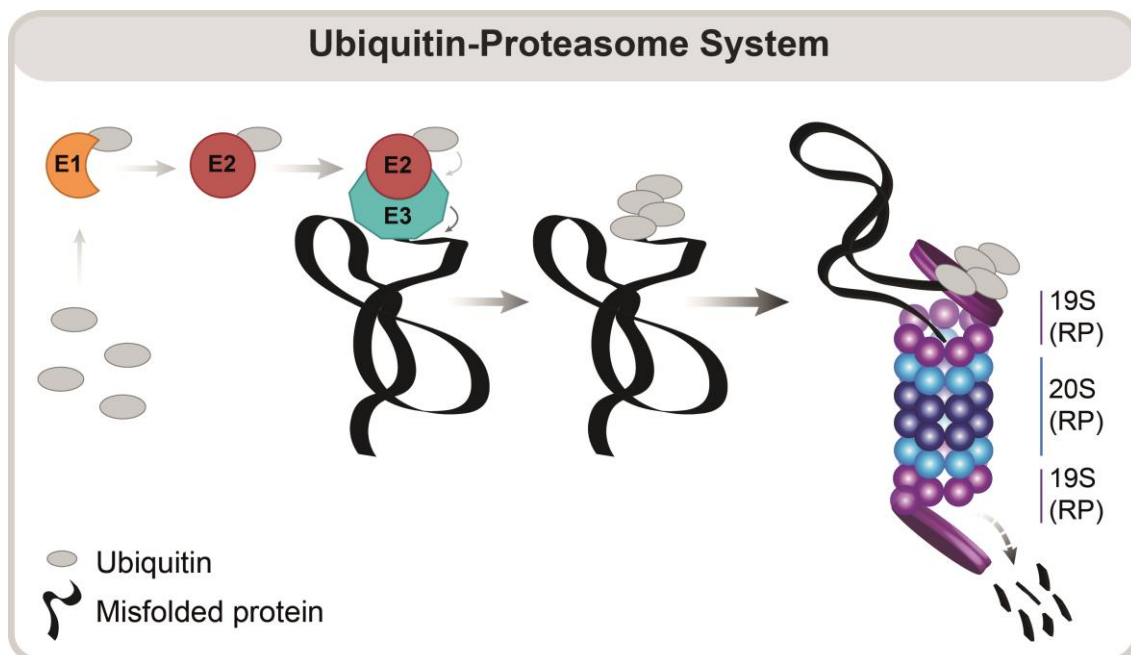
Figure 1. 4 - Degradation of misfolded proteins by the UPS.
Misfolded proteins are tagged with ubiquitin in a cascade reaction conducted by E1, E2 and E3 enzymes. E1 ubiquitin-activating enzymes bind and transfer ubiquitin to E2 ubiquitin-conjugating enzymes, and together with E3 ligases, transfer ubiquitin to the misfolded protein. The poly-ubiquitinated proteins are recognized and unfolded by the

proteasome lid (19S, regulatory particle) and then degraded in the core of the proteasome (20S, core particle) into small peptides.

3.2 *C. elegans* as a model organism

C. elegans is a transparent, free-living and non-parasitic nematode that exists in two sexes, hermaphrodites and males (Brenner 1974). Its genome was fully sequenced in 1998 and revealed that the 100 million base pairs encode for more than 19.000 genes (Consortium 1998). The nematode's genome is spread in six pairs of chromosomes (five autosomes and one sex). The number of the X chromosomes determines the sex. While hermaphrodites have a paired X sex chromosome, XX, males have only one X chromosome, X0. The incidence of males in a population is rare, and they account for only 0.1% of the population under normal growth conditions (Brenner 1974).

The nematodes have an exact cell number (hermaphrodites – 959, and males – 1031). Its tubular body is composed of distinct tissues, like muscle, neurons, intestine, excretory system, gonads, glands, and a hypodermis. The neuromuscular pharynx in its head region is responsible for food uptake (transferring food into the intestine) and the pumping rate can be used as readout for organismal fitness (Sulston et al. 1977, Altun 2017).

C. elegans has a short life cycle as it takes only 3.5 days (at 20°C) for an egg to develop into an egg-laying adult (Figure 2.1) (Brenner 1974). After egg development, animals hatch as larvae state 1 (L1) and mature through three additional larvae stages (L2, 3 and 4) until they reach adulthood. At 20°C, hermaphrodites lay approximately 300 eggs and live around two to three weeks reaching the maximum of 1 mm in length and 80 µm in diameter (Brenner 1974, Markaki et al. 2010). If L1 stage animals face starvation conditions or other stresses such as heat, they can enter into a dauer state and survive many months without access to food. When food is available, dauer larvae normally develop to L4 and adult animals (Byerly et al. 1976, Altun 2017).

C. elegans was first described as a model organism by Sidney Brenner in 1974 (Brenner 1974). In the laboratory, animals can be grown on agar plates or in liquid cultures supplied with bacteria as food source (Markaki et al. 2010). *C.*

elegans has been successfully employed as an animal model due to some attractive features such as a short lifespan, transparent body, known cell lineage and easy maintenance. In addition, the fact that approximately 80% of the nematode's proteome have a human ortholog, and the ability of genetically modifying the animals, for instance by depleting genes via RNA interference (RNAi), turned *C. elegans* into a powerful tool to study many disciplines such as developmental biology, cell biology or neurobiology (Lai et al. 2000, Hariharan et al. 2003, Sengupta et al. 2009, Markaki et al. 2010).
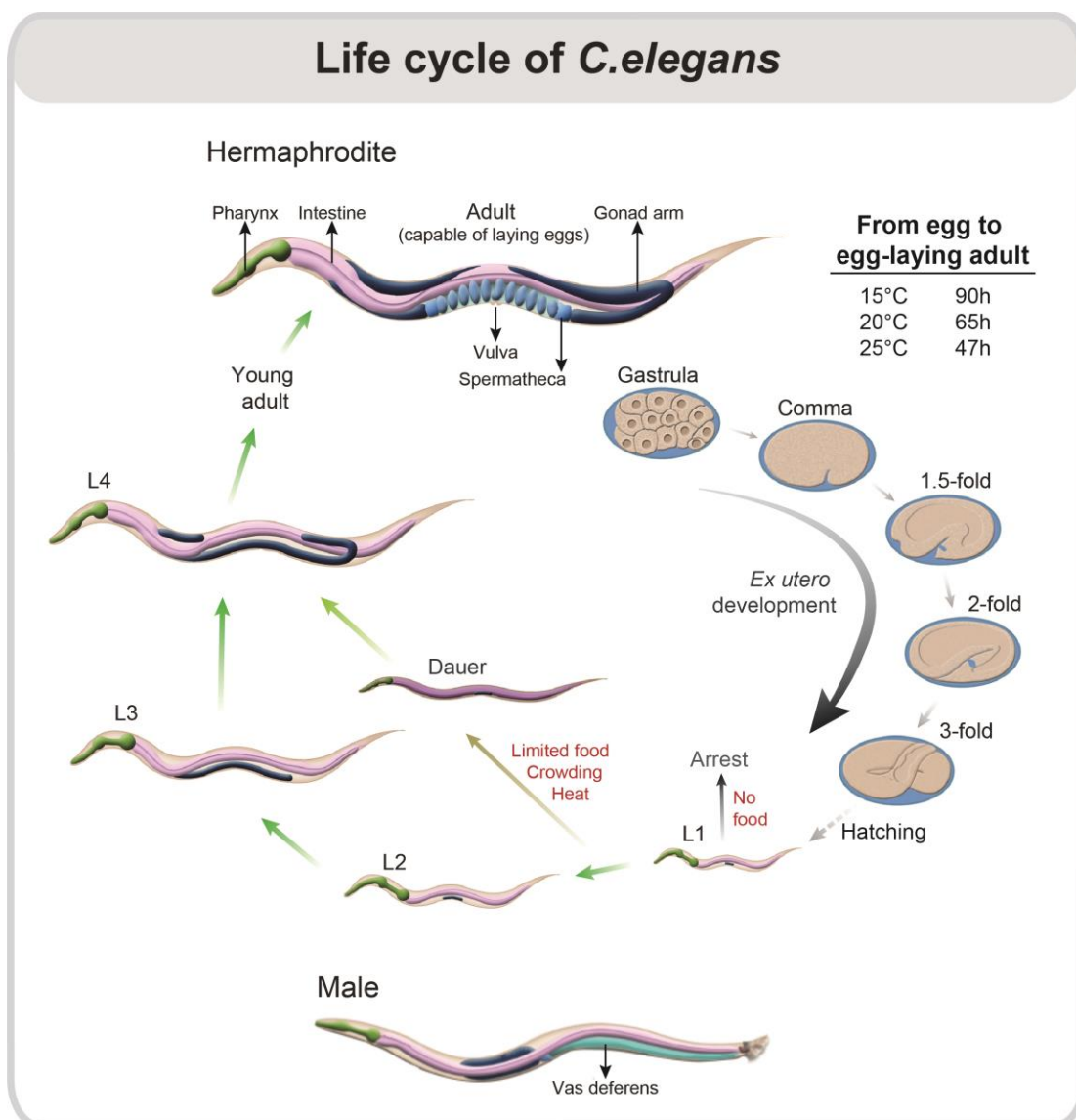
Figure 2. 1 - *C. elegans* development cycle (adapted from (Byerly et al. 1976, Altun 2017)).

The population of *C. elegans* is composed of hermaphrodites (99.9%) and males (0.1%). The development of *C. elegans* from egg to egg-laying adult involves many steps. Eggs mature into different stages and hatch as larvae stage 1 (L1). In normal condition, the L1 animals grow and enter three subsequent developmental stages (L2, 3 and 4), and reach adulthood (capable of laying eggs) after approximately 3.5 days. If L1 nematodes have no access to food, animals will arrest. Also, if L1 stage animals are exposed to stress conditions (e.g. heat stress or limited food), they can enter a dauer stage and survive several months. Dauer stage nematodes can develop normally into L4 and adult stages if growth conditions improve.

The temperature influences the life cycle of *C. elegans* in a time-wise manner, as the development from egg to egg-laying adult can take 90 h or 47 h if animals grow at 15°C or 20°C, respectively.

3.2.1 *C. elegans as a model to study aging*

A collapse in many cellular pathways is linked to the progression of aging. With the progression of aging, organisms are less capable of keeping a balanced cellular environment, and failure in maintaining proteostasis increases the protein misfolding and aggregation propensity (Naidoo et al. 2008, Ben-Zvi et al. 2009).

C. elegans is a suitable animal model for aging studies due to its short lifespan of about two to three weeks. It has been shown that while the age advances, the load of misfolded and aggregated proteins increase (David et al. 2010). In fact, around one-third of the proteome changes its abundance in old animals. An example of this are the ribosomal proteins, which decline in its abundance and lead to a decline in protein synthesis upon aging (Walther et al. 2015).

The modulation of signaling pathways such as the insulin pathway has revealed that aging is a programmed process that can be delayed (Greer et al. 2008). Mutants of the insulin pathway mutants, such as *daf-2* (insulin receptor) and *age-1* (catalytic subunit of PI3K) knockouts are long-lived (Friedman et al. 1988, Kenyon et al. 1993, Dorman et al. 1995). Both mutations in the insulin pathway lead to the activation of the transcription factor DAF-16, which induces the expression of numerous antioxidant, antimicrobial or chaperone genes (Mukhopadhyay et al. 2006). DAF-16 is the ortholog of the human FOXO3A,

which is associated with longevity in humans as well (Willcox et al. 2008). Besides the long-lived phenotype, these mutants are more resistant to heat, oxidative stress, and bacterial infection, demonstrating the important role of the insulin pathway for the organismal health (Lithgow et al. 1995, Honda et al. 1999, Garsin et al. 2003).

In addition to a proteostasis collapse discussed above, a number of different mechanisms have been proposed to explain the aging process, such as the telomere shortening, DNA/mitochondria damage, or cellular senescence (Harman 1956, Levy et al. 1992, Bhatia-Dey et al. 2016). While the telomere theory proposes that the shortening of telomeres after every cell division is the cause of aging, the mitochondria damage theory (known as "The free radical theory of aging") explains the aging process with the accumulation of reactive oxygen species that damage DNA, mitochondria, proteins, and lipids. The free radical theory of aging has produced some controversy, as it has been shown that both *C. elegans* and mice *Mclk1* mutants (mitochondrial enzyme) exhibit increased oxidative stress, yet they live longer than wt (Wong et al. 1995, Liu et al. 2005, Lapointe et al. 2008, Lapointe et al. 2009). Both telomere shortening and mitochondria damage can trigger cellular senescence (Di Micco et al. 2008, Bernadotte et al. 2016, Venkatachalam et al. 2017). The cellular senescence theory of aging states that aging is caused by an abnormal accumulation of senescent cells (cells that no longer divide), which consequently perturbs the physiology of multiple tissues (Bhatia-Dey et al. 2016, Ogrodnik et al. 2017).

Individually, the proposed theories do not entirely explain the process of aging and yet their arguments are not mutually exclusive. Aging is a complex process and may be caused or at least affected by a number of cellular signaling pathways or external factors.

3.2.1.1 Neurodegenerative diseases

The life expectancy for humans is continuously rising, and reports from the United Nations and World Health Organization predict that in 2050 the number of elderly people will have more than tripled in 2050 (WHO 2010, United Nations 2015). The increase of the human lifespan is associated with a higher

prevalence of diseases such as cancer, cardiovascular diseases or neurodegenerative diseases (Niccoli et al. 2012).

Alzheimer's disease

Alzheimer's disease (AD) is a devastating form of dementia that affects 25-50% of individuals that are older than 85 years (Duthey 2013). AD patients display severe memory loss and cognitive decline due to reduced brain mass in regions like the hippocampus (Schuff et al. 2009, Padurariu et al. 2012). The pathology is linked to mutations and post-translational modifications, and one of the hallmarks of AD is the accumulation of extracellular plaques and neurofibrillary tangles that contain Aβ and tau protein, respectively (Bloom 2014). Aβ peptides result from the cleavage of the amyloid precursor protein (APP), a transmembrane protein. APP cleavage by β- and γ-secretases generates fragments of 36 to 43 amino acids (Marsden et al. 2011). Despite the important role of the APP in the formation and function of synapses, its processing produces neurotoxic peptides such as $Aβ_{1-42/40}$ found in plaques in post-mortem AD brains (Milward et al. 1992, Klein et al. 1999, Torroja et al. 1999).

C. elegans has been employed to study AD by expressing Aβ in the muscle or neuronal cells (Figures 2.2 A+B). It has been shown that Aβ accumulation is associated with proteotoxicity that manifests in a reduced lifespan and early onset of paralysis (Link 1995, Link et al. 2003).

Polyglutamine diseases

The abnormal repetition of the aa CAG (above 35 repeats) in specific proteins is associated with nine neurodegenerative diseases like spinocerebellar ataxias, Machado-Joseph's disease, dentatorubral-pallidoluysian atrophy or Huntington's disease (HD) (Ikeda et al. 1996, Suzuki et al. 2010, Seidel et al. 2016).

HD is characterized by the extension of the polyQ region in the Htt protein. Htt protein is known to be involved in brain development and vesicular transport (e.g. synaptic, endosomal or autophagic) (Reiner et al. 2003, Cattaneo et al. 2005, Schulte et al. 2011). However, Htt aggregates and accumulates when the polyQ region is expanded, causing neuronal loss in the cerebral cortex (Goldberg et al. 1994, Gusella et al. 1998). The number of polyQ repeats is

directly associated with a stronger Htt aggregation and the severity of the symptoms, and inversely correlated with the age of disease onset (Andrew et al. 1993, Snell et al. 1993).

In nematodes expressing polyQ in muscle or neuronal cells (Figures 2.2 A+B), it has been shown that an increase of polyQ repetitions correlates with higher polyQ aggregation and toxicity (Faber et al. 1999, Morley et al. 2002).
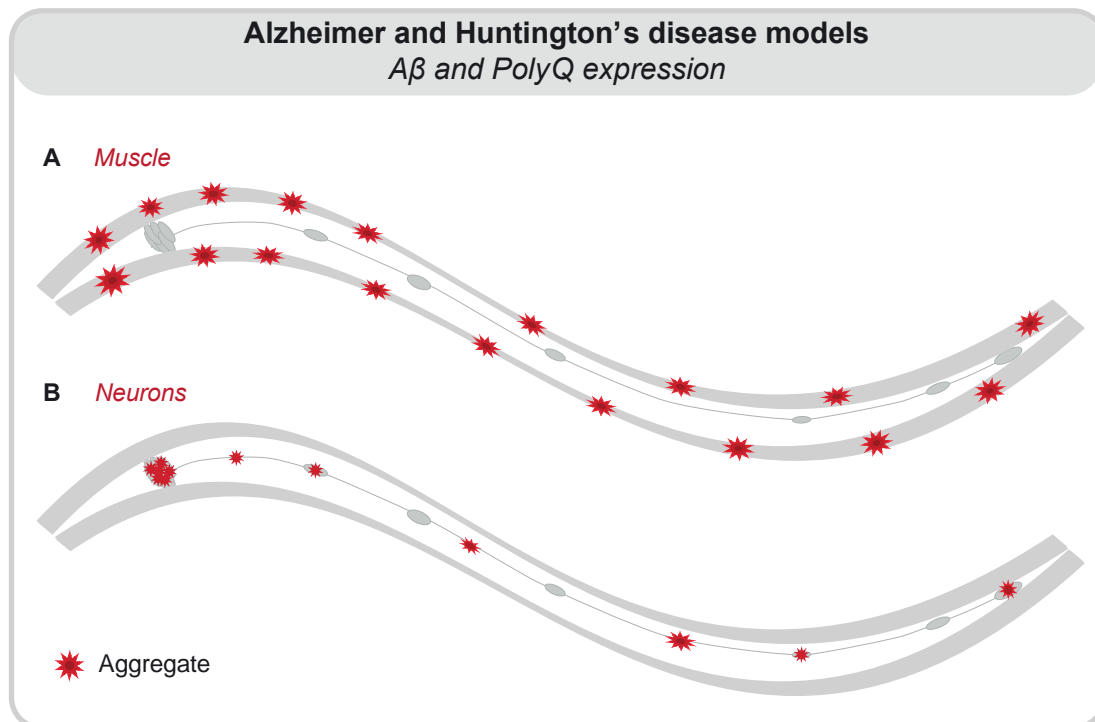
Figure 2. 2 - *C. elegans* **as a model for neurodegenerative diseases.**
Expression of an aggregation-prone protein involved in Alzheimer (Aβ) and Huntington's disease (polyQ) in the neuronal and muscle cells of *C. elegans.*

3.3 Aims of the study

A tight regulation and cooperation of the different proteostasis network components is critical to preserving a healthy cellular environment (Morimoto et al. 2014). Failure in PN pathways leads to an accumulation of protein aggregates, and is associated with aging and disease (Hipp et al. 2014, Kaushik et al. 2015). Protein misfolding and aggregation can be remodeled by the action of chaperones, UPS and autophagy (Wolff et al. 2014, Diaz-

Villanueva et al. 2015). However, it remains unclear how these three proteostasis mechanisms are regulated and coordinated on an organismal level with the progression of aging and in disease. In this thesis, I aimed to unravel the crosstalk between the chaperones that constitute the HSP110/70/J disaggregation complex with the autophagy and proteasome systems in *C. elegans* and HEK293 cells. In addition, the autophagy and proteasome functions were investigated during aging and in neurodegenerative disease models.

To understand how these three proteostasis mechanisms are coordinated, the following questions were addressed:

I. Can the protein clearance machinery compensate for a loss of HSP110/70/J complex members?
II. What is the impact of aging and disease on autophagy and proteasome pathways?
III. How do aging and loss of chaperone-mediated disaggregation capacity affect autophagy and proteasome?
IV. Does the depletion of non-disaggregating chaperones disturb the protein clearance machinery?

4 Results

4.1 Impact of proteostasis imbalances on autophagy and proteasome pathways

Cells are equipped with a powerful proteostasis network comprised of molecular chaperones and proteases to cope with proteotoxic stress and maintain a functional proteome (Kim et al. 2013, Labbadia et al. 2015). While autophagy and UPS are responsible for the elimination of non-functional cellular components, chaperones ensure the native state of proteins by assisting e.g. *de novo* folding and protein refolding. Furthermore, the HSP110/70/J chaperone complex can also prevent and reverse protein aggregation. These protein quality control mechanisms are key in maintaining proteostasis.

To understand the impact of the loss of disaggregation capacity on the maintenance of proteostasis, and in particular, on the clearance of protein aggregates, chaperones from the HSP110/70/J complex were depleted in *C. elegans* and HEK293 cells. The selection of the distinct members of the HSP/110/70/J complex was based on the following criteria: A) conservation from nematode to human and B) known involvement in protein disaggregation (Table 1).

The selected human and *C. elegans* J-proteins, together with HSP110/70 chaperones, can disaggregate amorphous (e.g. luciferase) and amyloid aggregates (α-syn and mHtt) (Rampelt et al. 2012, Gao et al. 2015, Nillegoda et al. 2015, Scior et al. 2018). The disaggregase complex requires three chaperones to be active: Hsp70 (substrate binding and folding), HSP110 (nucleotide exchange factor), and J-protein(s) (substrate recognition, targeting and activation of Hsp70).

The J-proteins act as an Hsp70 co-chaperones, and play a key role in the recognition of multiple substrates, and consequently in the composition of the disaggregation complex. Therefore, the composition of the chaperone complex can vary in response to different stress, substrates or aging. In case of amyloids, the disaggregation can be achieved with the involvement of a single type II J-protein, as shown for α-syn and mHtt, where the disaggregation is performed by HSP-70, HSP-110 and DNAJB1 (Gao et al. 2015, Scior et al. 2018). However, the disaggregation of amorphous aggregates is accelerated when members of

type I and II J-proteins are present. This phenomenon was demonstrated for luciferase, where the combination of HSP-70/HSP-110 with both, DNJ-12 and DNJ-13 exerts a synergistic effect and a more powerful disaggregation (Rampelt et al. 2012, Nillegoda et al. 2015). For this reason, and due to the diversity of the J-protein family, the depletion of three different J-proteins (two type-I and one type-II) that display the most robust disaggregation activity was employed.

Table 1 - Overview of the chaperones analyzed in this study.

Chaperone protein				Biological role	
Human	*C. elegans*	Identity*	Family	Disaggregation	Substrate
HSPA8	HSP-1	86%	Hsp70	Substrate binding; Protein folding	Luciferase (Rampelt et al. 2012, Nillegoda et al. 2015), α-syn (Gao et al. 2015), mHtt (Scior et al. 2018)
HSPA4	HSP-110	44%	Hsp70	Nucleotide exchange factor	Luciferase (Rampelt et al. 2012, Nillegoda et al. 2015), α-syn (Gao et al. 2015), mHtt (Scior et al. 2018)
DNAJA1	DNJ-12	53%	J-protein, type I	Substrate recognition; Co-chaperone	Luciferase (Rampelt et al. 2012, Nillegoda et al. 2015), α-syn (Gao et al. 2015)
DNAJB1	DNJ-13	54%	J-protein, type II	Substrate recognition; Co-chaperone	Luciferase (Rampelt et al. 2012, Nillegoda et al. 2015), α-syn (Gao et al. 2015), mHtt (Scior et al. 2018)
DNAJA2	DNJ-19	49%	J-protein, type I	Substrate recognition; Co-chaperone	Luciferase (Rampelt et al. 2012, Nillegoda et al. 2015)

* www.ensemble.org

The following genes were depleted in *C. elegans*: *hsp-1* (Hsc70)*, hsp-110* and the J-protein encoding genes *dnj-12, dnj-13* and *dnj-19*; and the respective mammalian orthologous genes in HEK293 cells: *hspa8, hspa4, dnaja1, dnajb1* and *dnaja2*. As shown in figure 3.1, the knockdown efficiencies were analyzed and revealed remaining chaperone protein levels of 20-40% in *C. elegans*, and 30-60% in HEK293 cells.
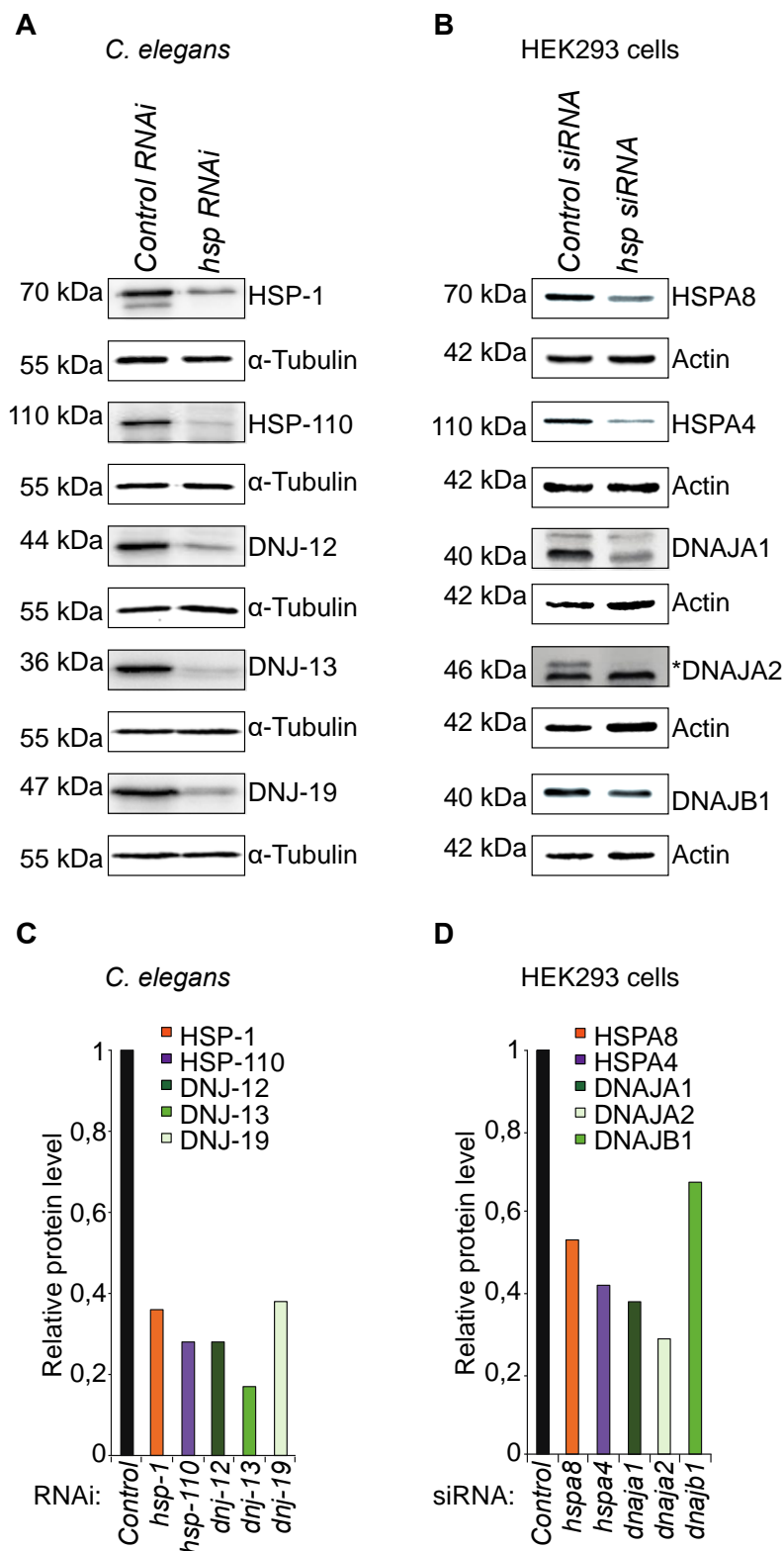
Figure 3. 1 - Analysis of RNAi and siRNA chaperone knockdown efficiencies in *C. elegans* and HEK293 cells.

A) Western blot analysis of chaperone levels of day 4 nematodes treated with RNAi against the indicated chaperones. B) Chaperone levels in HEK293 cells, which were transfected with the indicated siRNA for 48 h. C) The relative band intensity of each *C.*

elegans chaperone was normalized to α-tubulin levels and then to control RNAi (A). D) The relative band intensity of each mammalian chaperone was normalized to α-tubulin levels and then to control siRNA (B). The molecular weight is indicated on the left.

Based on the crucial role of the HSP/110/70/J chaperone complex, I hypothesized that the loss of disaggregase capacity would be likely to cause an accumulation of misfolded and aggregated proteins, which subsequently could trigger a compensatory activation of A) autophagy system and B) ubiquitin-proteasome system (Figure 3.2).

In the following sections, the responses of autophagy and proteasome pathways upon chaperone depletion in *C. elegans* and HEK293 cells will be depicted.
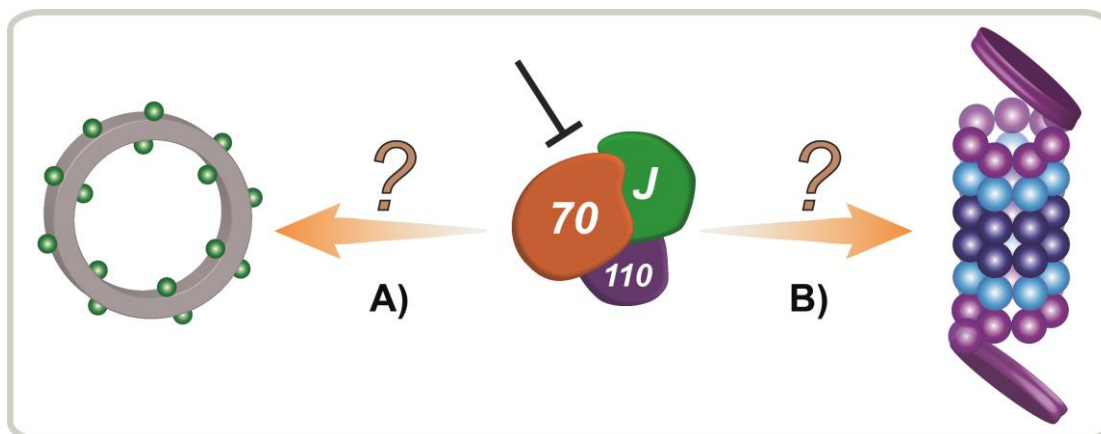
Figure 3. 2 - Analysis of the clearance machinery upon HSP110/70J complex members knockdown.
A) Autophagy and proteasome (B) pathways were investigated upon depletion of chaperones genes that constitute the disaggregation complex.

4.2 Autophagy response to proteostasis perturbations

4.2.1 *Autophagy is induced when chaperone disaggregase capacity is compromised*

In order to study the autophagy pathway, I used a well-established autophagy reporter strain (DA2123) that encodes the LGG-1 protein tagged with GFP expressed ubiquitously in the animal (Melendez et al. 2003). This reporter

enables the visualization of autophagic structures by light microscopy (Kang et al. 2007, Zhang et al. 2015).

Chaperones of the disaggregase complex were depleted in the DA2123 animals, and the GFP::LGG-1 expression pattern was analyzed on day 6 (Figure 3.3 A). Animals treated with control RNAi display a low basal level of autophagic vesicles in the head and intestine. Depletion of the chaperones led to a pronounced accumulation of autophagosomal structures mainly in the intestine. This accumulation was more prominent when animals were treated with RNAi during 6 days. Indeed, the increased number of GFP::LGG-1 positive structures detected by confocal microscopy was due to an increase of GFP::LGG-1 protein levels confirmed by western blot, using an anti-GFP antibody (Figures 3.3 B+C).
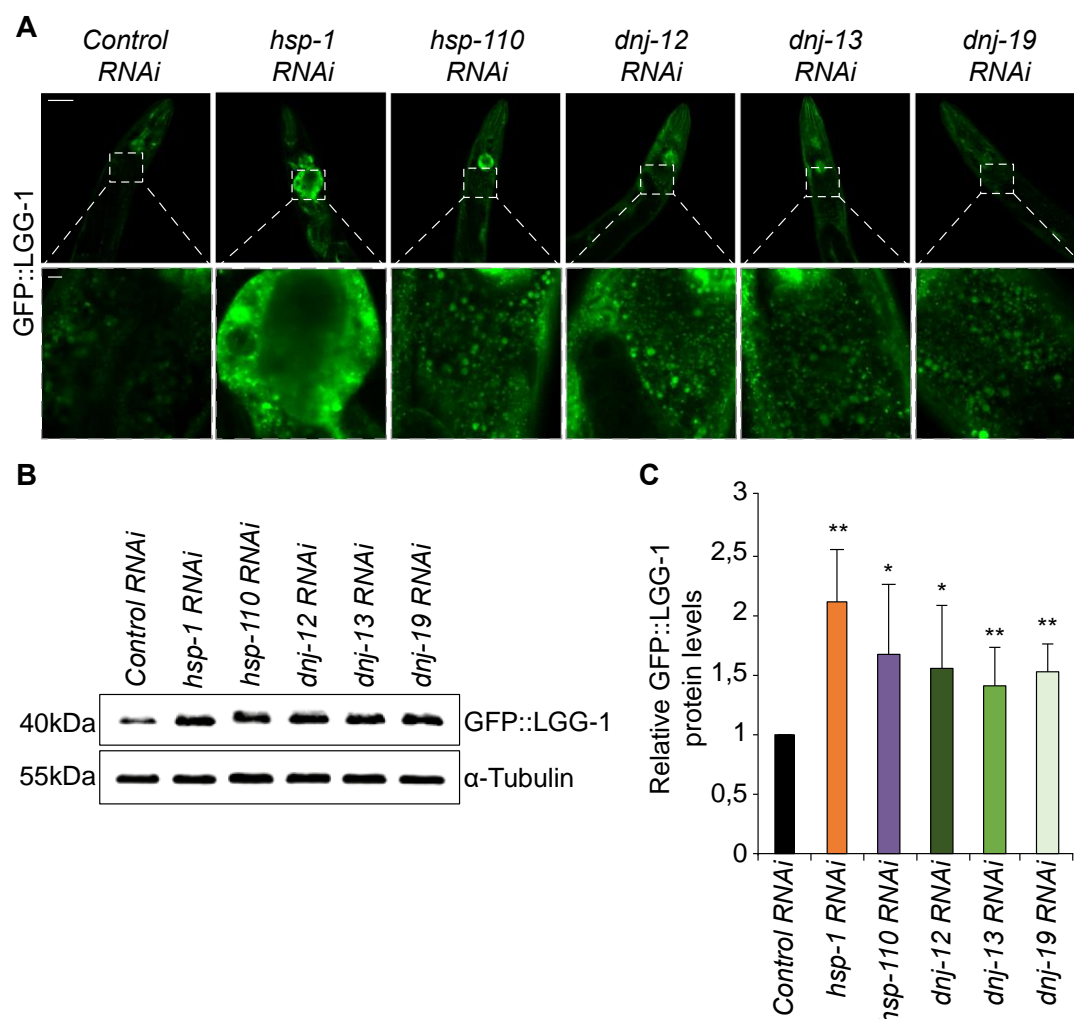
Figure 3. 3 - GFP::LGG-1 levels upon knockdown of members of the HSP110/70/J complex.

A) Fluorescent images of DA2123 (GFP::LGG-1) animals (day 6) that were subjected to RNAi treatment to deplete *hsp-1*, *hsp-110*, *dnj-12*, *dnj-13,* and *dnj-19*. The empty vector L4440 served as control. The upper panel shows the head/intestinal region of the animals and the lower panel is a magnification of the indicated regions of the upper panel. Scale bars: 50 μm (upper panel) and 5 μm (lower panel). B+C) Immunoblotting of lysates of DA2123 animals (day 6) treated with RNAi against the indicated genes. The relative band intensities of GFP::LGG-1 (anti-GFP) were normalized to the α-tubulin levels and then to control RNAi. The error bars represent the standard deviation from a minimum of four independent experiments.

To assess the endogenous levels of LGG-1 and to avoid the potential negative effects of the GFP fusion, an anti-LGG-1 antibody was generated. The specificity for LGG-1 was confirmed using a *lgg-1* knockdown that led to a reduction in the respective protein levels. (Figures 3.4 A+B). Moreover, *bec-1* RNAi led to an accumulation of LGG-1 protein due to autophagy blockage. The LGG-1 antibody detected the total amount of LGG-1 and consequently the levels of LGG-1-I/II could not be differentiated.
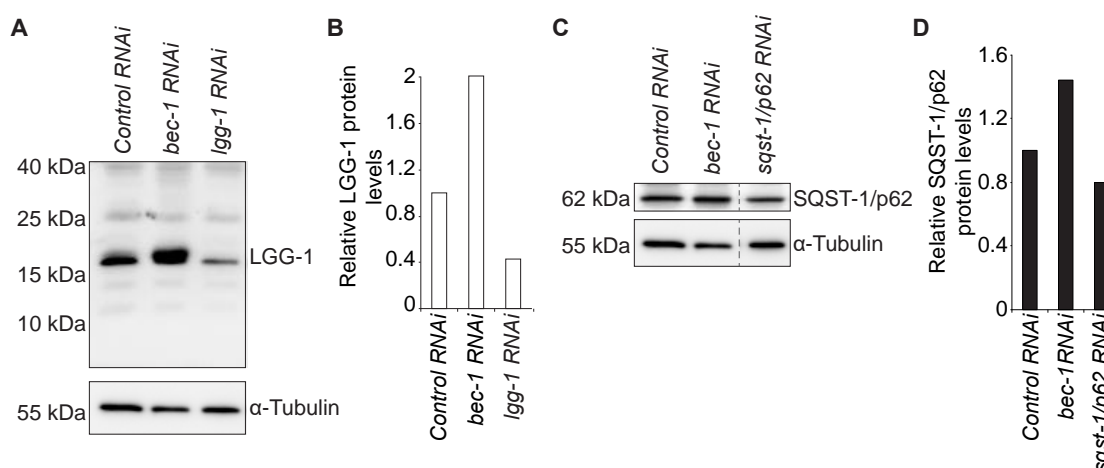
Figure 3. 4 - LGG-1 and SQST-1/p62 levels upon genetic modulations.
A-B) LGG-1 levels from day 4 wt animals treated with the indicated RNAi. The LGG-1 levels were normalized to α-tubulin levels and then to RNAi control (B). C-D) SQST-1/p62 levels from day 4 wt animals treated with the indicated RNAi. Some lanes were removed from the immunoblot as indicated by the dashed line (C). SQST-1/p62 levels were normalized to α-tubulin levels and then to RNAi control (D).

Using this antibody, I found that endogenous LGG-1 protein also accumulates in response to knockdown of the chaperone genes encoding the HSP110/70/J complex members and thus confirm the data obtained using the GFP::LGG-1 reporter (Figures 3.5 A+B). An accumulation of LGG-1 could be interpreted either as induction or impairment of autophagy, as both scenarios lead to an increase of LGG-1 protein levels. Therefore, it is critical to evaluate different autophagy markers to access the autophagic flux correctly.

In order to differentiate between these two possibilities, the levels of SQST-1/p62 were analyzed. SQST-1/p62 is an ubiquitin-binding protein that acts as an adaptor for the autophagy pathway, and is also degraded by autophagy, thus its levels can indicate the state of the autophagic flux (Bjorkoy et al. 2005). An SQST-1/p62 antibody was generated, and confirmed that the produced antibody recognizes the SQST-1/p62 protein (Figure 3.4 C+D). The levels of SQST-1/p62 were evaluated upon chaperone knockdown (Figure 3.5 A+C). Chaperone depletion, especially of *hsp-1* and *hsp-110,* led to a reduction of SQST-1/p62 levels when compared to the control condition, which indicates an increased autophagic flux.

The increase of LGG-1 and simultaneous decrease of SQST-1/p62 protein, suggests that the depletion of chaperones required for disaggregase activity in *C. elegans* is compensated by the activation of autophagy in young animals.
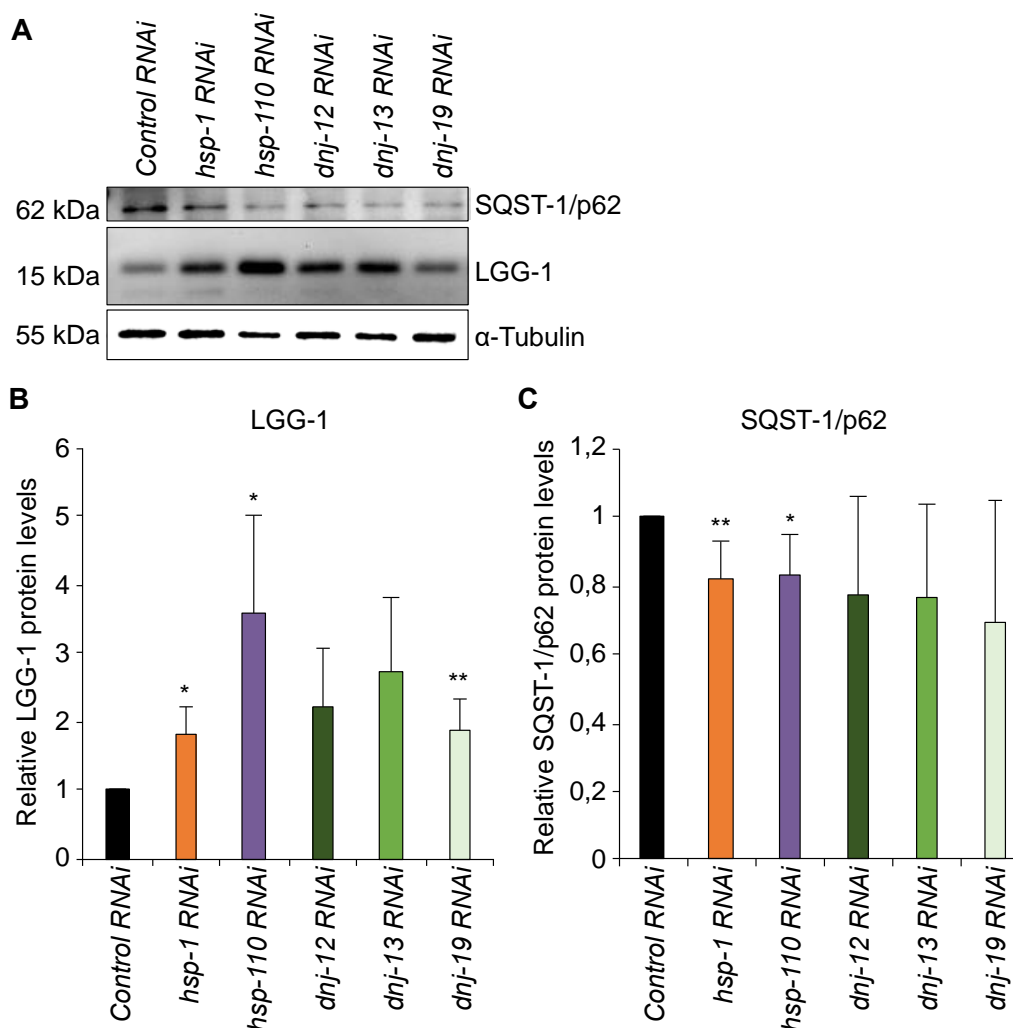
Figure 3. 5 - LGG-1 and SQST-1 protein levels upon RNAi-mediated knockdown of HSP110/70/J complex members.

A) LGG-1 and SQST-1/p62 protein levels from wt animals (day 6) treated with RNAi against the indicated chaperones. The LGG-1 (B) and SQST-1/p62 (C) levels were normalized to α-tubulin and then to control RNAi. The error bars represent the standard deviation of a minimum of three independent experiments.

To verify the relevance of these findings in a mammalian system, the autophagic flux was analyzed upon siRNA treatment of the orthologous chaperones in HEK293 cells. Analogously to the *C. elegans* data, chaperone depletion led to an increase of LC3-II protein levels (LGG-1 homolog) in HEK293 cells (Figures 3.6 A+B). LC3 levels are a well-established reporter of autophagy, and its levels correlate with the amount of autophagosomes

(Kabeya et al. 2000, Mizushima et al. 2010). Nevertheless, a distinction between induction and impairment of autophagic flux is required. In order to accurately differentiate between those two scenarios, cells were treated with Bafilomycin A1 (BafA1). BafA1 is a lysosome V-ATPase inhibitor that inhibits the autophagic flux and therefore unravels changes in autophagosome synthesis (Tanida et al. 2005, Fass et al. 2006). In the absence of BafA1, LC3-II levels are elevated upon knockdown of the chaperone genes, and the presence of BafA1 caused an increase of LC3-II levels compared to the siRNA control (Figures 3.6 A+B). The elevated LC3-II levels upon BafA1 treatment indicate an induction of autophagy, which is consistent with the data obtained using *C. elegans*.

A

B
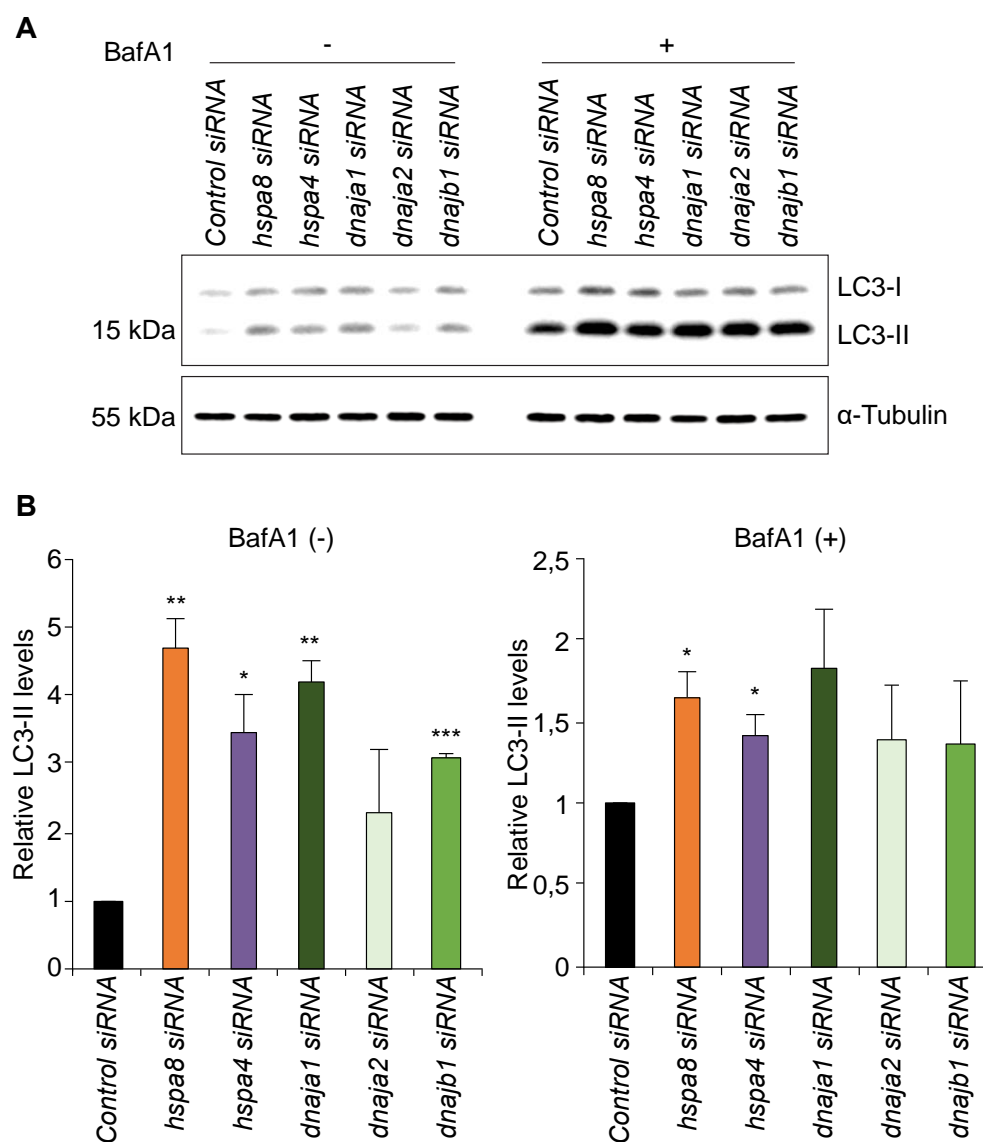
Figure 3. 6 - LC3 levels in HEK293 cells upon HSP110/70/J siRNA and Bafilomycin treatment.

A) Immunoblotting of HEK293 cells lysates, which were transfected with the respective chaperone siRNA. Cells were additionally treated with 200 nM Bafilomycin A1 4 h before harvest and lysis. The LC3-II levels were normalized to α-tubulin levels and then to siRNA control (B). The error bars represent the standard deviation of two independent experiments.

4.2.2 Autophagy is impaired in old animals and less responsive to chaperone depletion

With the progression of aging, misfolded and aggregated proteins accumulate and pose a burden to the PN. These aggregates are potential substrates for either remodeling by the disaggregation complex, or clearance by the proteasome or autophagic pathway. The analysis of the autophagy flux during aging has produced contradictory outcomes. While some laboratories have reported autophagy activation during aging (Chapin et al. 2015), others have suggested the opposite (Chang et al. 2017). The conflicting data could be due to different animal models and experimental conditions. I decided to take advantage of the short lifespan of *C. elegans* to investigate how autophagy is regulated with the progression of aging in the nematode.

In order to measure the autophagic flux over aging, the levels of LGG-1 and SQST-1/p62 were analyzed in animals of 4 (young), 6, 8 and 10 (old) days of life. As presented in figures 3.7 A+B, LGG-1, and SQST-1/p62 levels increase from young to old animals. This data strongly suggests an impairment of autophagy with the progression of aging, and it is in agreement with previous work (Chang et al. 2017).
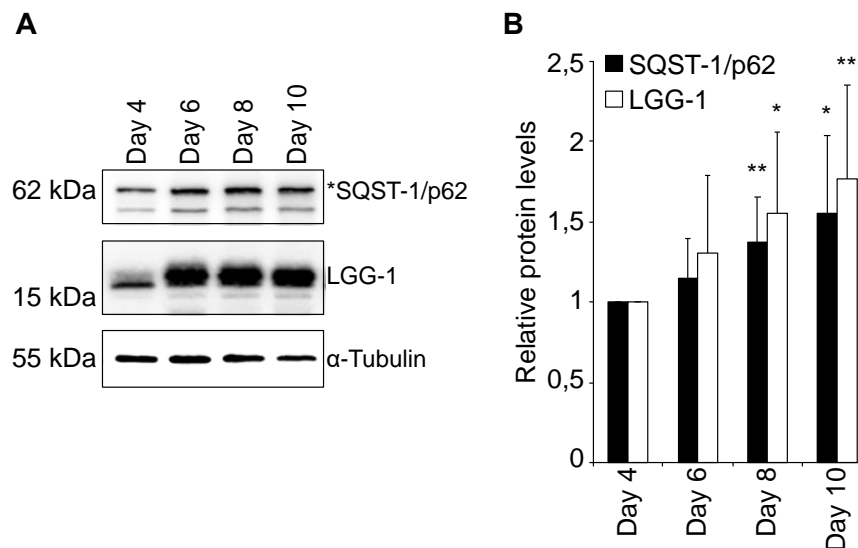
Figure 3. 7 – Autophagic flux with the progression of aging.

A) LGG-1 and SQST-1/p62 levels were determined in nematodes of 4, 6, 8 and 10 days of life. The LGG-1 and SQST-1/p62 levels were normalized to α-tubulin levels and then to day 4 (B). The error bars represent the standard deviation of five independent experiments.

Taking this data into account, I wondered how autophagy is regulated during aging upon depletion of the disaggregating chaperones. To address this question, I compared the autophagy flux upon knockdown of the HSP110/70/J complex members between young and old animals. The analysis of the autophagy reporter GFP::LGG-1 revealed an accumulation of LGG-1 positive structures in old animals (day 10) when compared to young animals (day 4), in the control condition (Figure 3.8). The higher LGG-1 protein levels in old animals presented in figure 3.7, supports the accumulation of LGG-1 positive structures in aged animals at day 10. An accumulation of LGG-1 positive structures in old animals was detected in all RNAi conditions including the control. Thus, the increase of LGG-1 positive structures detected in young animals upon chaperone knockdown compared to the control (Figure 3.3 A - day 6; Figure 3.8 – day 4), does not occur in old animals (Figure 3.8 – day 10).
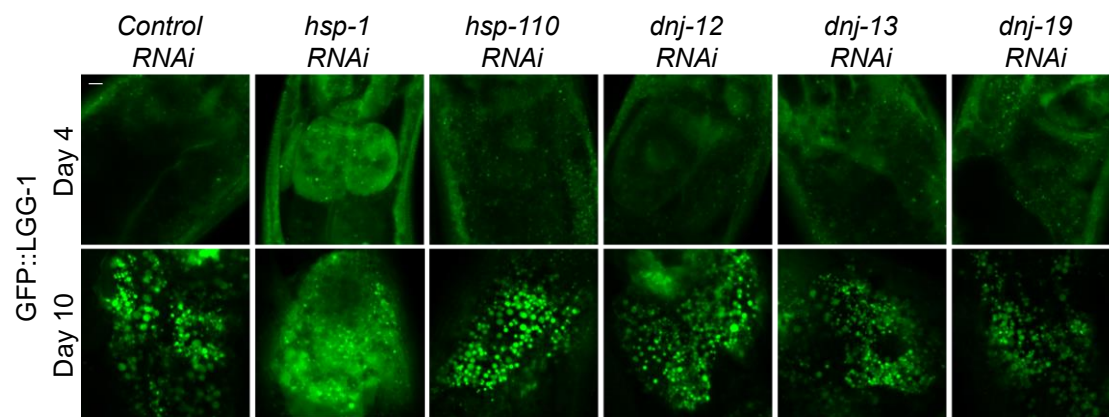
Figure 3. 8 – Analysis of GFP::LGG-1 fluorescence after chaperone RNAi on days 4 and 10.
DA2123 animals were subjected to RNAi treatment against the indicated genes. The fluorescent images are a magnification of the intestinal region and were acquired at day 4 (upper panel) and day 10 (lower panel). Scale bars: 5 µm.

These results imply that autophagy may be less responsive to chaperone depletion with the progression of aging. To analyze the autophagic flux, SQST-1/p62 and LGG-1 protein levels were assessed upon chaperone knockdown in a time-course experiment (day 4, 6, 8 and 10). As demonstrated in figures 3.9 A+B, LGG-1 protein levels peak for all distinct knockdowns at day 6, and SQST-1/p62 correspondingly exhibits the lowest levels between days 4 and 6. As aging progresses (day 6 to day 10), autophagy appears to be less activated in response to chaperone depletion. Nearly no differences can be observed in LGG-1 and SQST-1/p62 levels between control and the chaperone knockdowns. In order to analyze if the changes detected in the protein levels were associated with transcriptional regulation, the mRNA levels of *lgg-1* were analyzed upon *hsp-1*, *hsp-110* and *dnj-13* knockdown by qRT-PCR. As shown in figure 3.9 C, *lgg-1* mRNA levels are elevated only in young animals (days 4 and 6), indicating activation of autophagy at young age. No significant changes to the control were observed in older animals (day 10). The analysis of *sqst-1/p62* mRNA levels was not conclusive (data not shown).

This data suggests an induction of autophagy in young animals in response to the loss of HSP110/70/J complex members. However, in old animals autophagy does not respond to chaperone knockdown and is no longer induced.
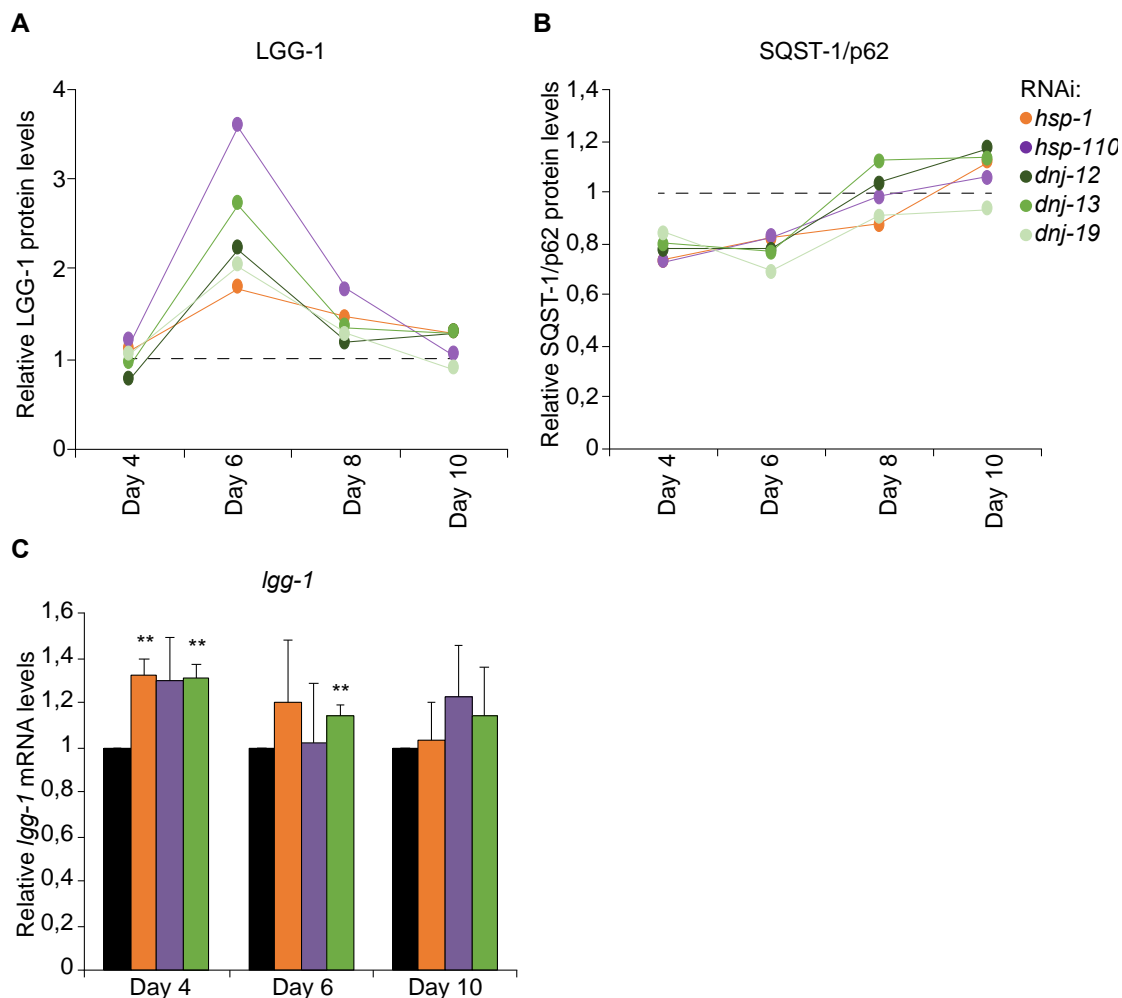
Figure 3. 9 - Analysis of protein and mRNA levels of LGG-1 and SQST-1/p62 upon chaperone depletion during aging.
A-B) The levels of LGG-1 and SQST-1/p62 were measured at day 4, 6, 8 and 10 of wt animals treated with RNAi against the indicated chaperones. The LGG-1 and SQST-1/p62 levels were normalized to α-tubulin levels and then to RNAi control. These graphs represent the average values from a minimum of two independent experiments (error bars were excluded for clarity). C) *lgg-1* mRNA levels from day 4, 6 and 10 animals treated with the indicated RNAi. The values were normalized to the control RNAi of the respective day. The graph represents the average values of three independent experiments.

4.2.3 Chaperone knockdown reduces lysosomal pool in C. elegans

To comprehensively understand how chaperone depletion affects autophagy, I analyzed the lysosomal function upon HSP110/70/J complex members knockdown.

The fusion between autophagosomes and lysosomes (Figure 1.3) is a crucial step in autophagy pathway, and it is dependent on the transport of both structures (Dunn 1990, Tooze et al. 1990, Lawrence et al. 1992, Berg et al. 1998, Fader et al. 2008). Therefore, the vesicular transport is essential for the autophagic flux (Longatti et al. 2009, Tooze et al. 2010). RAB proteins participate in vesicular trafficking, and RAB-7 is known to be involved in late-endosomal trafficking. RAB-7 assists in the maturation of autophagosomal structures by interacting with LMP-1 (Gutierrez et al. 2004, Lin et al. 2011). Upon maturation of autophagosomal structures a new vesicle, autophagolysosome, is formed and subsequently degraded. Thus, the lysosomal pool is affected by the autophagic flux and can be used as a read-out for either an impairment (accumulation of lysosomes) or activation of autophagy (decrease of lysosomes) (Yu et al. 2010). The lysosome pool can be quantified with LysoTracker, which is a fluorophore linked to a weak base that is highly selective for acidic organelles (Chen et al. 2015). The lysosomes have a pH between 4.5 and 5, which allows the accumulation and protonation of the fluorophore that subsequently leads to the emission of fluorescence.

The analysis of the lysosome pool was performed by assessing: A) the levels of LMP-1 in animals expressing LMP-1::GFP and the levels of RAB-7 in animals expressing RAB-7::GFP as well as B) the lysosomal abundance by LysoTracker-Red staining (Figures 3.10 A+B).
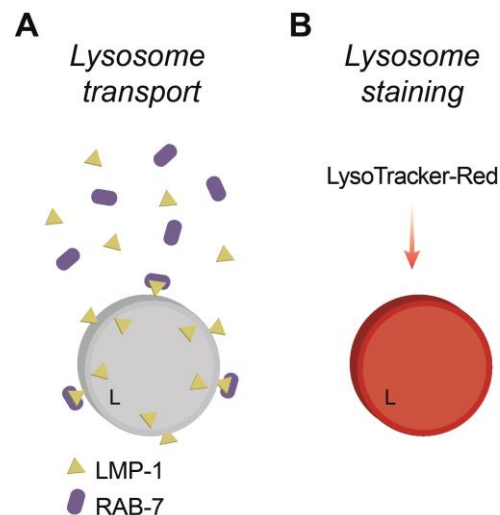
Figure 3. 10 – Lysosome function analysis.
A) LMP-1 is a lysosomal (L) membrane protein, which interacts with the vesicular transporter RAB-7 in order to fuse with autophagosomes. B) LysoTracker-Red accumulates within the lysosomes and its fluorescence allows the quantification of the lysosome pool.

To understand how these three lysosomal reporters (LysoTracker, RAB-7, and LMP-1) reflect changes in autophagy flux, animals were treated with established autophagy chemical modulators that either activate (rapamycin) or impair (3-Methyladenine (3-MA) and chloroquine (CQ)) the autophagic flux. While rapamycin strongly binds and inhibits mTOR leading to activation of autophagy, 3-MA impairs autophagy by inhibiting PI3K, which controls mTOR activation (Seglen et al. 1982, Noda et al. 1998). CQ accumulates in the lysosome and alters its acidification (Seglen et al. 1979). The increase of pH inhibits lysosomal enzymes and subsequently leads to autophagy impairment.

Activation (rapamycin) and impairment (3-MA or CQ) of autophagy led to a reduction and increase of the lysosome pool, respectively, detected by LysoTracker-Red staining (Figures 3.11 A+B). As shown in figures 3.11 E+F, RAB-7::GFP levels increased when autophagy was activated and were not affected upon inhibition of autophagy. LMP-1::GFP reporter did not exhibit a robust response to autophagy modulation (Figures 3.11 C+D). Therefore,

LysoTracker-Red staining was applied to accurately assess the lysosome pool in further experiments.
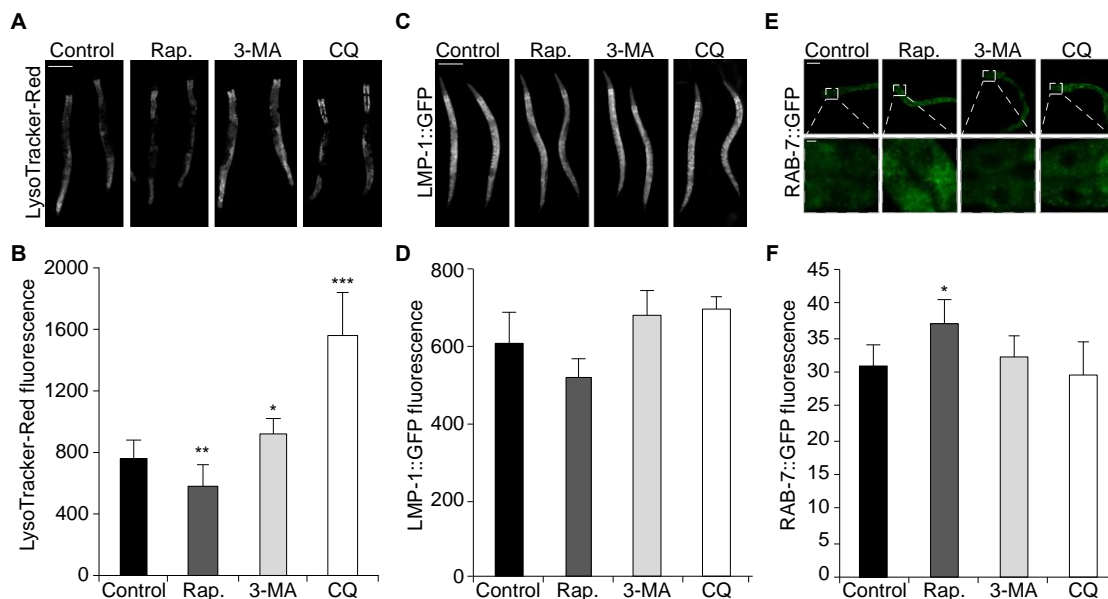
Figure 3. 11 - Modulation of the autophagy pathway.

A-B) Lysosomal pool of day 4 old animals treated with 200 µM Rapamycin, 10 mM 3-Methyladenine or 10 mM chloroquine for 20 h was stained with LysoTracker-Red and then imaged using a fluorescent microscope. LysoTracker-Red fluorescence was quantified and normalized to control animals (B). The error bars represent the standard deviation of 4-10 animals. Scale bar: 200 µm. C-D) Fluorescent imaging of day 4 LMP-1::GFP expressing animals treated with 200 µM Rapamycin, 10 mM 3-Methyladenine or 10 mM chloroquine for 20 h. GFP fluorescence was quantified and normalized to control animals (D). The error bars represent the standard deviation of 4-5 animals. Scale bar: 200 µm. E-F) Day 4 RAB-7::GFP expressing nematodes were imaged after 20 h of 200 µM Rapamycin, 10 mM 3-Methyladenine or 10 mM chloroquine treatment. The upper panel shows the intestinal cells of the nematodes, and the lower panel depicts a magnified region of the upper panel (E). GFP fluorescence was quantified and normalized to control animals (F). The error bars represent the standard deviation of 5-6 animals. Scale bars: 10 µm.

Next, the impact of the loss of chaperone disaggregation capacity in the lysosome function was analyzed. For that, the lysosomal pool was stained with LysoTracker-Red, and as displayed in figures 3.12 A+B, a notable reduction in

the lysosome pool stained was detected upon chaperone knockdown when compared to the control. The reduction in the lysosome pool supports the activation of autophagy upon chaperone depletion depicted in the section 4.2.1, which leads to the consumption of the lysosome pool.

In addition, the effect of chaperone knockdown in the RAB-7::GFP reporter strain was investigated. Depletion of genes encoding members of the HSP110/70/J complex, led to an accumulation of RAB-7 positive structures in intestinal cells, in particular upon knockdown of *hsp-110* (Figures 3.12 A+C). This result also points to an autophagy activation, as the activation of autophagy with rapamycin led to an increase of RAB-7::GFP fluorescence (Figures 3.11 E+F).

Taken together, these results confirm that the autophagy-lysosome pathway is activated when the disaggregase chaperone complex is compromised.
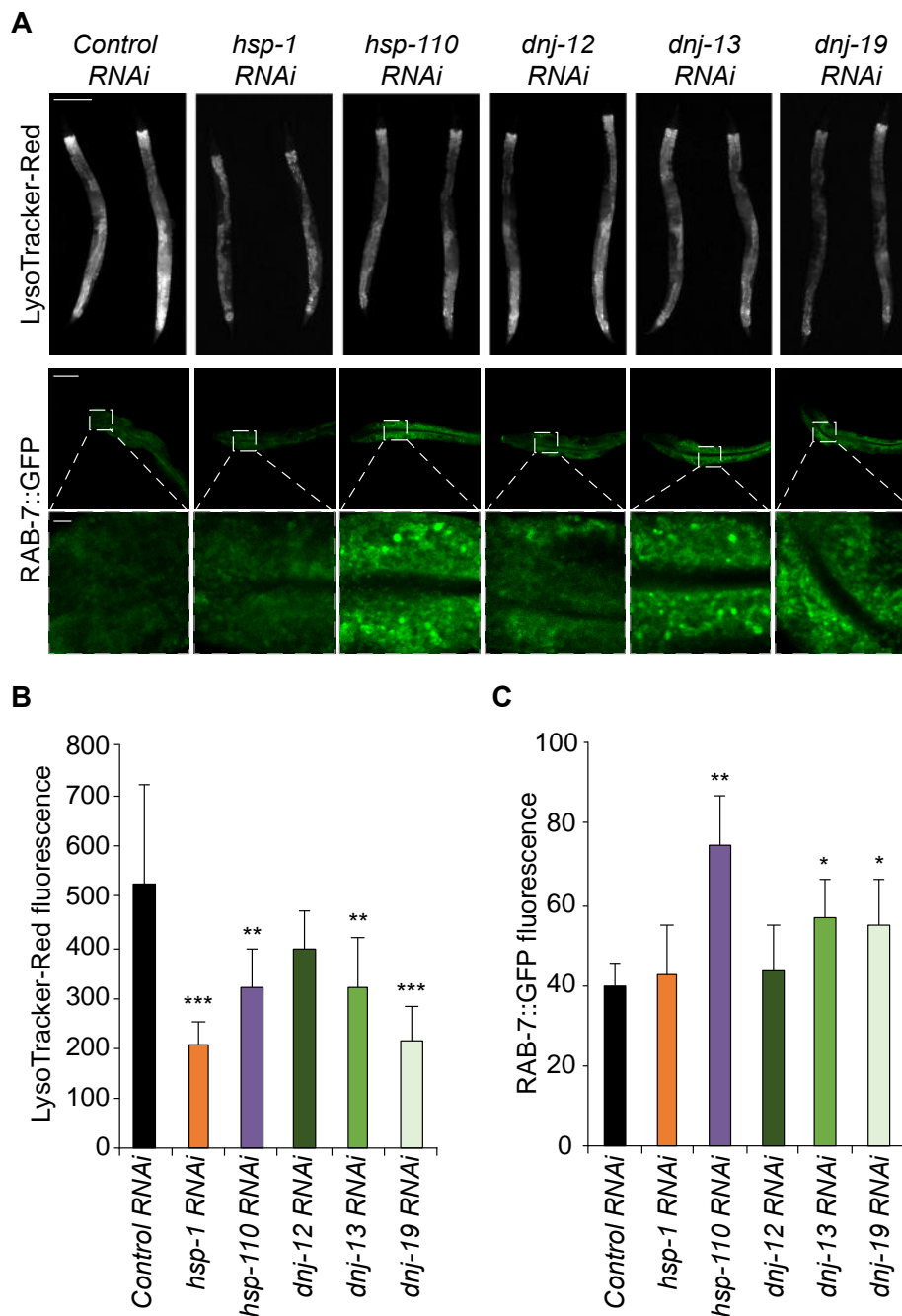
Figure 3. 12 - Lysosome pathway response to chaperone knockdown.

A) Lysosomal pool from day 4 old animals treated with the indicated RNAi was stained with LysoTracker-Red and then imaged using a fluorescent microscope (upper panel). RAB-7::GFP expressing nematodes were imaged after 4 days of RNAi treatment against the indicated genes (lower panel). B) LysoTracker-Red fluorescence was quantified and normalized to control RNAi. The error bars represent the standard deviation of 10-16 animals. Scale bar: 200 µm. C) RAB-7::GFP fluorescence was quantified and normalized to control RNAi. The error bars represent the standard deviation of 3-6 animals.

4.2.4 HLH-30 translocates to the nucleus upon chaperone depletion

Autophagy is tightly controlled on the transcriptional level. In mammals, transcriptional regulation of autophagy is controlled by the transcription factor EB (TFEB) (Settembre et al. 2011). In *C. elegans*, the activation of autophagy is regulated via HLH-30, a TFEB ortholog (Lapierre et al. 2013).

To elucidate the mechanism for the activation of autophagy upon depletion of chaperones, I employed an HLH-30::GFP reporter strain (Lapierre et al. 2013). In normal growth conditions, HLH-30 is mainly localized in the cytoplasm. However, upon autophagy activation, it translocates to the nucleus leading to the expression of autophagy-related genes (Figure 3.13).
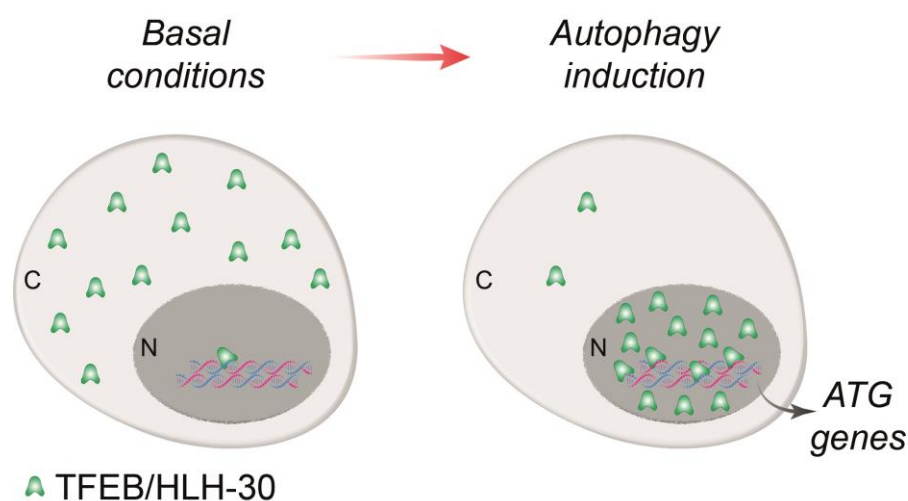
Figure 3. 13 - Mechanism of action of the autophagy transcriptional regulator TFEB/HLH-30.

Induction of autophagy leads to TFEB/HLH-30 translocation from the cytosol (C) to the nucleus (N), following the expression of autophagy-related genes.

This phenomenon can be observed in figure 3.14 A, where the activation of autophagy by rapamycin shows a nuclear translocation of HLH-30::GFP. Next, chaperones of the disaggregase complex were depleted in the HLH-30::GFP reporter strain. Notably, knockdown of *hsp-1* (30% of the animals*)* and *hsp-110* (45%) led to nuclear translocation of HLH-30 (Figures 3.14 B+C). This data

suggest that the activation of autophagy upon *hsp-1* and *hsp-110* depletion is regulated via the transcription factor HLH-30.
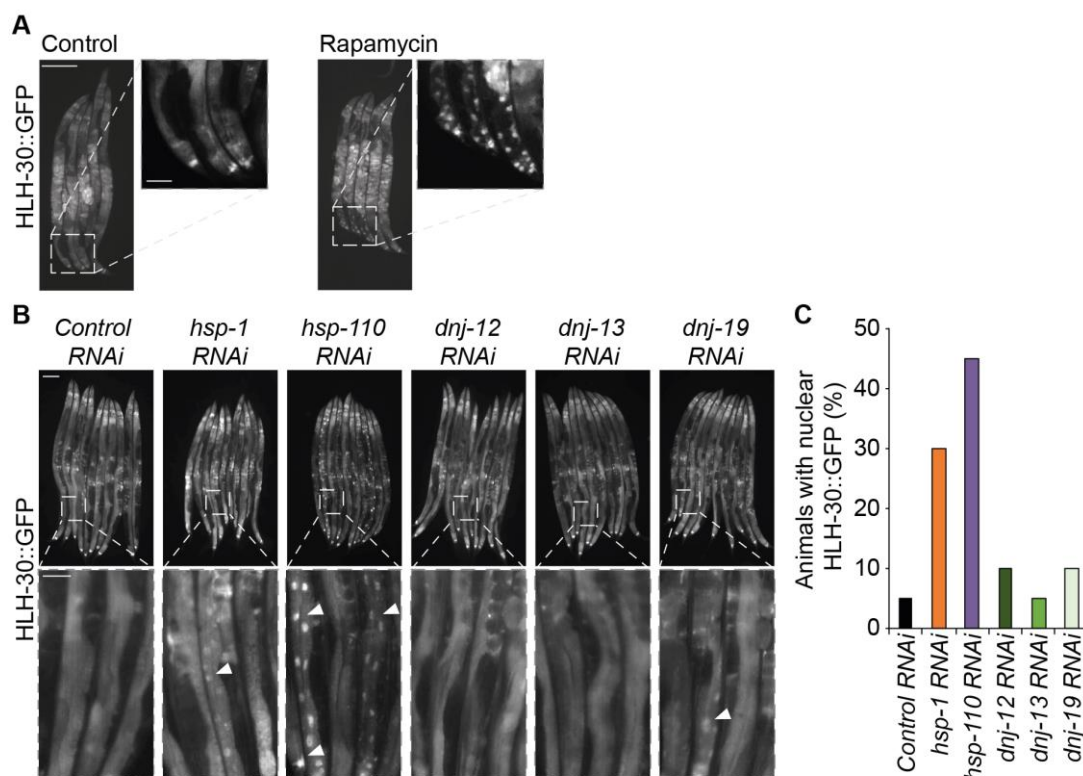
Figure 3. 14 - Translocation of HLH-30 in response to autophagy activation.
A) Day 4 animals expressing HLH-30::GFP were treated with 200 μM Rapamycin for 20 h or left untreated (control). The HLH-30::GFP nuclear translocation was analyzed in 10 animals. Scale bars: 200 μm (left panel) and 50 μm (right panel, magnification). B-C) Animals expressing HLH-30::GFP were subjected to RNAi treatment for 4 days before imaging. After image acquisition, the percentage of animals with HLH-30::GFP nuclear translocation was determined in 25 animals per condition (C). Scale bars: 200 μm (upper panel) and 50 μm (lower panel).

4.3 Proteasome function upon proteostasis perturbations

4.3.1 Proteasome capacity is diminished when HSP110/70/J machinery is compromised

The UPS plays a key role in the elimination of misfolded proteins. In this section, the UPS capacity in response to depletion of the disaggregating chaperones will be characterized.

To understand how UPS responds to the depletion of chaperones constituting the disaggregase complex, the *ex* and *in vivo* UPS capacity of *C. elegans* and HEK293 cells were investigated: A) *in vivo* – by measuring the degradation rates of UbG76V and B) *ex vivo* – by analyzing the cleavage of Suc-LLVY-AMC (Figures 4.1 A+B).
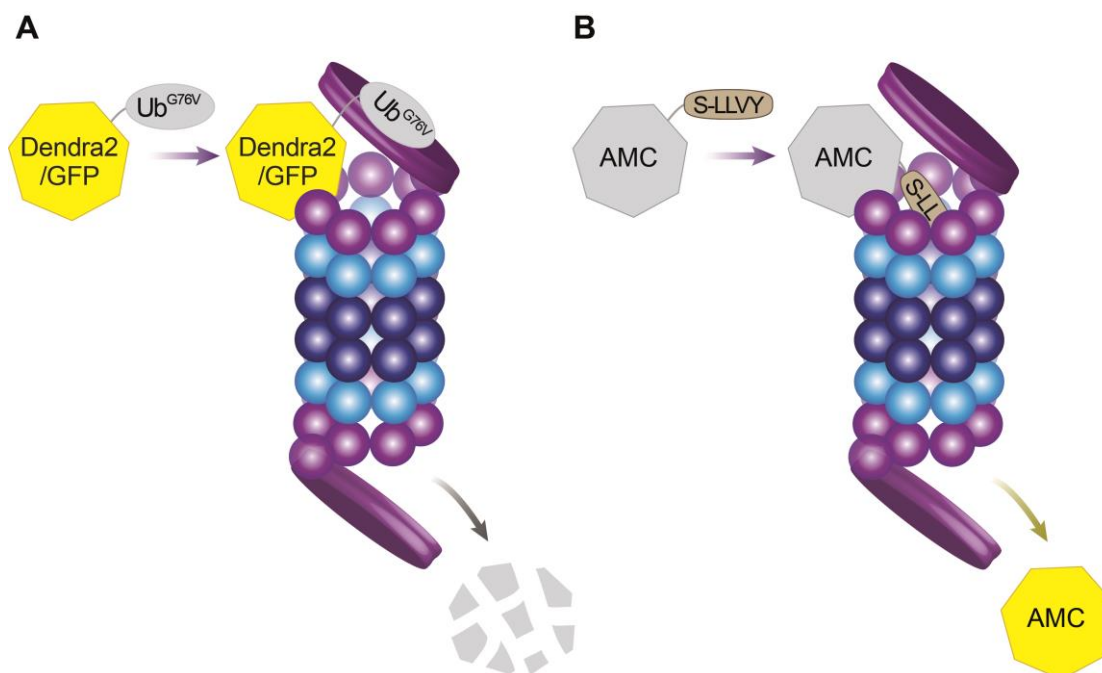
Figure 4. 1 - Scheme of the analysis of proteasome activity.
A) The *in vivo* UPS activity was analyzed by measuring the degradation rates of UbG76V. B) The cleavage of the Suc-LLVY-AMC peptide was used to monitor UPS activity in protein lysates.

As proteasome function has been reported to be regulated in a cell type specific manner, I decided to investigate the degradation of a proteasomal substrate in different tissues of *C. elegans* (Hamer et al. 2010). For that, *C. elegans* reporters that express UbG76V::Dendra2 either in the body wall muscle tissue (using the *unc-54* promoter), or in the GABAergic neurons (using the *rgef-1* promoter) were employed (Figures 4.2 A+B). Dendra2 is a fluorescent protein that has been used to study the fate of specific proteins, as it can be irreversibly photo-converted from the green to red emission spectrum upon excitation at 405 nm (Chudakov et al. 2007). In the analyzed reporter lines, Dendra2 is fused

to a non-cleavable ubiquitin moiety, UbG76V, which allows the correct poly-ubiquitination and subsequent targeting of the Dendra2 fusion protein for proteasomal degradation (Stack et al. 2000). This sensor is a specific proteasomal substrate and enables the quantification of proteasome activity in the neuronal and muscle tissue of a whole animal or on a single-cell level by monitoring the red fluorescence after photo-conversion (Figure 4.2 B).
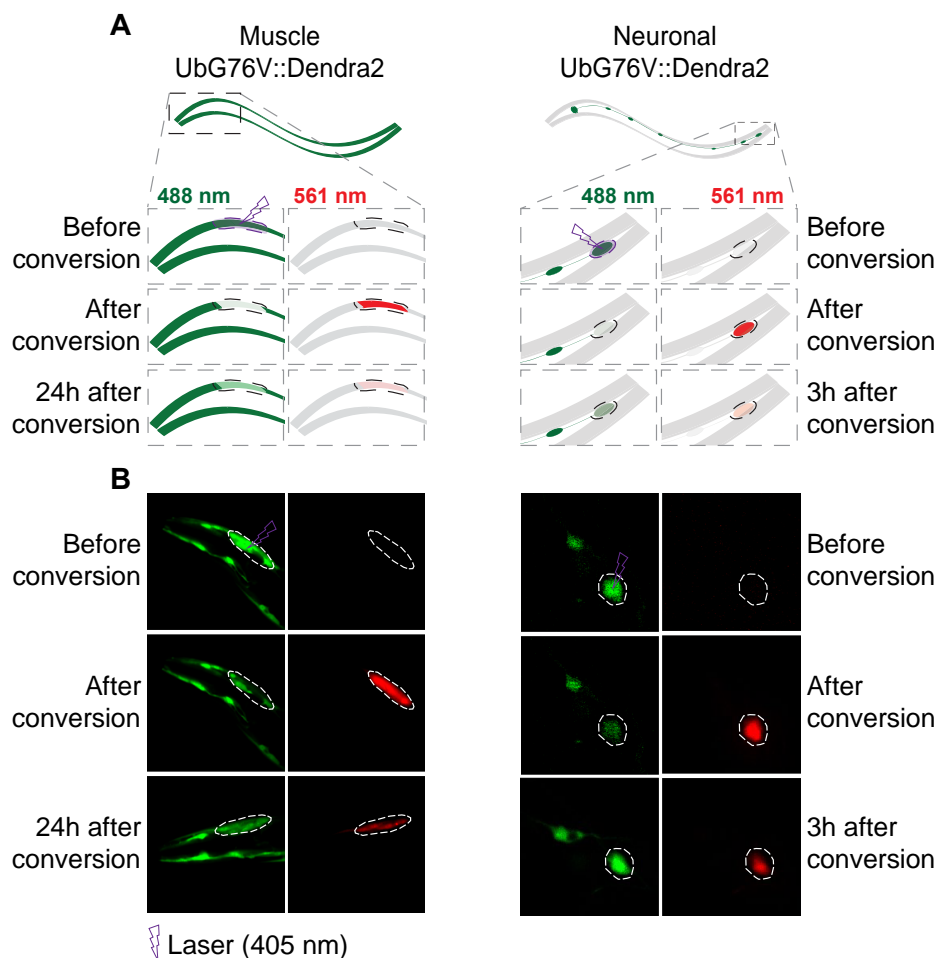
Figure 4. 2 – Photo-conversion of UbG76V::Dendra2 in muscle and neurons.
A) Representative scheme of the photo-conversion of UbG76V::Dendra2 in muscle (right panel) and neuronal cells (left panel) of *C. elegans*. B) Representative fluorescent images of photo-conversion of UbG76V::Dendra2 in single muscle (right panel) and neuronal cells (left panel) of *C. elegans*. UbG76V::Dendra2 protein was converted by exposure to 405 nm and imaged 3 (neurons) or 24 (muscle) hours post-conversion.

UbG76V::Dendra2 was developed to be specifically targeted and degraded by proteasomes. As can been observed in figure 4.3, depletion of an essential 20S proteasome subunit (*pas-5*) leads to reduced turnover of UbG76V::Dendra2, which then accumulates due to the loss of proteasome function (Hamer et al. 2010).
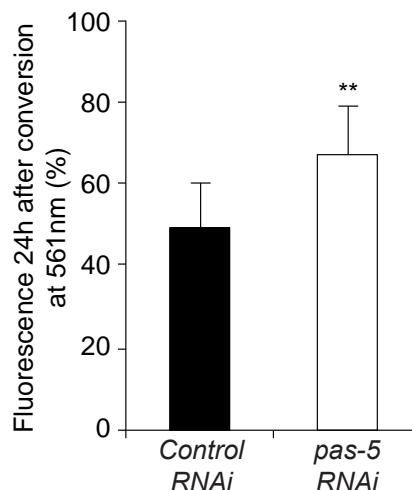
Figure 4. 3 – Degradation rates of UbG76V::Dendra2 upon *pas-5* depletion

Animals expressing UbG76V::Dendra2 in the muscle cells were treated with *pas-5* RNAi for 72 h. UbG76V::Dendra2 protein was converted, and the animals were imaged 24 h post-conversion. To determine the degradation rates, the fluorescence (561 nm) acquired 24 h post-conversion was divided by the fluorescence immediately after conversion. The error bars represent the standard deviation of 5-6 animals.

Next, chaperones from the disaggregase complex were depleted and the degradation rates of UbG76V::Dendra2 were analyzed in muscle and neuronal cells. As shown in figure 4.4 A, a pronounced accumulation of photo-converted UbG76V::Dendra2 was detected upon depletion of *dnj-12* (+27%), *dnj-13* (+17%), and particularly upon *hsp-110* (+45%) when compared to the control condition 24 h after photo-conversion. In neuronal cells the degradation of UbG76V::Dendra2 is much faster, therefore its levels were measured 3 h after photo-conversion. Depletion of *hsp-1* (+18%) and *hsp-110* (+16%) led to a slight accumulation of UbG76V::Dendra2 compared to the control in the neurons (figure 4.4 B).

This data indicates a reduction of proteasome activity in muscle and neuronal cells upon loss of some members of the disaggregase complex, mainly triggered by the depletion of *hsp-110*.
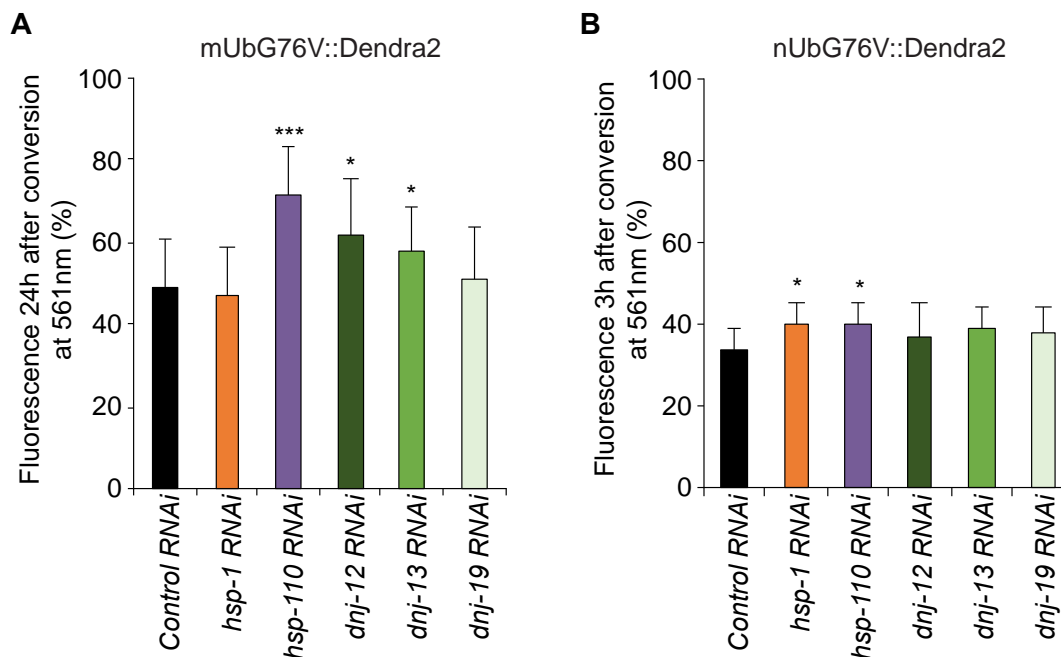
Figure 4. 4 - UbG76V::Dendra2 degradation rates in muscle and neurons upon chaperone knockdown.

A-B) Animals expressing UbG76V::Dendra2 in the muscle (YD3) cells (A) or neuronal cells (YD12) (B) were treated with RNAi against the indicated genes. UbG76V::Dendra2 protein was converted by exposure to 405 nm and imaged 3 (neurons) or 24 (muscle) hours post-conversion. To determine the degradation rates, the fluorescence (at 561 nm) acquired 3 or 24 h after conversion was divided by the fluorescence directly after conversion. The error bars represent the standard deviation of 9-15 animals.

To validate these observations in mammalian cells, a similar experiment in HEK293 cells was carried out, where I analyzed the proteasome function upon loss of disaggregating chaperones. Cells were transfected with a non-cleavable ubiquitin moiety fused to GFP, UbG76V-GFP, (Dantuma et al. 2000) while the orthologous chaperone genes were depleted. As a control, cells were treated with MG-132. MG-132 is a potent and reversible inhibitor of the proteolytic activity of the 26S proteasome complex (Lee et al. 1996). As expected, cells

treated with MG-132 showed an accumulation of the proteasome substrate UbG76V-GFP (Figures 4.5 A+B). An accumulation of UbG76V-GFP was also detected upon *hspa4* siRNA *(hsp-110* ortholog) (2-fold) (Figures 4.5 A+B), thus confirming the data obtained in *C. elegans*. Moreover, a reduction in the degradation rates of UbG76V::GFP upon depletion of *hspa8* (*hsp-1* ortholog) and *dnaja1* (*dnj-12*) was also detected, suggesting that depletion of members of the disaggregase complex exert an inhibitory effect on UPS activity in mammalian cells, too.
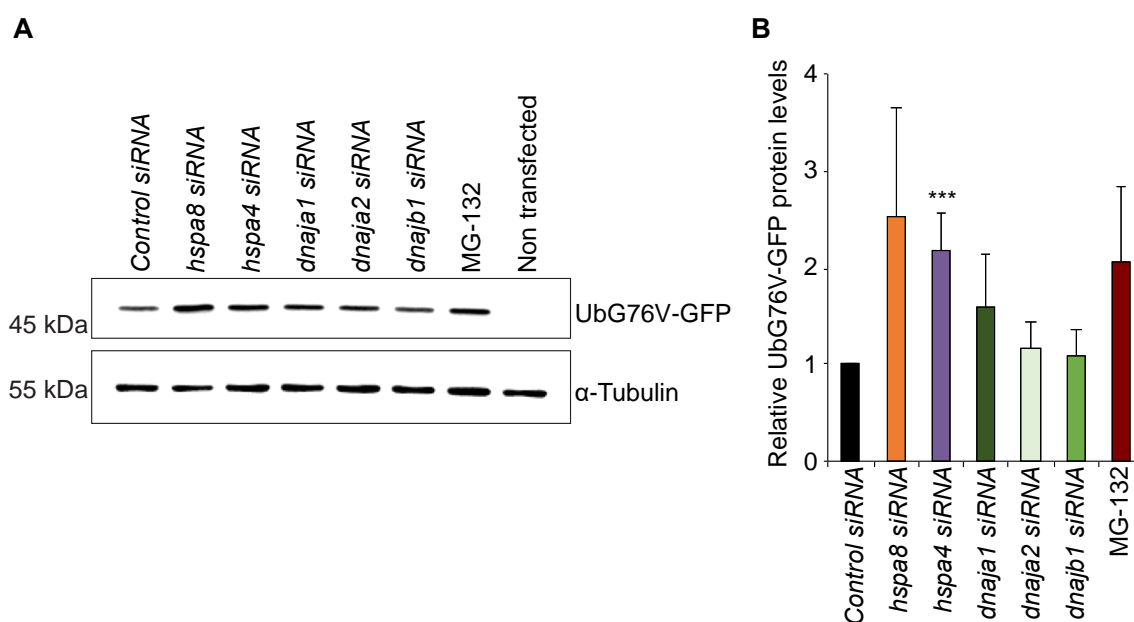
Figure 4. 5 – UbG76V-GFP levels upon chaperone depletion in HEK293 cells.
A) Immunoblotting of lysates of HEK293 cells, which were transfected with the respective chaperone siRNA for 48 h and UbG76V-GFP in the subsequent 24 h. As a positive control, cells were also treated with 20 µM MG-132 for 4 h. The UbG76V-GFP levels were normalized to α-tubulin levels and then to siRNA control (B). The error bars represent the standard deviation of three independent experiments.

To complement and expand the analysis of the proteasome function, the *ex vivo* proteasome activity was monitored in protein lysates of either complete nematodes or HEK293 cells. By taking advantage of a fluorogenic proteasome-specific substrate, Suc-LLVY-AMC, the chymotrypsin-like proteasome activity was accessed (Kisselev et al. 2005, Vilchez et al. 2012). Suc-LLVY-AMC is

recognized and cleaved by the chymotrypsin-like subunit (β5). Upon cleavage, the AMC peptide emits fluorescence that can be monitored. As shown in figures 4.6 A+B, AMC fluorescence increases over time revealing the proteasome activity of wt *C. elegans* protein lysate. The increase of AMC fluorescence is due to proteasome activity as inhibiting the proteasome with MG-132 inhibits Suc-LLVY-AMC cleavage in a concentration-dependent manner.
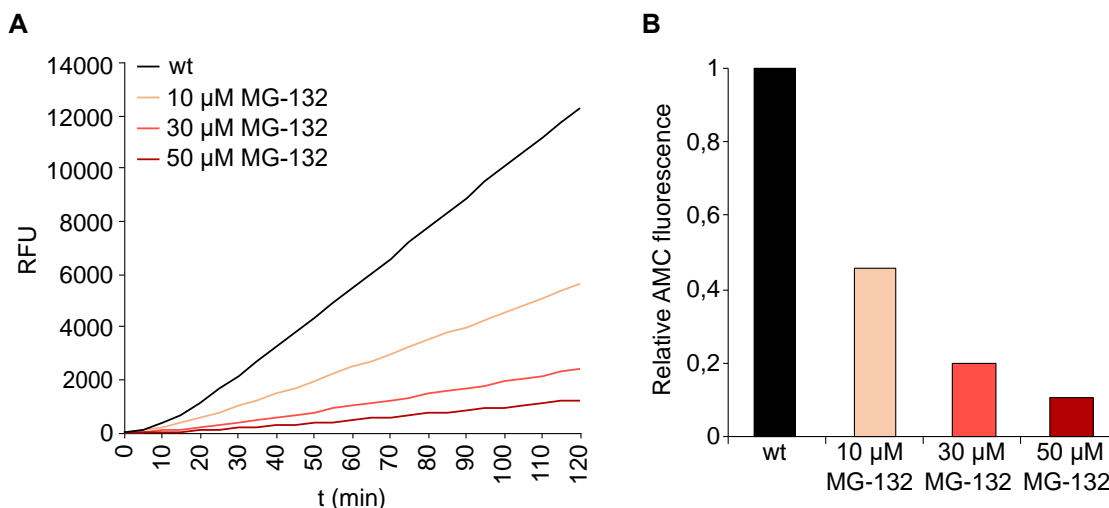
Figure 4. 6 - Suc-LLVY-AMC cleavage by *C. elegans* lysate.
A) Chymotrypsin-like proteasome activity was measured every 5 min of lysates of day 4 wt nematodes. As a control, 10, 30 and 50 µM MG-132 was incubated with the lysates. B) The relative activities were calculated and normalized to the untreated condition.

Subsequently, chaperones from the disaggregase complex were depleted, and the AMC release was monitored in the lysate of *C. elegans* and HEK293 cells. As depicted in figures 4.7 A+B, animals treated with *hsp-110*, *dnj-12* and *dnj-13* RNAi display a reduction of 20-30% of AMC release over time compared to the control indicating a reduction of proteasome capacity. In HEK293 cells, a diminished chymotrypsin-like proteasome activity could also be observed upon *hspa4*, *dnaja1*, *dnaja2* and *dnajb1* siRNA compared to control condition (Figures 4.7 C+D). These observations corroborate the UbG76V data, especially for *hsp-110/hspa4* depletion that led to a strong decrease of UbG76V degradation in *C. elegans* and HEK293 cells (Figures 4.4 + 4.5).
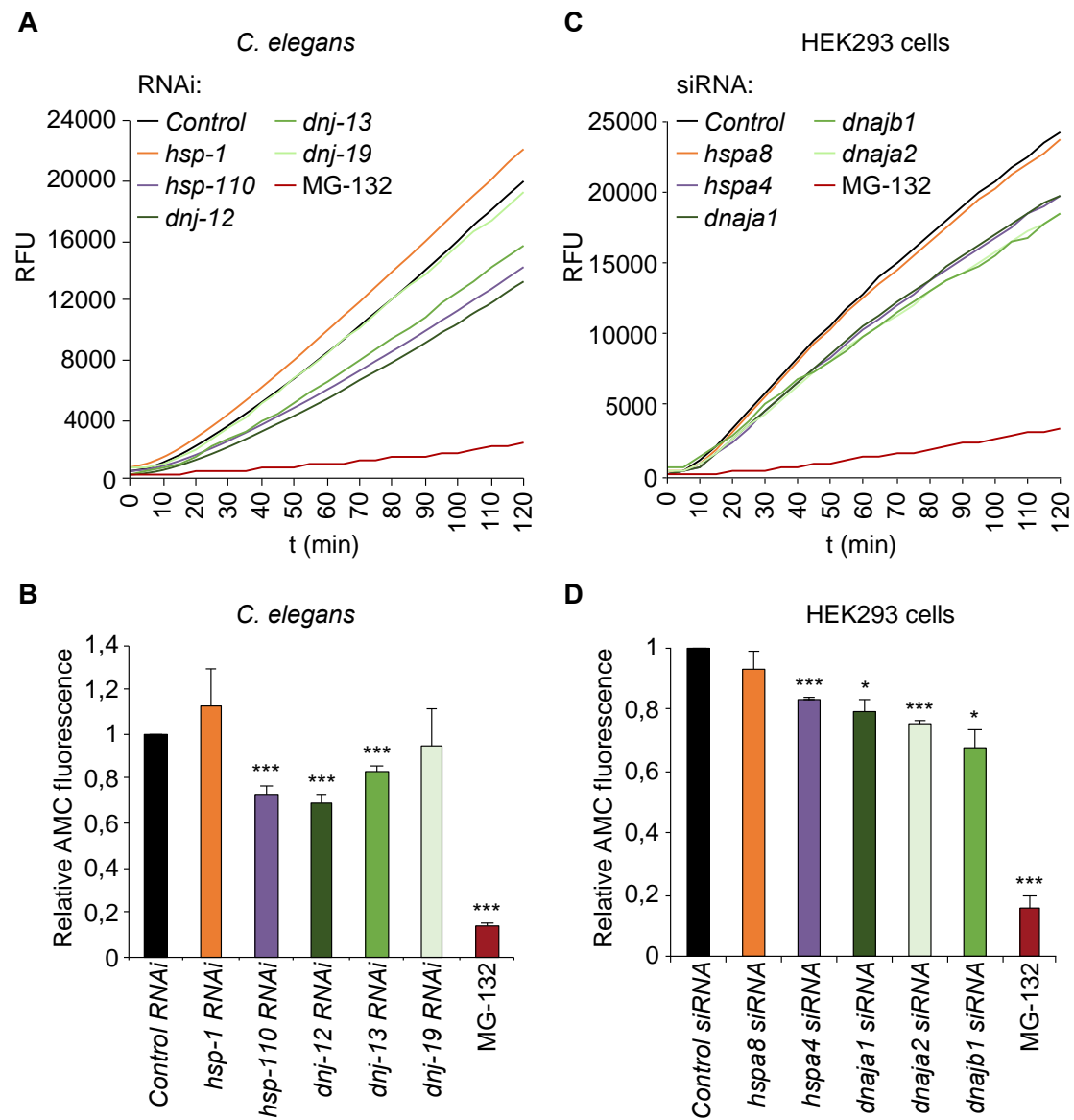
Figure 4. 7 - Proteasome activity of *C. elegans* and HEK293 cells upon chaperone depletion.

A) Chymotrypsin-like proteasome activity was measured every 5 min in lysates of wt nematodes treated with the indicated RNAi for 4 days. The relative activities were calculated and normalized to RNAi control (B). The error bars represent the standard deviation of three independent experiments. C) Chymotrypsin-like proteasome activity was measured every 5 min in lysates of HEK293 cells treated with the indicated siRNA for 48 h. The relative activities were calculated and normalized to RNAi control (D). The error bars represent the standard deviation of three independent experiments.

A decrease in the UPS capacities upon chaperone depletion could be either due to decreased activities or reduced abundance of the proteasome. An analysis of the 20S α-subunit levels would allow differentiating between reduced proteasome activity and lower abundance of the proteasomes. Interestingly, depletion of *hsp-110*, *dnj-12* and *dnj-13* in *C. elegans* (Figures 4.8 A+B)*,* and *hspa4*, *dnaja2* and *dnajb1* in HEK293 led to lower levels of 20S α-subunits compared to the control condition (Figures 4.8 C+D). The reduction of the 20S α-subunit levels correlate with proteasome activity described above and could explain or at least contribute to a decreased proteasome capacity upon chaperone depletion.
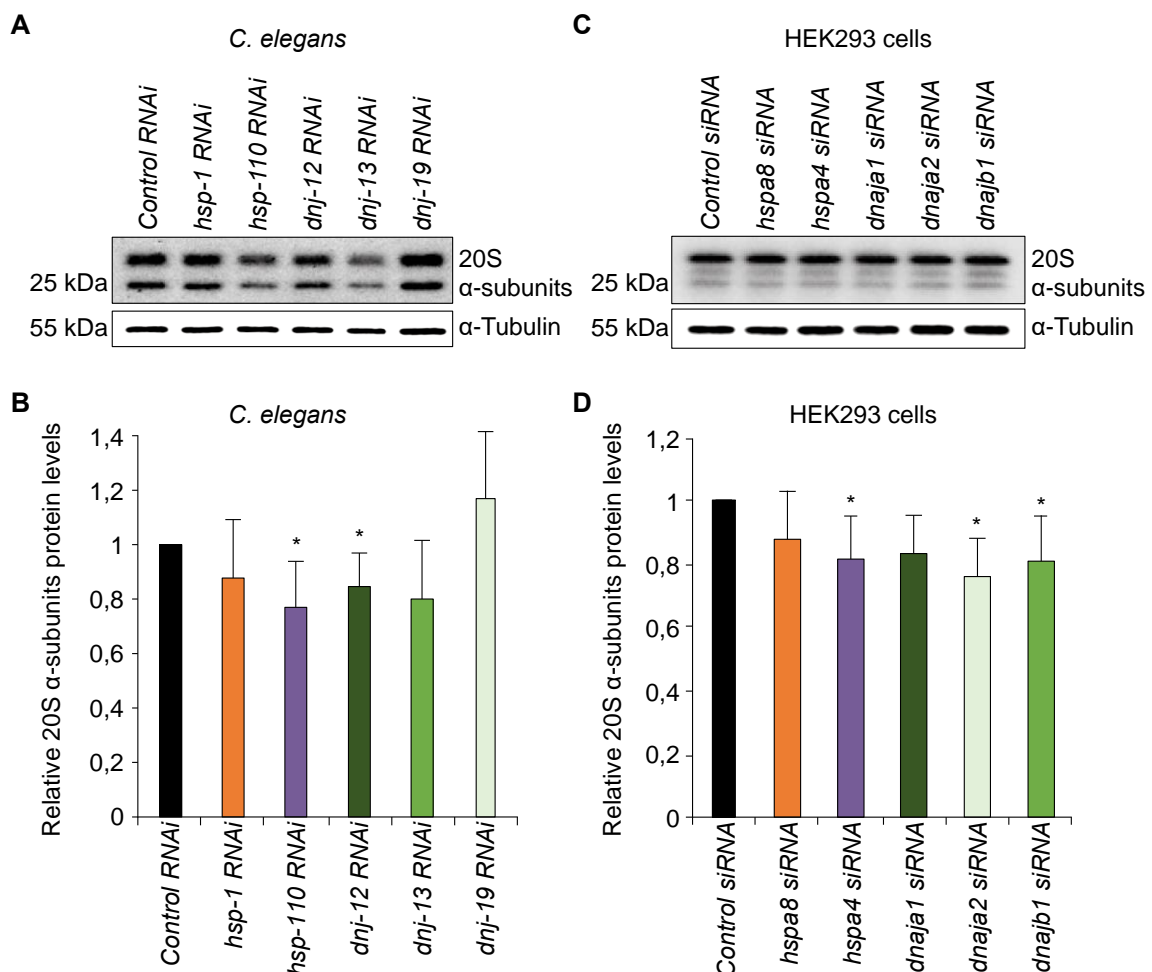
Figure 4. 8 - 20S α-subunits upon chaperone knockdown in *C. elegans* and HEK293 cells.

A) Relative protein levels of 20S α-subunits of wt animals treated with RNAi against chaperone genes. The 20S levels were normalized to α-tubulin levels and then to

control RNAi (B). The error bars represent the standard deviation of three independent experiments. C) Relative protein levels of 20S α-subunits of HEK293 cells treated with siRNA against the indicated genes. The 20S levels were normalized to α-tubulin levels and then to control siRNA (D). The error bars represent the standard deviation of a minimum of six independent experiments.

4.3.2 Proteasome function is altered in older animals

In order to assess how the proteasome capacity is affected with the progression of aging, I analyzed first the 20S α-subunit protein levels of nematodes at day 4, 6, 8 and 10 of life (Figures 4.9 A+B). A strong increase (+63%) in the 20S α-subunit levels can be observed in old animals (day 10) when compared to young animals (day 4). To assess if the increase in 20S levels correlates with increased activity, I analyzed the chymotrypsin-like proteasome activity in young versus old animals and did not observe a significant difference (Figure 4.9 C). This prompted me to study the UPS capacity in different tissues as differences between cell types might be masked when analyzing the lysate of the whole animal. Thus, I analyzed degradation rates of UbG76V::Dendra2 in muscle and neuronal tissue of day 4 and day 7 old nematodes. While muscle cells displayed lower levels of converted UbG76V::Dendra2 at day 7 compared to day 4 (36% vs. 49%), neuronal cells exhibited higher UbG76V::Dendra2 in old animals (48% vs. 34%) (Figure 4.9 D). This data suggests an increase of proteasome activity with the progression of aging in muscle cells, yet a reduction of UPS activity in neurons, as previously reported (Hamer et al. 2010).
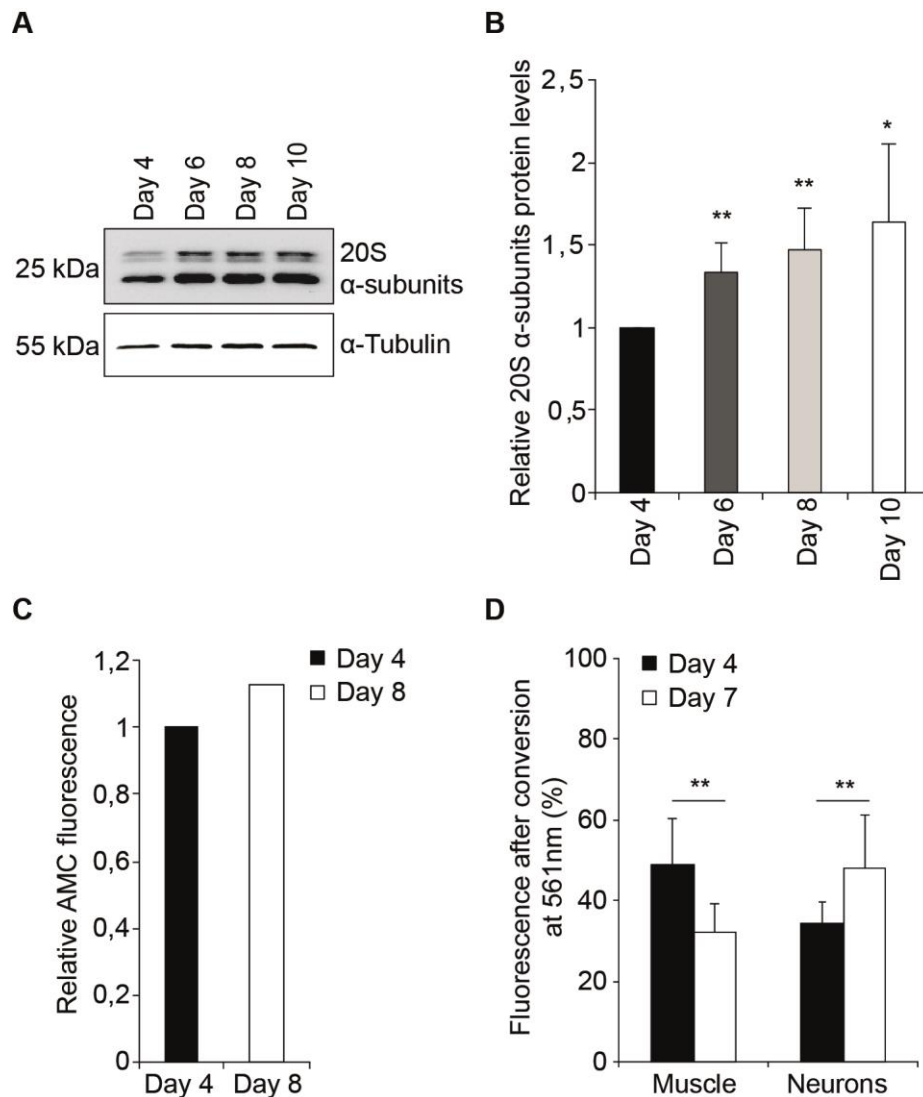
Figure 4. 9 - Proteasome function with the progression of aging.

A) 20S α-subunit levels were determined in nematodes of 4, 6, 8 and 10 days of life. The 20S levels were normalized to α-tubulin levels and then to day 4 animals (B). The error bars represent the standard deviation of five independent experiments. C) Chymotrypsin-like proteasome activity was measured in day 4 or 8 old wt nematodes. The relative activities were calculated and normalized to day 4. D) The degradation rates of UbG76V::Dendra2 animals were measured at day 4 and day 7 of age in muscle cells and neuronal cells. UbG76V::Dendra2 protein was converted, and the animals were imaged 3 or 24 h after conversion (as in Fig. 4.2). To determine the degradation rates, the fluorescence (561 nm) acquired 3 or 24 h after conversion was divided by the fluorescence immediately after conversion. The error bars represent the standard deviation of 6-16 animals.

To assess how chaperone depletion affects the UPS capacity with the progression of aging, I quantified the 20S α-subunit protein levels upon chaperone depletion between days 4 and 10 (Figure 4.10 A). As shown above (section 4.3.1), 20S α-subunits are reduced in young animals when chaperones are depleted. However, in old animals, 20S α-subunits are no longer decreased and are now more abundant compared to control when *hsp-110*, *dnj-12*, *dnj-13,* and *dnj-19* are depleted (days 8 and 10). Taking into account these changes in the 20S α-subunits levels, I decided to monitor proteasome activity in older animals. As described in the section 4.3.1, the UPS activity is reduced upon *hsp-110*, *dnj-12* and *dnj-13* RNAi at day 4. Yet, old animals show no significant difference to the control in the degradation rates of UbG76V::Dendra2 (muscle and neurons) or the cleavage of Suc-LLVY-AMC (Figures 4.10 B+C+D). Together, this data shows that aging alters proteasomal levels and activity in a tissue-specific manner. In addition, depletion of chaperones does not affect proteasome levels and activity of aged nematodes.
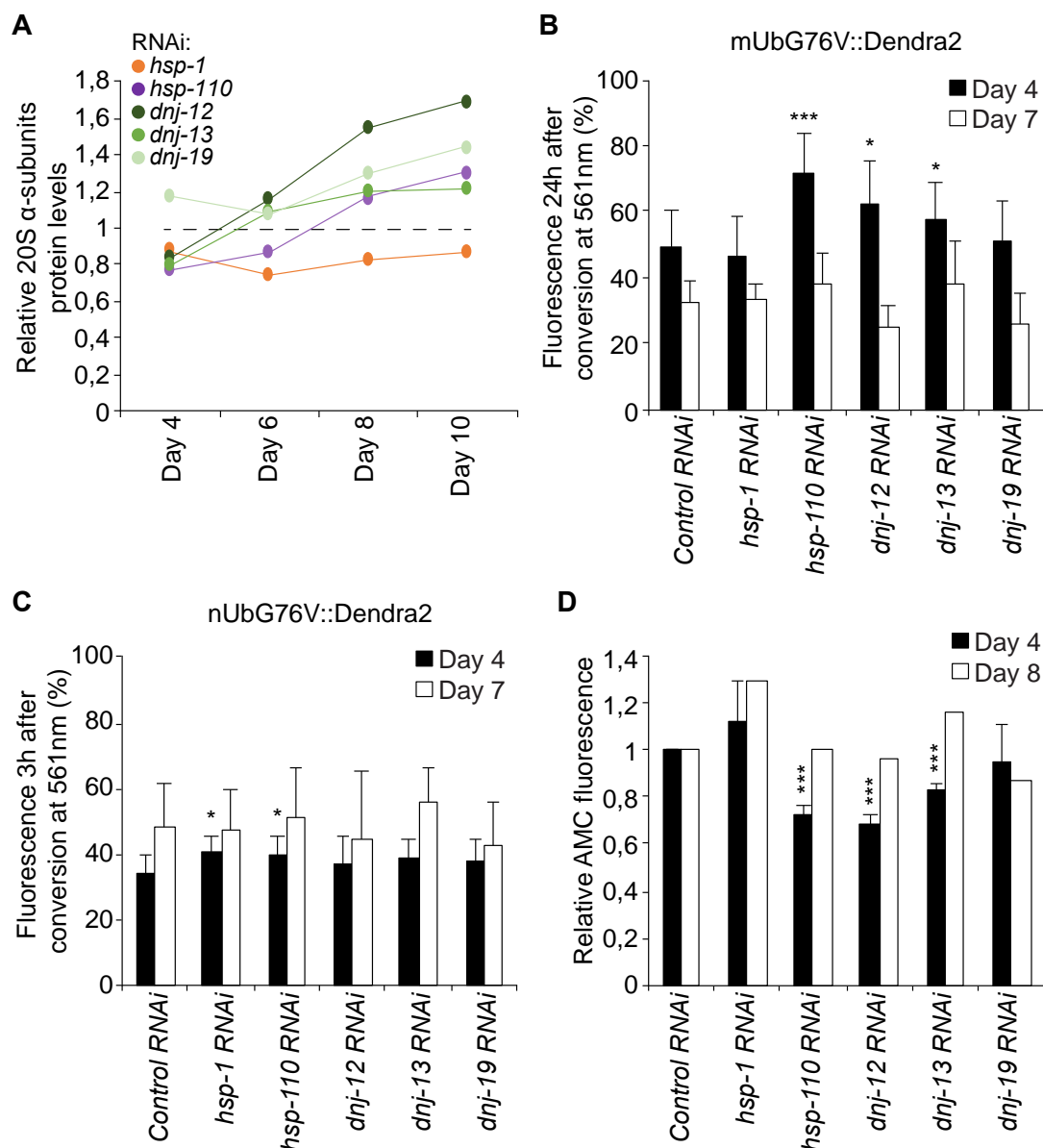
Figure 4. 10 - Proteasome levels and activity after chaperone depletion.

A) The levels of 20S α-subunits were measured at day 4, 6, 8 and 10 of wt animals treated with RNAi against the indicated chaperones. The 20S α-subunit levels were normalized to α-tubulin levels and then to RNAi control. Depicted is a graph representing the average values from a minimum of three independent experiments (error bars were excluded for clarity). B-C) The degradation rates of UbG76V::Dendra2 animals were measured at day 4 and day 7 of age in muscle cells (B) or neuronal cells (C). UbG76V::Dendra2 protein was converted, and the animals were imaged 3 or 24 h after conversion. To determine the degradation rates, the fluorescence (561 nm) acquired 3 or 24 h after conversion was divided by the fluorescence immediately after conversion. The error bars represent the standard deviation of 6-16 animals. D) Chymotrypsin-like proteasome activity was measured every 5 min of lysates of wt

nematodes treated with the indicated RNAi for 4 or 8 days. The relative activities were calculated and normalized to RNAi control in the respective day.

4.4 Proteolytic pathways response to *hsp-16.41* and *hsp-17* depletion

4.4.1 *Autophagy and proteasome pathways are not affected by the loss of two small heat shock proteins*

In the sections described above, the impact of the depletion of chaperones from the disaggregation complex in the proteolytic pathways was demonstrated. To further validate the correlation between the loss of disaggregation capacity with the autophagy and proteasome responses, and eliminate the possibility that our observations are due to a general chaperone effect, I analyzed both proteolytic pathways upon depletion of two additional chaperones. It was important to carefully select chaperones that do not display pleiotropic roles in cellular signaling pathways such as Hsp90. In addition, the selected chaperones should not be members of the Hsp70, Hsp110 or J-protein families. For that reason, I chose two small heat shock proteins, *hsp-16.41* and *hsp-17* that do not exhibit any disaggregation activity (data from Kirstein lab).

As shown in figure 5.1, the depletion of *hsp-16.41* or *hsp-17* has no impact either on autophagy (LGG-1 and SQST-1 protein levels) or proteasome pathways (20S α-subunits levels and Suc-LLVY-AMC cleavage). This data indicates that the clearance machinery responds specifically to a loss in the capacity of chaperone-mediated disaggregation.
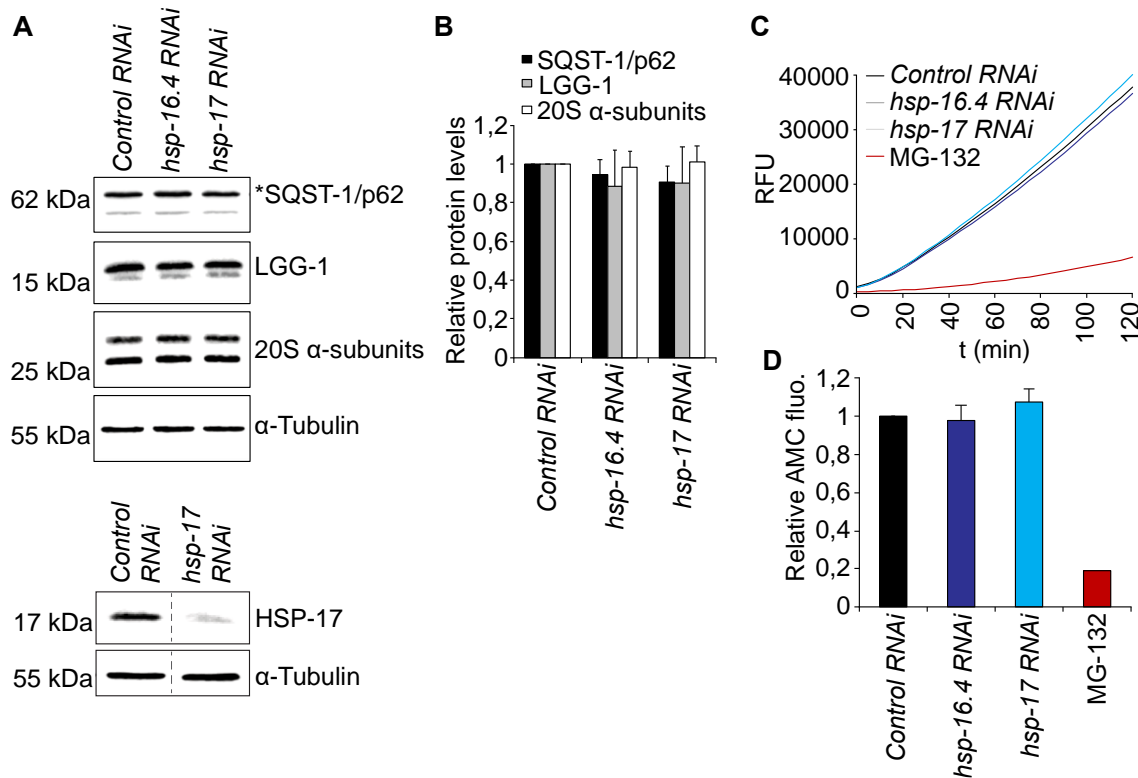
Figure 5. 1 - Proteolytic pathways are not affected by a depletion of *hsp-16.41* and *hsp-17*.

A) LGG-1, SQST-1/p62, 20S and HSP-17 protein levels of nematodes treated with the indicated RNAi for 4 days. B) LGG-1, SQST-1/p62, and 20S levels were normalized to RNAi control. The error bars represent the standard deviation from five independent experiments. C-D) Chymotrypsin-like proteasome activity of nematodes treated with the indicated RNAi for 4 days. The relative activities were calculated and normalized to RNAi control (D). The error bars represent the standard deviation of two independent experiments.

4.5   Autophagy and proteasome response to protein misfolding

4.5.1   Depletion of chaperones promotes cytosolic protein misfolding which triggers the induction of autophagy and proteasome impairment

To better understand how the loss of HSP110/70/J affects the cellular folding capacity and the crosstalk with the proteolytic pathways, I employed a well-established protein-folding sensor. The sensor is a GFP-tagged destabilized

luciferase variant, FlucDM-GFP expressed in HEK293 cells (Gupta et al. 2011, Park et al. 2013, Raychaudhuri et al. 2014). FlucDM contains two point mutations (R188Q, R261Q) that lead to rapid misfolding and aggregation in response to proteostasis perturbations. The enzymatic activity of luciferase can be assessed in the form of released light upon conversion of luciferin to oxyluciferin (Thorne et al. 2010).

To monitor FlucDM-GFP misfolding and aggregation in real-time, I designed a live-cell imaging experiment where cells were imaged using a confocal microscope. As seen in figure 6.1 A, when cells were treated with MG-132, a strong increase of FlucDM aggregates is detectable after 6 h. The enzymatic activity of luciferase was monitored in parallel in the intact cells (Gupta et al. 2011). The luciferase aggregation resulting from MG-132 treatment corresponded to a decrease of 45% of luciferase activity compared to control (Figure 6.1 B).
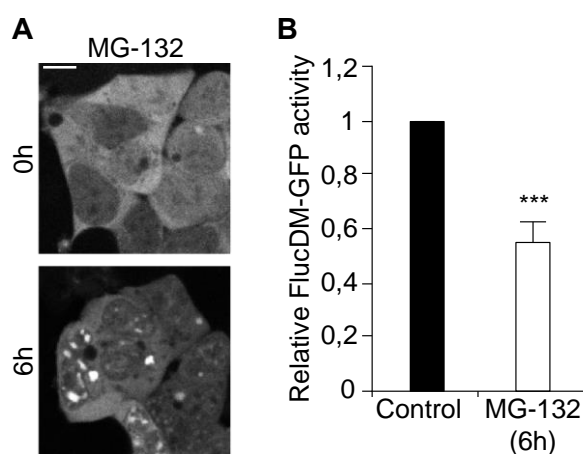
Figure 6. 1 - FlucDM-GFP aggregation and activity upon proteasome inhibition.
A) HEK293 cells expressing FlucDM-GFP were treated with 20 µM MG-132. The depicted images were acquired at 0 and 6 h after treatment. Scale bars: 10 µm. B) The FlucDM-GFP activity was measured in cells treated with 20 µM MG-132 for 6 h. The error bars represent the standard deviation of three independent experiments.

Taking advantage of this reporter line, I aimed to determine the time-point by which luciferase starts to aggregate (and loses its activity) in response to chaperone depletion, and then correlate it to the induction of autophagy and inhibition of proteasome activity. To address this question, cells were treated

with siRNA against HSP110/70/J complex members and imaged for 48 h. The formation of the first foci representing aggregated FlucDM-GFP in response to chaperone depletion was detected 24 h post siRNA transfection (Figures 6.2 A+B). At 48 h of siRNA treatment, the chaperone knockdown conditions displayed visible accumulation of aggregated luciferase, particularly upon depletion of *hspa8*, *dnaja2*, and *dnajb1*. In parallel, the enzymatic activity of the luciferase was monitored. The luciferase activity measured at different time-points after chaperone depletion confirmed that the misfolding and subsequent loss of activity of luciferase occurs 24 h after siRNA transfection and at the 48 h time-point all chaperone siRNA conditions exhibit a prominent reduction (25-45%) of luciferase activity (Figure 4D).
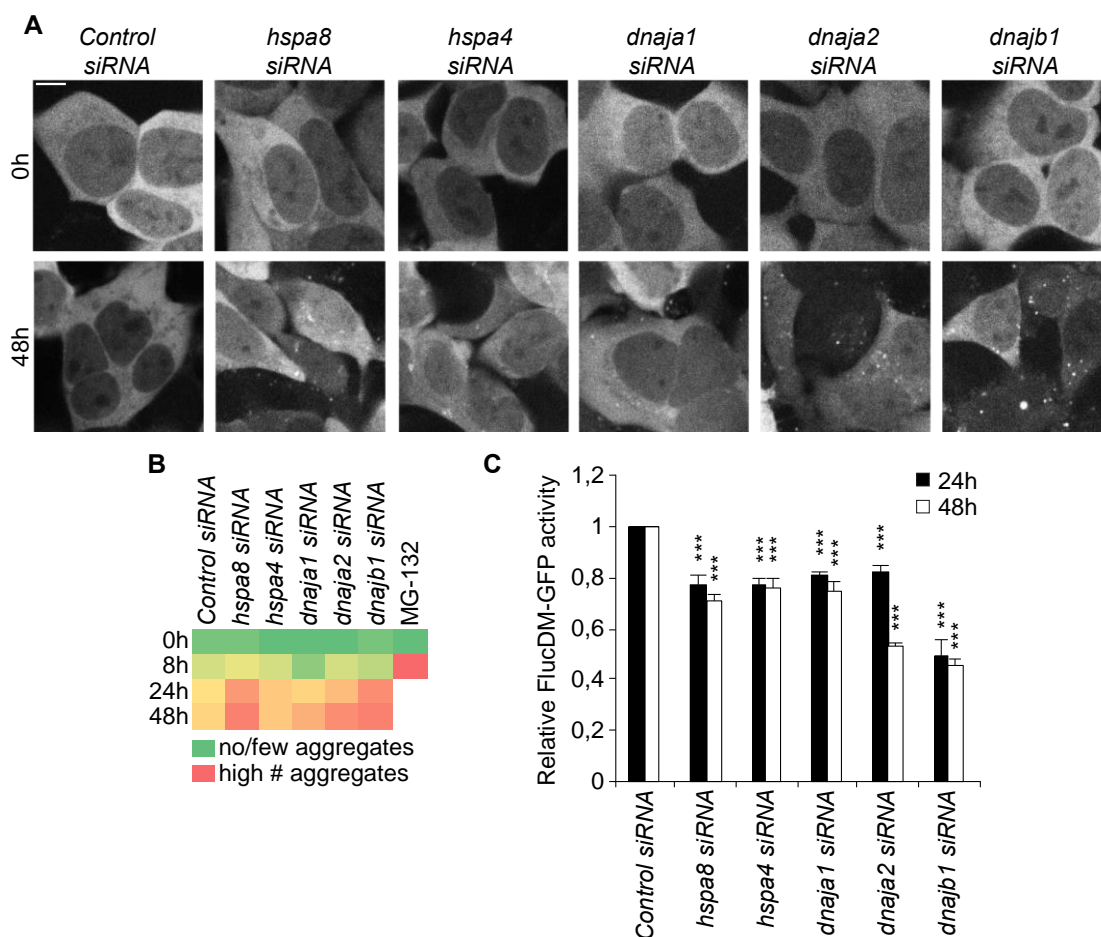
Figure 6. 2 - FlucDM-GFP aggregation and activity upon chaperone depletion.
A) HEK293 cells expressing FlucDM-GFP were treated with siRNA against the indicated genes and subjected to live-cell imaging (A). The images shown were acquired at 0 and 48 h after transfection. Scale bars: 10 µm. B) Aggregation analysis of

the images acquired at 0, 8, 24 and 48 h of the live FlucDM-GFP cell imaging experiment (A). The green color represents no or a low number of cells with aggregates, whereas the red color indicates a high number of cells with aggregates. C) The FlucDM-GFP activity was measured 24 and 48 h after siRNA transfection. The luciferase activity of the chaperone knockdown conditions was normalized to the control siRNA luminescence of the respective time-point. The error bars represent the standard deviation of three independent experiments.

This data prompted me to question if the protein clearance mechanisms were already affected when the cells were treated with siRNA for 24 h (previous experiments were performed 48 h after siRNA). Therefore, autophagy and proteasome pathways were additionally assessed at 24 h post siRNA treatment. First, the LC3-II autophagy marker was analyzed upon chaperone knockdown. As depicted in figure 6.3 A, LC3-II levels are slightly increased at 24 h post transfection but exhibit the highest level at 48 h siRNA time-point.

Second, to assess UPS capacity, I analyzed UbG76V levels and chymotrypsin-like proteasome activity upon siRNA treatment for 24 and 48 h. The accumulation of UbG76V-GFP, in particular upon *hspa4* depletion, is only detected after 48 h of siRNA treatment (Figure 6.3 B). Despite this, a reduction in chymotrypsin-like proteasome activity can already be detected at the 24 h time-point in *hspa4* and *dnajb1* siRNA conditions (Figure 6.3 C). This data indicates that the UPS activity is already compromised 24 h post siRNA transfection, yet the accumulation of UPS substrates becomes prominent only 48 h after depletion of the chaperones.

In sum, these results suggest that depletion of chaperones leads to an accumulation of protein aggregates, which triggers the induction of autophagy and simultaneously leads to a reduction of proteasome capacity.
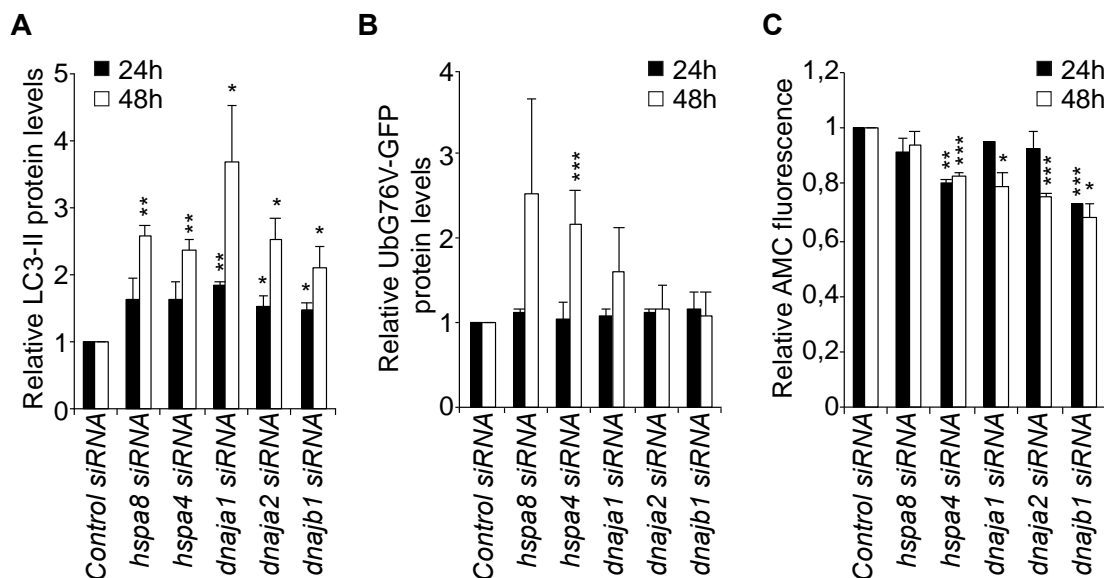
Figure 6. 3 - Analysis of the autophagy and UPS capacity in HEK293 cells treated with HSP110/70/J siRNA for 24 and 48 h.

A) LC3-II levels from lysates of HEK293 cells, which were transfected with the respective chaperone siRNA for 24 and 48 h. The LC3-II levels were normalized to α-tubulin levels and then to siRNA control. The error bars represent the standard deviation of two independent experiments. B) UbG76V-GFP levels from lysates of HEK293 cells, which were transfected with the respective chaperone siRNA and UbG76V-GFP for 24 and 48 h (data shown in figure 4.5). The UbG76V-GFP levels were normalized to α-tubulin levels and then to siRNA control. The error bars represent the standard deviation of a minimum of two independent experiments. C) Chymotrypsin-like proteasome activity of lysates of HEK293 cells treated with the indicated siRNA for 24 and 48 h (data shown in figure 4.7). The relative activities were calculated and normalized to siRNA control. The error bars represent the standard deviation of a minimum of two independent experiments.

4.6 Alzheimer and Huntington's disease models exhibit compromised proteolytic pathways

4.6.1 Aβ and PolyQ$_{40}$ C. elegans models display autophagy impairment

Aggregation and accumulation of toxic protein aggregates are a hallmark of neurodegenerative disorders (Ross et al. 2004). It is known that the presence of such toxic proteins destabilizes cellular and organismal proteostasis (Hipp et al.

2014). Yet, little is known on how these protein aggregates affect the concerted action of protein clearance pathways.

To understand how autophagy pathway is affected by disease-associated protein aggregates, animals expressing Aβ (CL2006 [Aβ$_{3\text{-}42}$]) or polyglutamine (AM1066 [Q$_{40}$::RFP]) in the body wall muscle tissue were crossed with animals expressing the autophagy reporter GFP::LGG-1. As shown in figure 7.1 A, the expression of Aβ$_{3\text{-}42}$ and Q$_{40}$ led to a prominent accumulation of GFP::LGG-1 not just in muscle tissue, but also in the head region. The levels of GFP::LGG-1 were also determined by western blot and confirmed that Aβ$_{3\text{-}42}$ (3-fold) and Q$_{40}$ (2-fold) expressing animals have elevated GFP::LGG-1 protein levels compared to control (Figures 7.1 B+C).
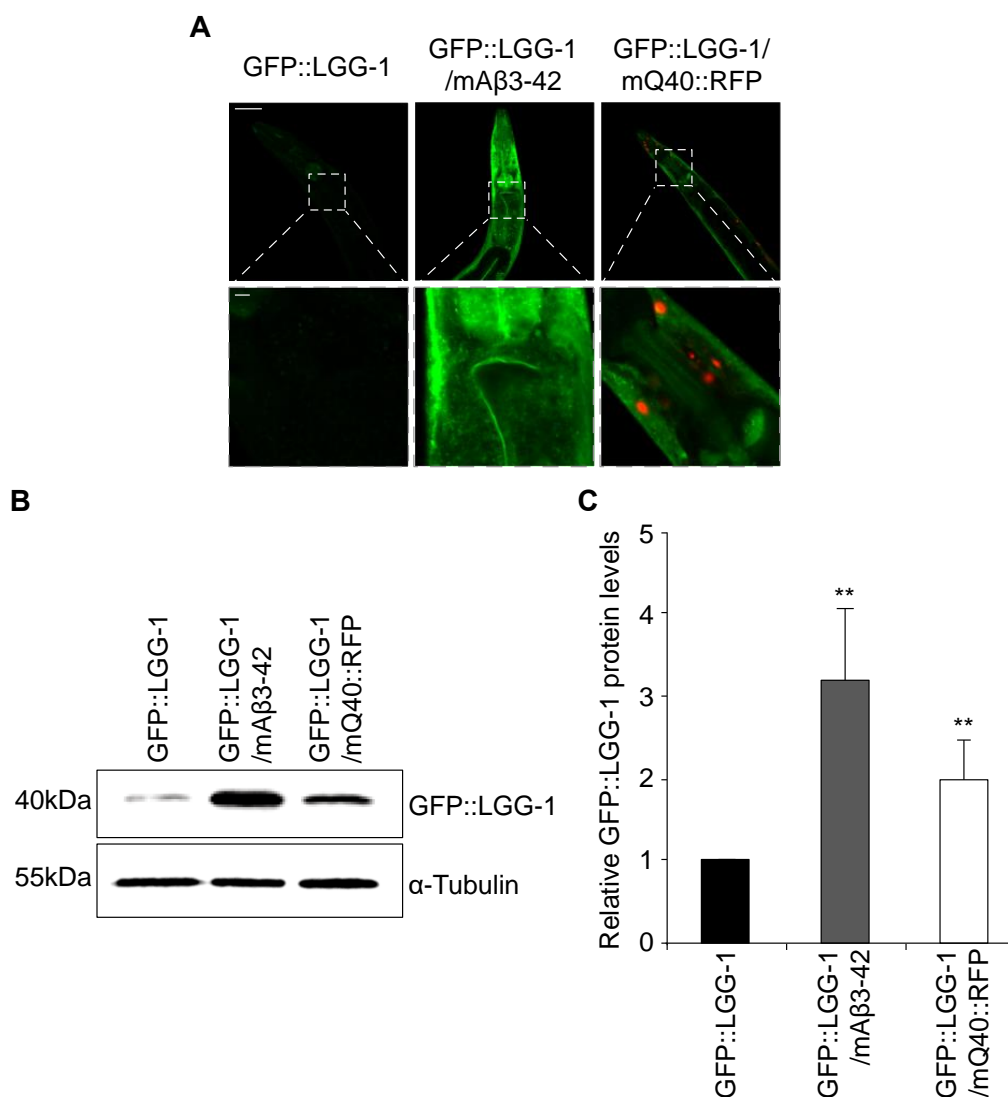
Figure 7. 1 - GFP::LGG-1 levels in neurodegenerative disease *C. elegans* models

A) Fluorescent images of DA2123 (GFP::LGG-1), DA2123/CL2006 (GFP::LGG-1; mAβ_{3-42}) and DA2123/AM1066 (GFP::LGG-1; mQ$_{40}$::RFP) animals at day 5 of life. The lower panel is a magnification of the head region. Scale bars: 50 μm (upper panel) and 5 μm (lower panel). B-C) GFP::LGG-1 levels of DA2123, DA2123/CL2006 and DA2123/AM1066 animals at day 5. The relative band intensities of GFP::LGG-1 were normalized to the α-tubulin levels and then to DA2123 (C). The error bars represent the standard deviation of four independent experiments.

Neurodegenerative diseases are generally late age of onset diseases (Morimoto et al. 2014). Thus, I decided to investigate the autophagic flux in young and old Aβ_{3-42}/Q$_{40}$ animals. As depicted in figure 7.2 A, both young and aged Aβ_{3-42}/Q$_{40}$ expressing nematodes display increased GFP::LGG-1 fluorescence compared to wt animals, yet day 10 Aβ_{3-42}/Q$_{40}$ animals have similar GFP::LGG-1 signal when compared to day 4. Subsequently, the SQST-1/p62 and LGG-1 protein levels were monitored in animals expressing Aβ and Q$_{40}$ in the body-wall muscle cells (CL2006 [Aβ_{3-42}] and AM141 [Q$_{40}$::YFP]), and in neuronal cells (CL2355 [Aβ_{1-42}] and AM101 [Q$_{40}$::YFP]). As shown in figure 7.2 B+C, all disease proteins led to a strong increase of LGG-1 and a slight increase of SQST-1/p62 in young adults, indicating that autophagy is impaired in those animals. As aging progresses, the impact of the disease proteins becomes less pronounced, and the LGG-1 and SQST-1/p62 levels are not or only moderately elevated in the Aβ and Q$_{40}$-expressing animals compared to wt animals. This is supported by the fact that old animals exhibit an already impaired autophagic system, resulting in increased LGG-1 and SQST-1/p62 levels (Figure 3.7). To substantiate the data set, I examined also the lysosome pool. Indeed, young animals expressing Aβ/Q$_{40}$ either in muscle or neurons exhibit a prominent accumulation of the lysosome pool when compared to the wt (Figure 7.2 D). Taken together, this data demonstrates that autophagy is compromised in young Aβ and Q$_{40}$ animals.
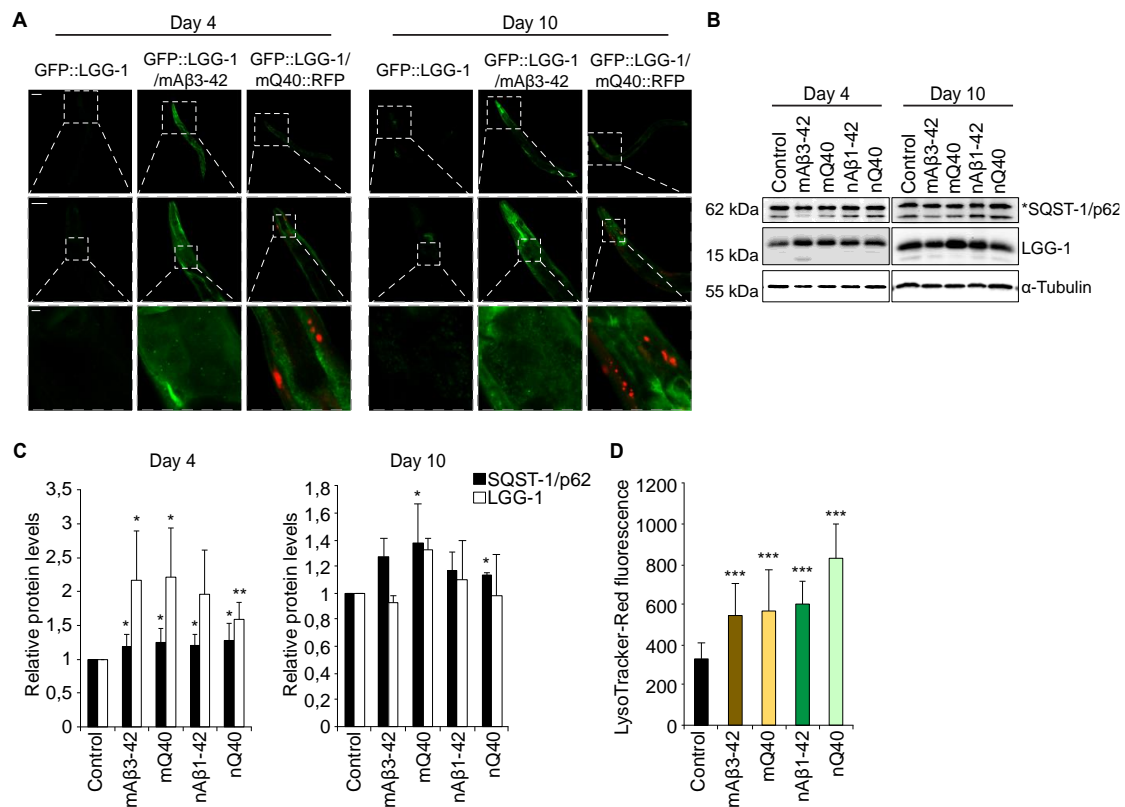
Figure 7. 2 - Autophagic flux analysis in neurodegenerative disease *C. elegans* models during aging.

A) Fluorescent images of DA2123 (GFP::LGG-1), DA2123/CL2006 (GFP::LGG-1; mAβ$_{3-42}$) and DA2123/AM1066 (GFP::LGG-1;mQ$_{40}$::RFP) animals were acquired at day 4 (left panel) and day 10 (right panel) of age. The upper, middle and lower panels show the whole animal, the head and a magnification of the head region, respectively. Scale bars: 20 µm (upper panel), 50 µm (middle panel) and 5 µm (lower panel). B-C) LGG-1 and SQST-1/p62 levels were determined in control, CL2006 (mAβ$_{3-42}$), CL2355 (nAβ$_{1-42}$), AM141 (mQ$_{40}$::YFP) and AM101 (nQ$_{40}$::YFP) nematodes of 4 and 10 days of age. The LGG-1 and SQST-1/p62 levels were normalized to α-tubulin levels and then to DA2123 (GFP::LGG-1) (C). The error bars represent the standard deviation of a minimum of three independent experiments. D) The lysosomal pool of control, CL2006 (mAβ$_{3-42}$), CL2355 (nAβ$_{1-42}$), AM141 (mQ$_{40}$::YFP) and AM101 (nQ$_{40}$::YFP) animals at day 4 was stained with LysoTracker-Red and then imaged using a fluorescent microscope. LysoTracker-Red fluorescence was quantified and normalized to control animals. The error bars represent the standard deviation of 12-20 animals.

4.6.2 Aβ models display proteasome impairment across tissues

My observations that the autophagic flux is compromised in neurodegenerative disease models, posed the question whether the proteasome system would also be affected by the presence of toxic disease-associated protein aggregates. To address this question, the chymotrypsin-like proteasome activity (described in section 4.3) was monitored in animals expressing Aβ in muscle and neurons. As depicted in figure 7.3 A+B, nematodes expressing Aβ$_{3-42}$ either in muscle cells or Aβ$_{1-42}$ in neuronal cells exhibited reduced chymotrypsin-like proteasome activity (-40% and -48%, respectively). The 20S α-subunit protein levels were also analyzed, and a reduction of 20S α-subunits in the Aβ-expressing animals was detected (Figures 7.3 C+D). The reduction in the 20S α-subunits protein levels likely causes or at least contributes to the reduction of proteasome activity.

Figure 7. 3 - *Ex vivo* **proteasome function in Aβ expressing animals.**

A-B) Chymotrypsin-like proteasome activity was measured every 5 min from lysates of control, CL2355 (nAβ$_{1-42}$) and CL2006 (mAβ$_{3-42}$) day 4 old animals. The relative activities were calculated and normalized to control (B). The error bars represent the standard deviation of three independent experiments. C-D) 20S α-subunit levels were determined in control, CL2355 (nAβ$_{1-42}$) and CL2006 (mAβ$_{3-42}$) day 4 old animals. The 20S levels were normalized to α-tubulin levels and then to control (D). The error bars represent the standard deviation of three independent experiments.

As the chymotrypsin-like proteasome activity reflects the *ex vivo* activity on an organismal level, I decided to analyze the *in vivo* proteasome activity in distinct tissues. Animals expressing Aβ were crossed with the *in vivo* neuronal and muscle proteasome-sensor UbG76V::Dendra2 (Figure 7.4 A). Both, the muscle and neuronal model, express Aβ without a fluorescence tag, which enables an accurate Dendra2 quantification. As presented in figure 7.4 B+C, animals expressing Aβ$_{3-42}$ in the muscle tissue displayed reduced degradation rates of UbG76V::Dendra2 in muscle (-30%) and neurons (-45%) compared to control. Analogously, Aβ$_{1-42}$ expressed in neurons also led to a diminished proteasome activity in muscle (-25%) and neuronal cells (-48%). This data shows that Aβ expression exerts a cross-tissue effect, which leads to defective proteasome function within the same and even across tissues.
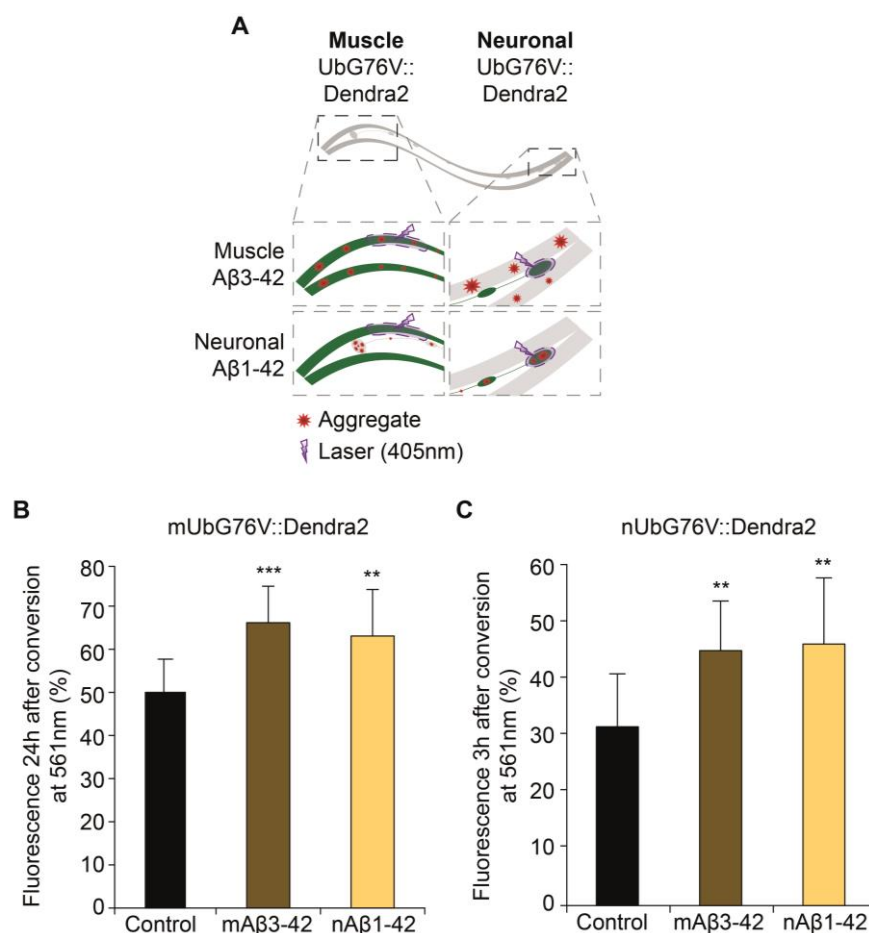
Figure 7. 4 - *In vivo* proteasome function in Aβ expressing animals.

A) The UbG76V::Dendra2 degradation rates were measured in YD3 (mUbG76V::Dendra2), YD3/CL2006 (mUbG76V::Dendra2; mAβ$_{3-42}$), YD3/CL2355 (mUbG76V::Dendra2; nAβ$_{1-42}$), YD12 (nUbG76V::Dendra2), YD12/CL2006 (nUbG76V::Dendra2; mAβ$_{3-42}$), YD12/CL2355 (nUbG76V::Dendra2; nAβ$_{1-42}$) animals. B-C) UbG76V::Dendra2 protein was converted upon exposure to 405 nm, and the animals were imaged immediately and 3 (C) or 24 (B) hours after at 561 nm. To determine the degradation rates, the fluorescence (561 nm) acquired 3 or 24 h after the conversion was divided by the fluorescence immediately after conversion. The error bars represent the standard deviation of 11-15 animals.

4.6.3 PolyQ and mHtt expression reduces proteasome capacity

Subsequently, the proteasome function was investigated in animals expressing expanded polyglutamine stretches in muscle and neurons. Interestingly, whereas expression of Q$_{40}$ in muscle tissue led to a reduction of chymotrypsin-

like proteasome activity of 30% and analogously of the 20S α-subunit levels (Figures 7.5 A-D), neuronal expression of Q_{40} did not affect proteasomal activity (Figures 7.5 E). Similar results were obtained in animals expressing a longer polyglutamine stretch, Q_{67}, as neither the *ex vivo* nor *in vivo* proteasome function were altered (Figures 7.5 F+G).
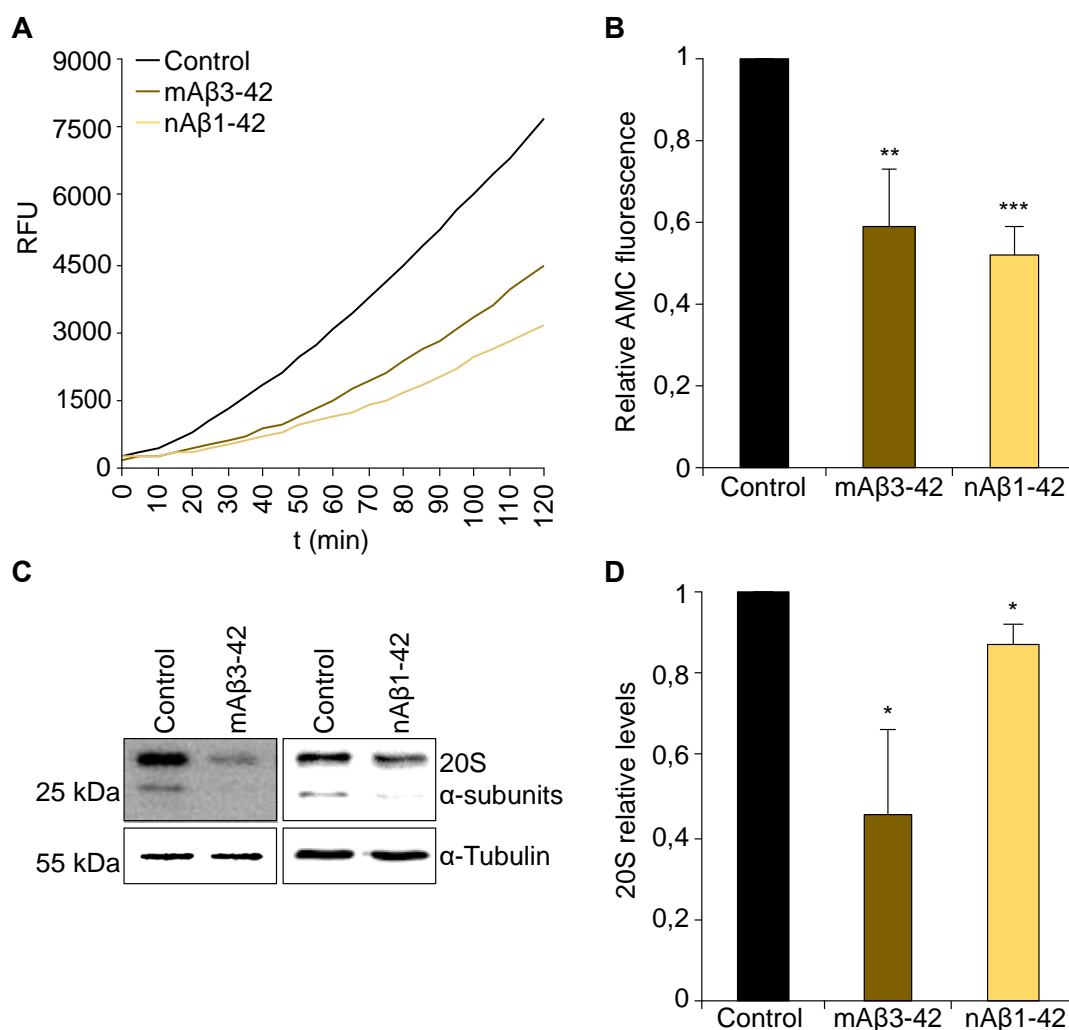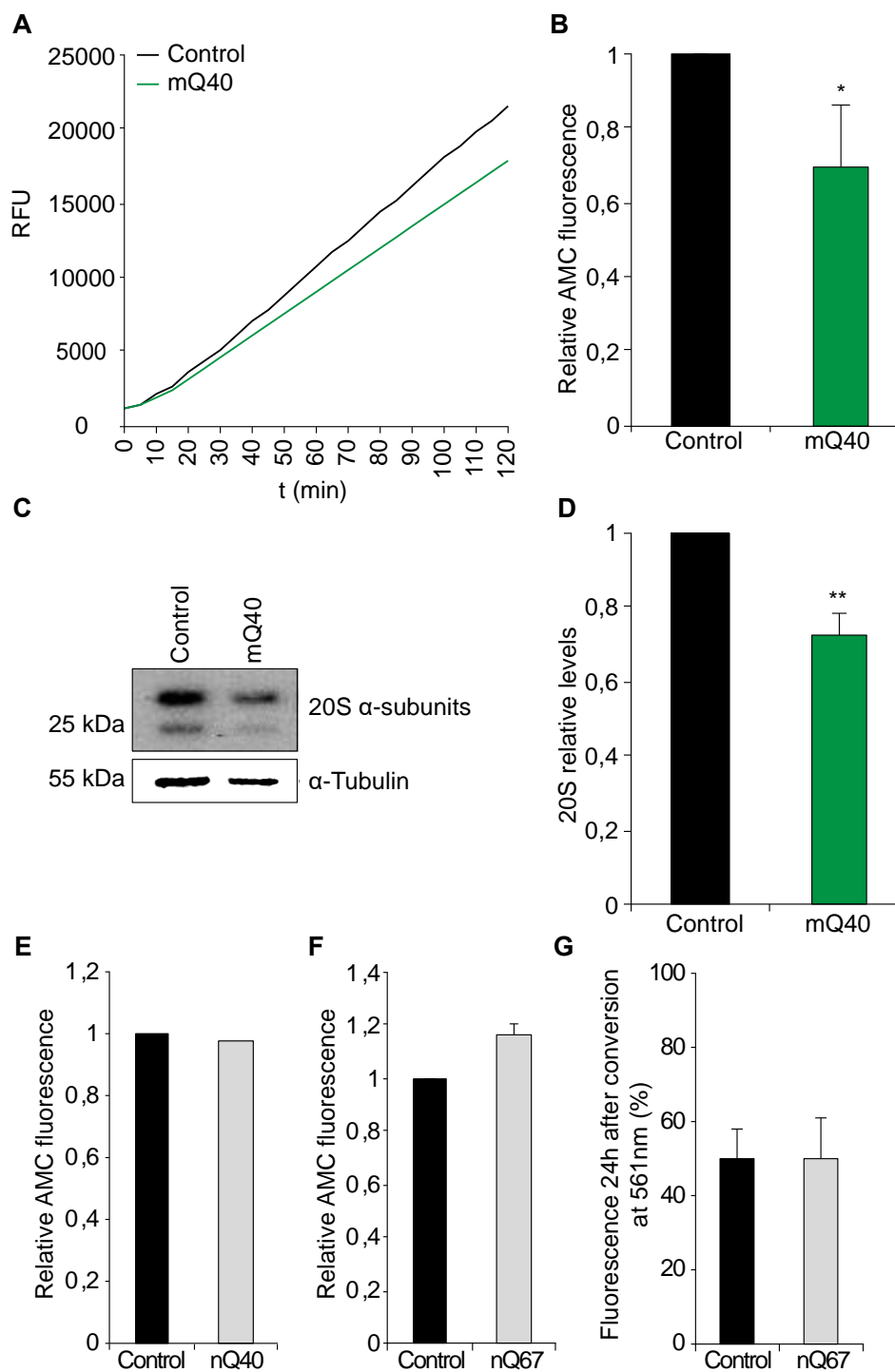

Figure 7. 5 - Proteasome function in polyglutamine expressing animals

A-B) Chymotrypsin-like proteasome activity was measured every 5 min from lysates of control and AM141 (mQ_{40}::YFP) day 4 old animals. The relative activities were calculated and normalized to control (B). The error bars represent the standard deviation of three independent experiments. C-D) 20S α-subunit levels were determined in control and AM141 (mQ_{40}::YFP) day 4 old animals. The 20S levels were normalized to α-tubulin levels and then to control (D). The error bars represent the standard deviation of three independent experiments. E) Chymotrypsin-like proteasome activity was measured every 5 min from lysates of control and AM101 (nQ_{40}::YFP) day 4 old animals. The relative activities were calculated and normalized to control. F) Chymotrypsin-like proteasome activity was measured every 5 min from lysates of control and AM44 (nQ_{67}::CFP) day 4 old animals. The relative activities were calculated and normalized to control. The error bars represent the standard deviation of two independent experiments. G) The UbG76V::Dendra2 degradation rates were measured in YD3 (mUbG76V::Dendra2), YD3/AM44 (mUbG76V::Dendra2; nQ_{67}::CFP) animals. UbG76V::Dendra2 protein was converted upon exposure to 405 nm, and the animals were imaged immediately and 24 h after at 561 nm. To determine the degradation rates, the fluorescence (561 nm) acquired 24 h after the conversion was divided by the fluorescence immediately after conversion. The error bars represent the standard deviation of 11 animals.

To validate the data obtained in the nematode, I set out to analyze the proteasome function in response to mHtt aggregation in mammalian cells. As demonstrated in figures 7.6 A+B, HEK293 cells were transfected with GFP (control), HttExon1Q_{25}-GFP (non-aggregating control), and HttExon1Q_{97}-GFP (aggregation-prone).
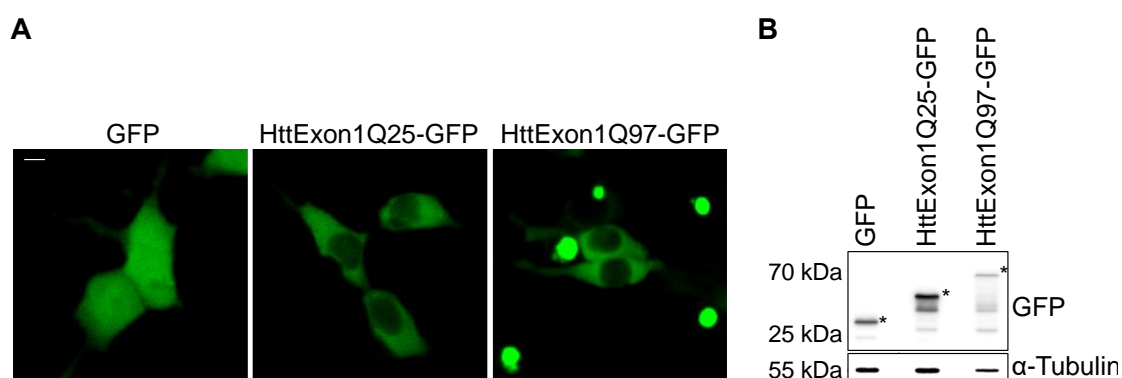
Figure 7. 6 - mHtt expression in HEK293 cells

A-B) HEK293 cells were transfected with GFP, HttExon1Q$_{25}$-GFP, and HttExon1Q$_{97}$-GFP. 24 h after transfection, cells were imaged in a fluorescent microscope (A). The expression of GFP, HttExon1Q$_{25}$-GFP, and HttExon1Q$_{97}$-GFP was also confirmed by western blot (B). Scale bar: 5 µm.

The expression of the aggregation-prone HttExon1Q$_{97}$-GFP led to a reduction of chymotrypsin-like proteasome activity by 16% compared to controls (GFP and HttExon1Q$_{25}$-GFP) (Figures 7.7 A+B). Unlike the *C. elegans* data, the presence of amyloid-like aggregates in HEK293 cells did not affect the 20S levels (Figures 7.7 C+D).

Together, these results demonstrate that Huntington's disease models display a compromised proteasome function likely associated with the presence of toxic amyloid aggregation-prone proteins in the nematode, as well as in mammalian cells.
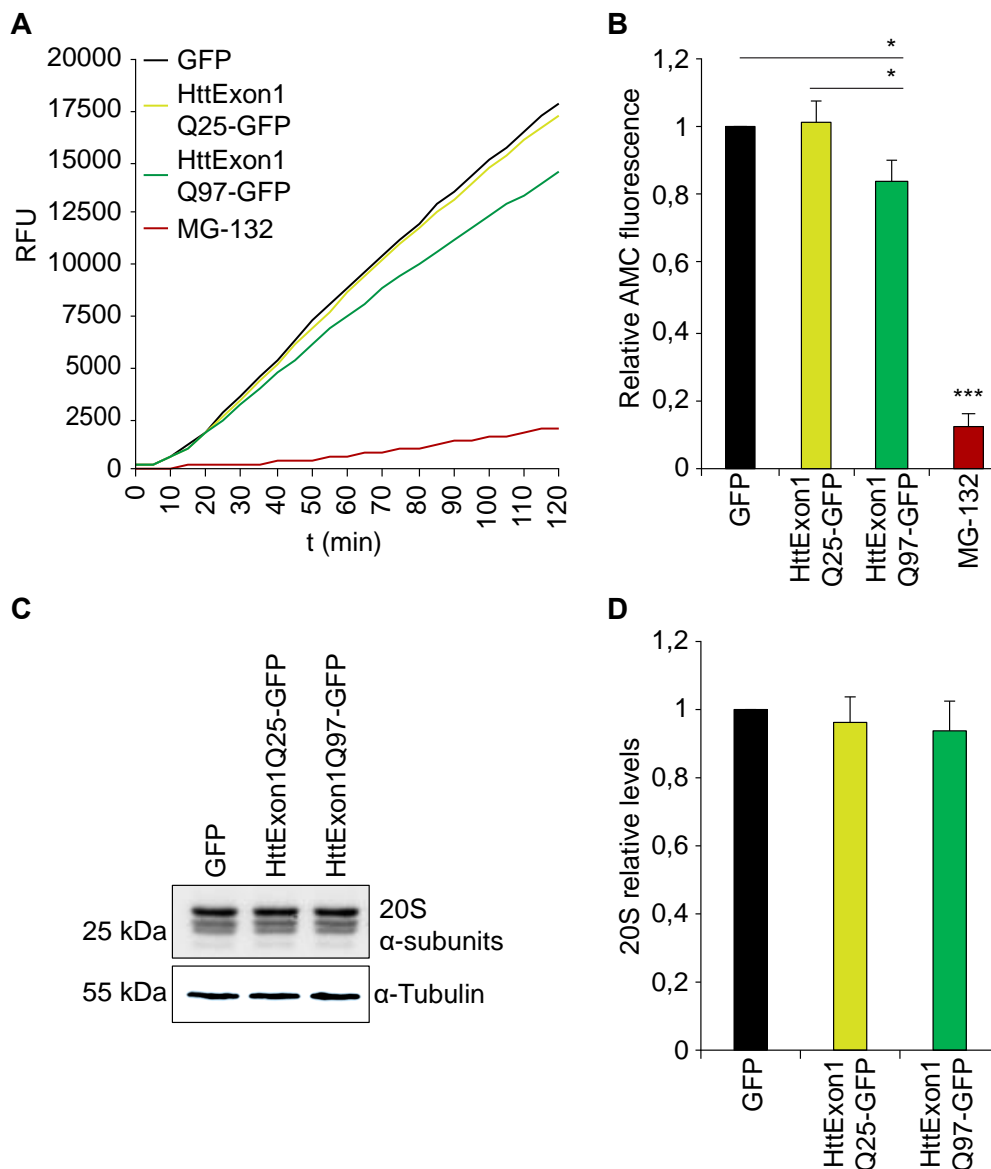
Figure 7. 7 - Analysis of the proteasome activity and abundance in mHtt expressing HEK293 cells.

A-B) Chymotrypsin-like proteasome activity was measured every 5 min of lysates of HEK293 cells transfected with GFP, HttExon1Q_{25}-GFP or HttExon1Q_{97}-GFP. The relative activities were calculated and normalized to GFP (B). The error bars represent the standard deviation of three independent experiments. C-D) 20S α-subunit levels were determined in HEK293 cells transfected with GFP, HttExon1Q_{25}-GFP or HttExon1Q_{97}-GFP. The 20S levels were normalized to α-tubulin levels and then to GFP (D). The error bars represent the standard deviation of four independent experiments.

4.6.4 PolyQ$_{40}$ ultrastructure by CLEM and EM

The fact that animals expressing amyloidogenic protein aggregates exhibit an impairment of protein clearance pathways suggests a cellular collapse. To gain insight into the structural changes of the affected cells and tissues within the nematode, I decided to perform a more detailed analysis of the morphology of the Q$_{40}$ aggregates. The fluorescent features of the Q$_{40}$::RFP aggregates allow its visualization by confocal microscopy and subsequent transmission electron microscopy analysis. Therefore, Correlative Light Electron Microscopy (CLEM) was applied to determine the ultrastructure of Q$_{40}$ aggregates. Nematodes were embedded in HM20 resin that retained enough fluorescence enabling the detection of Q$_{40}$::RFP, and together with nuclear DAPI staining allowed the alignment of confocal images with transmission electron microscopy images (Figure 7.8, upper panel). The RFP signal was associated with a cytoplasmic part of muscle cells, and ultrastructural observation indeed revealed that the bright RFP foci were associated with a cytoplasmic region containing an electron dense fibrilar meshwork (Figure 7.8, lower panel). Similar to observations from transfected mouse primary cells, HeLa cells and yeast (Bauerlein et al. 2017, Gruber et al. 2018), the obtained Q$_{40}$ aggregates in an animal reveal that the aggregates are devoid of ribosomes and are not enclosed by any membranous structure. Despite the increased GFP::LGG-1 signal observed on the confocal level (Figure 7.1 A), autophagy-related membranes were not found in proximity to the aggregate.
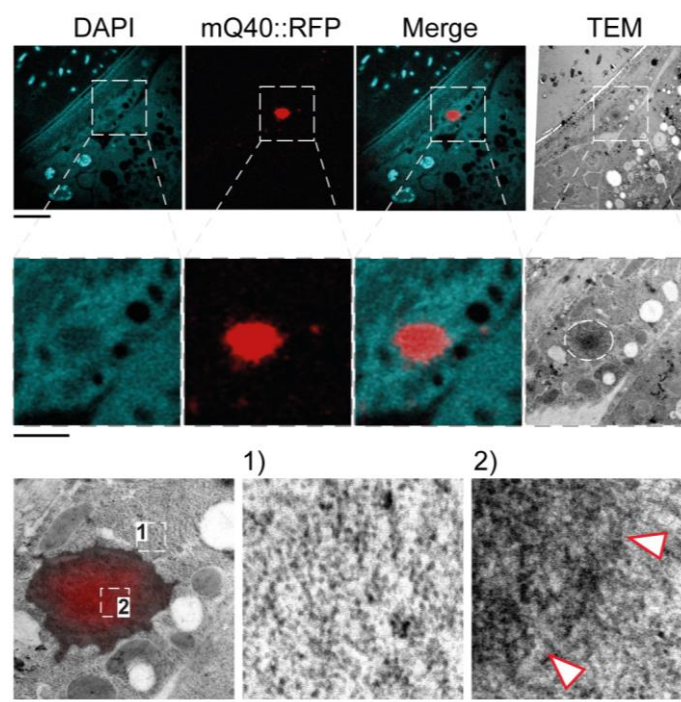
Figure 7. 8 - CLEM analysis of a Q_{40}::RFP aggregate.
Confocal microscopy images (DAPI and RFP) were aligned with transmission electron images (upper and middle panel). The lower panel displays an electron microscopy image merged with the Q_{40}::RFP signal. Image 1 is a magnification of the cytosol and image 2 depicts the Q_{40} aggregate. Triangles indicate the aggregate boundary. Scale bars: 5 µm (upper panel), 2 µm (middle panel) and 1 µm (lower panel).

The Q_{40} aggregates were also analyzed in standard Epoxy embedded/osmium fixed nematodes to obtain a better image contrast (Figure 7.9). The Q_{40} aggregate displayed an amyloid-like fibril structure, resembling *in vitro* generated HttExon1Q_{48} fibrils (Gao et al. 2015, Scior et al. 2018) and HttExon1Q_{97}-GFP structures in transfected cells (Bauerlein et al. 2017). The diameter of the depicted Q_{40} aggregate is about 2 µm (Figure 7.9, top image; the dimension of the Q_{40} aggregate is indicated by the red triangles). Inset 1 depicts a magnified region of a cell section outside of the polyQ aggregate that shows a regular distribution of ribosomes. The interface between aggregate and the remaining cytosol is depicted by inset 2 and demonstrates the lack of any membranous structure, and inset 3 depicts a magnified region within the aggregate that shows the amyloid fibrils and the complete lack of ribosomes.

Together, the CLEM and EM analysis show that the polyQ aggregates display an amyloid-like structure that easily can interact with cytosolic components due to the lack of any surrounding membrane.
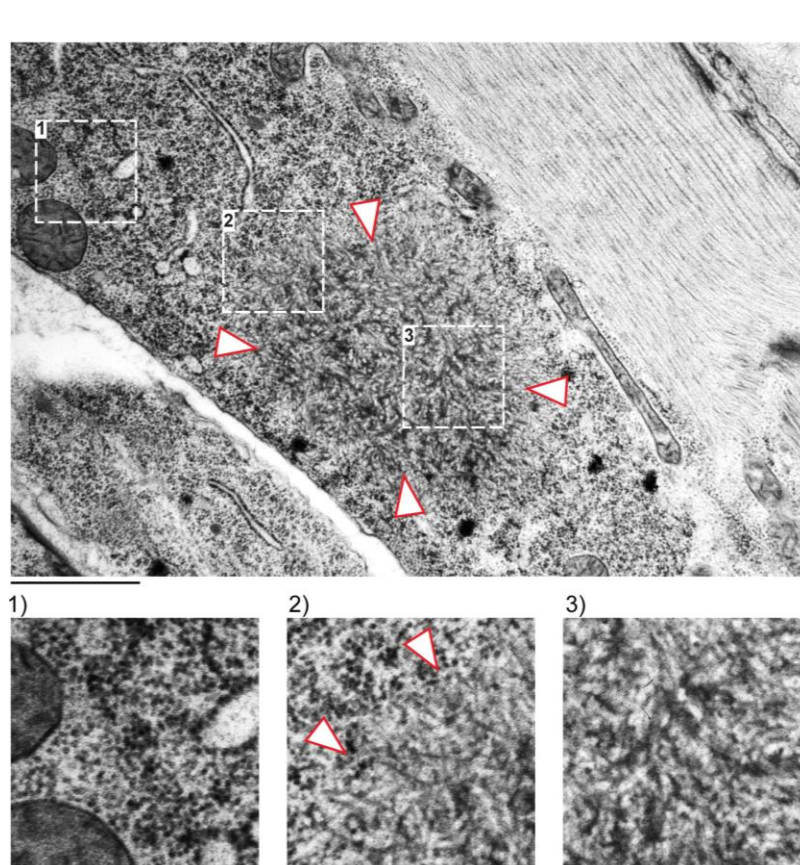
Figure 7. 9 - EM analysis of a Q_{40}::RFP aggregate.

In the lower panel are magnified images from the indicated regions. Image 1 is a magnification of the cytosol; image 2 shows the interface of the aggregate and image 3 is a magnification of the aggregate. The arrows point out the boundaries of the aggregate. Scale bars: 1 μm (upper panel) and 500 nm (lower panel).

5 Discussion

The proteostasis network is a well-orchestrated system that tightly regulates protein synthesis, folding, refolding and proteolysis to maintain the function of the proteome and the cellular physiology (Wolff et al. 2014, Diaz-Villanueva et al. 2015, Sala et al. 2017). The interplay between different protein quality control pathways has been the focus of many studies. However, the precise regulation of the proteostasis machinery, especially during aging and disease, is still far from being completely understood (Rubinsztein et al. 2011, Kaushik et al. 2015).

For this reason, I decided to investigate the crosstalk between the disaggregase constituting chaperones and the two major proteolytic pathways, the UPS and autophagy (Figure 8.1 A). A response of autophagy and UPS was observed when proteins of the HSP110/70/J disaggregation complex were depleted in *C. elegans* and HEK293 cells. Notably, the depletion of chaperones that are not involved in protein disaggregation did not affect autophagy and proteasome pathways.

Moreover, the UPS and autophagy pathways were assessed with the progression of aging and in neurodegenerative disease models (Figure 8.1 B). I found that the protein clearance pathways are altered in old animals, and animals expressing disease-associated amyloid proteins.
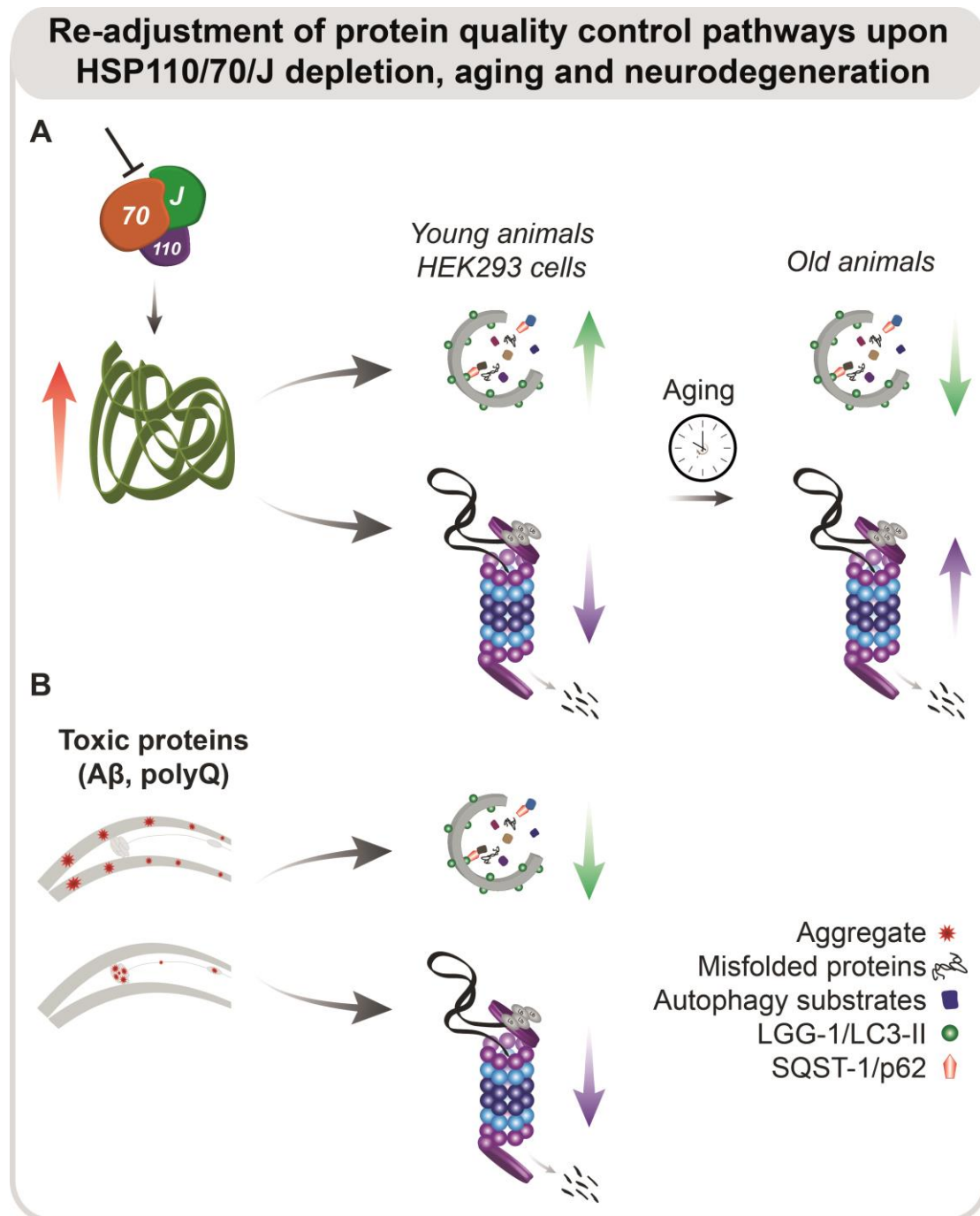
Figure 8. 1 - Summary scheme.

A-B) Depletion of HSP110/70/J disaggregation complex members leads to an increase of misfolded proteins, which induces autophagy and impairs proteasome function in young animals and HEK293 cells (A). With the progression of aging in *C. elegans*, autophagy is not activated, and proteasome activity is no longer reduced in response to chaperone loss. Autophagy and proteasome pathways are perturbed in the presence of amyloid-like proteins in the muscle and neurons of *C. elegans* (B).

5.1 Autophagy is induced upon loss of disaggregation capacity

The recently described HSP110/70/J disaggregation complex can prevent and reverse the aggregation of multiple substrates, thus providing the cell with an alternative protein aggregate clearance pathway (Rampelt et al. 2012, Nillegoda et al. 2015, Kirstein et al. 2017, Scior et al. 2018). In this study, I demonstrated that the depletion of chaperones that form the disaggregation complex leads to an activation of autophagy in *C. elegans* and HEK293 cells (section 4.2). The activation of autophagy was detected in young animals, which displayed elevated LGG-1 and reduced SQST-1/p62 protein levels, in response to chaperone depletion. Also, chaperone knockdown led to a decrease of the lysosome pool in *C. elegans* confirming the activation of autophagic flux. I was also able to show that chaperone siRNA induced autophagy in HEK293 cells. Moreover, I could demonstrate that the activation of autophagy is regulated at the transcriptional level as *hsp-1* and *hsp-110* depletion leads to a nuclear translocation of the transcription factor HLH-30 that initiates the gene expression program to activate autophagy.

Aging is marked by an accumulation of misfolded proteins due to the collapse of protein quality control mechanisms (Ben-Zvi et al. 2009, David et al. 2010, Kirstein-Miles et al. 2013). However, the regulation of autophagy during aging is far from consensual. An impairment (Chang et al. 2017) as well as activation of autophagy (Chapin et al. 2015) during aging have been reported for *C. elegans*, which emphasizes the need to further investigate the autophagic flux in aged animal models. Here, I monitored the LGG-1 and SQST-1/p62 protein levels of both young and old animals and detected an increase in the levels of both proteins in aged animals. Thus, it can be concluded that the autophagic flux is less active with the progression of aging, supporting a previous study (Chang et al. 2017). Additionally, I found that the induction of autophagy in response to chaperone depletion is diminished in old animals, implying that the compensatory effect of autophagy to maintain proteostasis is limited to the reproductive phase of animals. This observation is supported by previous work from Ben-Zvi and colleagues, which demonstrated that the maintenance of proteostasis occurs only until the reproductive phase (progeny production) and

then collapses in the adulthood phase (Ben-Zvi et al. 2009, Shemesh et al. 2013). Particularly, after the reproductive stage, there is a sharp decline in the capability to activate proteostasis mechanisms like the heat-shock response (Ben-Zvi et al. 2009). So, it is possible that autophagy is regulated analogously, restricting an activation of the autophagic flux in response to stress to a narrow window until adulthood is reached.

In summary, I was able to show that autophagy is activated in response to the loss of chaperone-mediated disaggregation in HEK293 cells and *C. elegans*. Yet, as aging progresses, the autophagic flux is diminished, and old animals can no longer activate autophagy to compensate for the loss of disaggregating chaperones.

5.2   Proteasome capacity is diminished when HSP110/70/J machinery is compromised

The capacity of the proteasome system was also studied in response to the loss of disaggregation activity. Both *ex* and *in vivo* analysis of proteasome function revealed that depletion of some chaperones constituting the disaggregation complex leads to a decreased proteasome activity, and accumulation of proteasomal substrates in *C. elegans* and HEK293 cells (section 4.3). Interestingly, the depletion of *hsp-110/hspa4* showed the most robust phenotype. The knockdown of *hsp-110* led to a prominent reduction of chymotrypsin-like proteasome activity and a notable accumulation of UbG76V in the muscle and neurons of *C. elegans*. Similar results were obtained in HEK293 cells when *hspa4* was depleted. The distinct biological function of HSP-110 described so far may explain these results. HSP-110 is essential for protein disaggregation, due to its nucleotide exchange factor activity as part of the disaggregation complex (Rampelt et al. 2012). No other function has been described so far yet for HSP-110. Moreover, the *C. elegans* genome encodes for only one *hsp-110* gene, which implies that the knockdown of *hsp-110* completely abrogates the disaggregation activity.

A reduction of proteasome capacity can be attributed to a failure in substrate recognition, enzymatic activity deficiencies or reduced proteasome proteins. The latter is likely to be the case, as the levels of the 20S α-subunit proteins are decreased when *hsp-110* and *dnj-12* are depleted in *C. elegans*, and upon knockdown of *hspa8*, *dnaja2* and *dnajb1* in HEK293 cells.

Intriguingly, the depletion of chaperones from the J-protein family led to the highest discrepancies in the phenotypes detected between *C. elegans* and HEK293 cells. These observations may be related to the huge diversity of J-proteins. The J-protein family is comprised of 32 and 49 members in *C. elegans* and humans, respectively (Hageman et al. 2009, Craig et al. 2017). The precise biological role for every J-protein family member is still unknown and the orthologous proteins between species may exhibit different functions. In addition, compensatory effects have been observed between distinct J-protein members, where a depletion of a specific J-protein led to an upregulation of another (unpublished data, Kirstein laboratory).

Furthermore, the diversity of the Hsp70 protein family could also explain the variation of the phenotypes observed upon *hsp-1* depletion. The complete disaggregation of amorphous and amyloid aggregates (e.g. luciferase and mHtt) is only possible when HSP-1 acts together with HSP-110 and a J-protein (Rampelt et al. 2012, Nillegoda et al. 2015, Kirstein et al. 2017, Scior et al. 2018). However, other Hsp70s (C12C8.1, F11F1.1 an F44E5.4) also possess a residual disaggregation activity. It was shown that C12C8.1 is able to solubilize in part aggregated luciferase, and that an excessive amount of C12C8.1, F11F1.1 or F44E5.4 can prevent mHtt aggregation (Kirstein et al. 2017, Scior et al. 2018). Interestingly, the depletion of *hsp-1* leads to an upregulation of more than six-fold of C12C8.1 (Guisbert et al. 2013). Yet, the increasing levels of C12C8.1 do not compensate for the loss of the disaggregation activity of HSP-1 (Kirstein et al. 2017).

The high complexity of the Hsp70 and J-protein family, needs to be taken into account when analyzing the severity of the observed phenotypes in the knockdown conditions, as they could be underestimated and masked by compensatory effects.

Analogous to autophagy, the proteolytic capacity of the UPS is a vital node of the proteostasis network and plays an important role during aging. Yet, the

regulation of proteasome function with the progression of aging requires additional studies, as opposing data have been published. While it has been reported that the lung, liver, heart and spinal cord of aged rat exhibit a decreased proteasome activity (Keller et al. 2000, Bulteau et al. 2002, Breusing et al. 2009), others have reported that muscle, liver, and spleen display an increased proteasome function (Shibatani et al. 1996, Zhang et al. 2007, Altun et al. 2010). Moreover, impaired proteasome function or even no change was detected in aged *Drosophila* and mice, respectively (Vernace et al. 2007, Cook et al. 2009, Tonoki et al. 2009, Caniard et al. 2015). In *C. elegans*, the chymotrypsin-like proteasome activity was reported to be increased on day 10 when compared to day 3 animals (Raynes et al. 2017). Also, the degradation of UbG76V::GFP in the epithelial cells of *C. elegans* revealed an increased proteasome activity during aging (detected 48 h after L4 stage) (Liu et al. 2011).

In this thesis, I further analyzed the proteasome function during aging in *C. elegans*, and found that the 20S α-subunit protein levels increase as the nematodes age, but the overall chymotrypsin-like activity remained unchanged. These results prompted me to analyze the *in vivo* proteasome activity in different cellular compartments. I observed that while old animals display an increased proteasome activity in muscle cells, the UPS activity declines in neurons (Hamer et al. 2010), revealing a coordinated tissue-specific regulation of the proteasomal activity with aging. Notably, the reduced proteasome capacity in response to the depletion of some disaggregating members (*hsp-110*, *dnj-12* and *dnj-13*) is no longer observed in old animals, likely due to an increase of the 20S α-subunit levels when *hsp-110*, *dnj-12*, *dnj-13,* and *dnj-19* are depleted.

This data demonstrates that proteasome function is decreased in young nematodes and HEK293 cells when specific chaperones from the disaggregation complex are depleted. With the progression of aging, the proteasome capacity is altered in *C. elegans*, and it exhibits a tissue-specific proteasome regulation.

5.2.1   The decline of the proteolytic pathways during aging

Proper regulation of the proteolytic pathways is vital for healthy aging, as a decline in degradative pathways leads to the accumulation of damaged proteins, organelles, and reduced ability to adapt and respond to stress conditions such as bacterial infection (Shintani et al. 2004, Vilchez et al. 2014). Besides, the activity of the protein degradation pathways is crucial for the immune system and protein synthesis, as its proteolytic activity generates antigenic peptides that will be presented to the immune system and free amino acids that will be transformed to obtain energy or recycled to synthesize new proteins (Gaczynska et al. 1993, Mizushima et al. 2011). The latter is of high relevance due to the observed decrease in protein synthesis during aging (Kirstein-Miles et al. 2013, Walther et al. 2015). Therefore, the reduced activity of the UPS and autophagy during aging, not only leads to the accumulation of damaged organelles, increase in the half-life and stability of proteins, but also may contribute to the reduction of protein synthesis.

Supporting the importance of proteasome and autophagy pathways during aging is the fact that their activities are increased and contribute to the lifespan extension observed in the *daf-2* mutants (Melendez et al. 2003, Ghazi et al. 2007, Hansen et al. 2008, Matilainen et al. 2013). Indeed, the extension of lifespan can be achieved by the activation of the proteolytic pathways, as this was reported when autophagy was activated in *C. elegans* (Kenyon 2010), *Drosophila* (Bjedov et al. 2010) or mice (Harrison et al. 2009), or when proteasome activity was increased in *C. elegans* (Chondrogianni et al. 2015), *Drosophila* (Tonoki et al. 2009) or yeast (Kruegel et al. 2011).

Although my data helped to get more insight into the role of the diverse proteostasis pathways during aging, many open questions remain regarding the mechanism of how the activity of the proteolytic pathways are adjusted with aging. Further analysis should ideally be carried out in different model organisms to corroborate the obtained data.

5.2.2 Are the proteolytic pathways reacting to the loss of disaggregation capacity due to an increase in protein misfolding?

It is challenging to untangle the crosstalk between the disaggregating chaperones and the proteolytic pathways. Is there a strict sequence of events upon loss of cellular disaggregation capacity that leads to a subsequent regulation of autophagy and proteasome? I aimed to address this question and found that HSP110/70/J complex member depletion leads to a prominent increase of amorphous aggregates and loss of protein function, followed by the activation of autophagy and reduction of proteasome function (section 4.5). The expected accumulation in cytosolic protein misfolding in consequence of chaperone depletion, likely triggers the induction of autophagy as a compensatory mechanism to rebalance protein homeostasis. However, a clear separation of the functional role of chaperones as constituents of a disaggregase complex and the two proteolytic pathways is difficult.

This aspect is of particular relevance for Hsp70 family members that fulfill pleiotropic functions and are not only active in a trimeric disaggregase complex. Hsp70 is known to participate in the autophagy process, particularly its role in chaperone-mediated autophagy (CMA) is well established (Cuervo et al. 2014). Therefore, the involvement of other chaperones from the disaggregase complex in targeting substrates for degradation cannot be excluded. Indeed, a possible involvement of DNAJB1 in the autophagy pathway was proposed due to its interaction with WIPI2, an autophagy-related protein (Behrends et al. 2010).

In addition, it has been shown that heat-shock can promote the induction of autophagy via HSF-1 in *C. elegans* (Kumsta et al. 2017). Moreover, the depletion of specific chaperones (*hsp-1/Hsp70*, *daf-21/Hsp90*) induces a robust heat-shock response in *C. elegans,* thus interfering with the autophagy-signaling pathway (Guisbert et al. 2013, Haslbeck et al. 2013).

The interplay between the UPS and chaperones has been investigated as well, and for instance, Hsp70 was shown to be involved in the targeting of misfolded poly-ubiquitinated proteins to the proteasome (Esser et al. 2004, Kriegenburg et al. 2012). The targeting of misfolding proteins to the proteasome by other disaggregation chaperones like the HSP-110 has not yet been proposed.

However, it cannot be excluded that additional chaperones that participate in disaggregation events also play a role in the proteasomal degradation of specific substrates.

Furthermore, the proteasome complex assembly is assisted by five chaperones, the proteasome assembly chaperones, PAC1-4 (Rousseau et al. 2018). A recent study showed that yeast proteins from the Hsp70 family are required in the proteasome assembly cascade, and thus achieving a functional proteasome structure (Hammack et al. 2017). As discussed above, the depletion of some disaggregating chaperones leads to a reduction of essential proteasome complex subunits. A plausible explanation would be the involvement of these chaperones either in the folding of proteasome-related proteins, or even in proteasome assembly. Another scenario would be linked to a reduction in the stability of the proteasome subunits upon chaperone down-regulation and may affect its stability in the cell. As the depletion of chaperones activates autophagy, one might also speculate that the reduction of proteasome levels can be linked to increased degradation. In the last years the degradation of proteasomes by autophagy (proteophagy) has been described (Marshall et al. 2015, Cohen-Kaplan et al. 2016, Marshall et al. 2016, Waite et al. 2016). Yet, this mechanism has not been demonstrated in *C. elegans*, and therefore further studies are required to reveal if the nematodes exhibit the ability to degrade proteasome via autophagy.

These results demonstrate that the depletion of chaperones diminish the cellular folding capacity, leading to the accumulation of misfolded proteins, which subsequently trigger the induction of autophagy and a reduction of proteasome function.

5.3 Alzheimer and Huntington's disease models exhibit an impaired autophagy

The formation and accumulation of amyloid-like aggregates is a shared characteristic of multiple neurodegenerative diseases such as Alzheimer's or Huntington's disease (Ross et al. 2004, Park et al. 2013). The aggregation of

disease-related proteins is associated with a collapse of protein quality mechanisms that fail to maintain the solubility of these aggregation-prone proteins or to eliminate them by disaggregation or proteolysis.

A failure in the autophagy pathway has been linked to neurodegeneration (Wong et al. 2010, Zheng et al. 2016). In this study, I investigated the autophagic flux in Alzheimer and Huntington's disease models. The analysis of animals expressing disease-associated amyloid proteins revealed that autophagy is impaired irrespective of the type of amyloid (Aβ and Q_{40}) and expression pattern (neuronal and muscle tissue). An accumulation of LGG-1, SQST-1/p62, and an increase in the lysosome pool indicates that the amyloid-like proteins block the autophagy pathway (section 4.6.1). These toxic proteins are targeted to autophagy, thus the degradation attempt may lead to an overload of autophagosomes and subsequently lysosomes. Similar observations were reported in other disease models, suggesting a more general inhibitory effect on autophagy by amyloid-like proteins (Li et al. 2008, Winslow et al. 2010, Nixon 2013, Menzies et al. 2015). Moreover, a direct interaction of the amyloid protein either in its soluble, oligomeric or aggregated state with autophagic components is likely to occur, as demonstrated for mHtt which can interact with *bec-1* resulting in autophagy impairment (Ashkenazi et al. 2017).

In sum, the expression of both Aβ and Q_{40} in the muscle or neurons of *C. elegans* leads to the impairment of autophagy, supported by the accumulation of the LGG-1 and SQST-1/p62 proteins, and lysosomes.

5.4 Proteasome function is diminished in Alzheimer and Huntington's disease models

Proteasome dysfunction has been linked to many neurodegenerative diseases. Despite the ability of proteasomes to degrade aggregation-prone proteins, various studies show that amyloid proteins can lead to an impairment of proteasome function (Bence et al. 2001, Lopez Salon et al. 2003, Bennett et al. 2005, Juenemann et al. 2013)

Indeed, the presence of Aβ and Q_{40} diminishes the proteasome capacity in *C. elegans* (sections 4.6.2 and 4.6.3). I was able to demonstrate that the reduction in chymotrypsin-like proteasome activity correlates with a substantial reduction in the 20S α-subunit protein levels in *C. elegans*, particularly in animals expressing Aβ in the muscle cells. In addition, I detected that the expression of the aggregation-prone HttExon1Q_{97}-GFP in HEK293 cells also leads to a reduction of the chymotrypsin-like proteasome activity, confirming previous data involving similar mHtt aggregation-prone constructs (Bence et al. 2001, Bennett et al. 2005, Hipp et al. 2012).

Furthermore, I found that the presence of Aβ in the muscle cells led to a diminished proteasome capacity within the muscle cells, but notably also in the neurons. A similar phenomenon was also observed when Aβ was expressed in the neurons. A suppression of UPS activity in a distal tissue by the expression of Aβ has not yet been reported.

What could be a potential mechanism by which Aβ expression leads to UPS dysfunction across tissues? The presence of Aβ exerts a severe organismal proteotoxic stress, which likely explains the failure of protein quality control mechanisms in diverse tissues. A possible explanation for this effect could be a transmission of Aβ peptides, oligomers or aggregates between different cell types. Spreading of toxic proteins plays a critical role in the manifestation of neurodegenerative diseases (Guo et al. 2014). Interestingly, the transmission of toxic proteins between tissues has been observed in *C. elegans* for the NM region of the prion Sup35 (Nussbaum-Krammer et al. 2013). In a recent study, the release of Q_{128} and Aβ$_{1-42}$ was observed from neurons of *C. elegans* (Melentijevic et al. 2017). The neurotoxicity caused by expression of the amyloid-like proteins, led to the excretion of vesicles (named exophers) containg organelles, Q_{128}, and Aβ$_{1-42}$, which likely disturb the neighboring tissues.

Also, the signaling communication between different cell types must be considered. Notably, a trans-tissue chaperone signaling mechanism has been demonstrated in *C. elegans* (van Oosten-Hawle et al. 2014). It was shown that Hsp90 overexpression in muscle cells leads to the upregulation of Hsp90 in the neuronal and intestinal cells (van Oosten-Hawle et al. 2013). Moreover, the toxicity observed in animals expressing Aβ in muscle cells was dramatically

reduced after overexpression of Hsp90 in the neurons, demonstrating the impact of transcriptional regulation in a trans-tissue manner (O'Brien et al. 2018). So, it is possible that chaperones involved in disaggregation events share a similar trans-tissue signaling regulation.

How do amyloid-like proteins affect UPS function?

Many studies have shown that protein aggregates of disease-related proteins sequester numerous endogenous proteins, and amongst those components of the clearance pathways (e.g. proteasome proteins) and chaperones (Bence et al. 2001, Park et al. 2013, Walther et al. 2015, Yang et al. 2016, Thibaudeau et al. 2018). The mechanisms by which the amyloid-like proteins associate and impair the proteasome have been studied (Bence et al. 2001, Yang et al. 2016, Thibaudeau et al. 2018). A recent *in vitro* analysis revealed that Aβ, mHtt and α-syn oligomers directly bind to the proteasome preventing the opening of the 19/20S subunits, and consequently leading to proteasome dysfunction (Thibaudeau et al. 2018).

The sequestration of proteasomes by amyloid-like protein aggregates has also been demonstrated and is of particular interest because it was shown that active proteasomes co-localize with mHtt aggregates (Schipper-Krom et al. 2014). Also, a recent study, demonstrated that proteasomes strongly accumulate and are trapped within a poly-Gly-Ala aggregate, an amyloid aggregate associated with ALS (Guo et al. 2018). Together, the binding of amyloid aggregates to proteasomes and subsequent sequestration may lead to the reduction of the available proteasomal pool and likely explains the diminished proteasome function.

This data shows the challenge that the proteostasis network faces in the presence of amyloid-like proteins. The proteasome capacity is diminished in Q_{40}, but especially in Aβ-expressing animals, which display proteasome loss of function across tissues.

5.5 Q40 aggregates exhibit an amyloid fibril structure without a surrounding membrane

Amyloid-like aggregates are found in most neurodegenerative diseases (Chiti et al. 2006). However, it remains unclear how these aggregates structurally affect diverse cellular components. In this study, I aimed to address this question and analyzed the Q_{40} aggregate ultrastructure by CLEM and EM (section 4.6.4). I found that Q_{40} aggregates are a rounded amyloid fibril structure with a diameter of about 2 µm that is not enclosed by a membrane. The lack of a surrounding membrane exposes the amyloid fibrils directly to all cytosolic components. Thus, the aggregate can easily interfere with cellular functions by sequestration of for instance, chaperones and components of the clearance pathways (Holmberg et al. 2004).

This amyloid-like aggregate ultrastructure obtained from *C. elegans* is similar to a recent cryo-electron tomographic analysis of mouse primary and HeLa cells transfected with $HttExon1Q_{97}$-GFP (Bauerlein et al. 2017). Interestingly, Bauerlein and colleagues found that polyQ aggregates are also not membrane-enclosed and that the fibrilar structures protrude the endoplasmic reticulum (ER) membranes, altering its dynamics. Another recent work (discussed above) showed that the poly-Gly-Ala aggregate sequesters proteasomes instead of interacting with ER membranes (Guo et al. 2018).

The recent ultrastructure analysis of disease-associated protein aggregates demonstrates the need to comprehend the exact content composition of the toxic aggregates further and elucidate how the sequestration of cellular components affects global cellular physiology. The sequestration of cellular components by the aggregates is likely to perturb numerous cellular functions, which consequently causes the collapse of proteostasis.

5.6 Conclusion and future perspectives

The interplay between different proteostasis mechanisms is vital to preserve a cellular physiology and prevent the development of numerous diseases.
In this thesis, I investigated the crosstalk between the chaperone-mediated disaggregation and degradation pathways, which comprise the proteostasis

network. I was able to show that in *C. elegans* and HEK293 cells, the proteolytic pathways (autophagy and UPS) respond distinctly to a loss of chaperone disaggregation capacity (HSP110/70/J). While autophagy is activated to compensate for the increase of protein misfolding generated by the depletion of HSP110/70/J complex members, the proteasome function is diminished in particular upon knockdown of *hsp-110/hspa4*.

Interestingly, the activation of autophagy is restricted to the reproductive phase of *C. elegans*, which supports a collapse of proteostasis mechanisms with the progression of aging. Indeed, I found that the autophagic flux is reduced in old animals, and the UPS function is diminished in the neurons of *C. elegans*. However, the muscle cells exhibit increased proteasomal degradation, indicating that UPS function is regulated in a tissue-specific manner.

Moreover, I demonstrated that both proteolytic pathways (autophagy and UPS) are impaired in Alzheimer and Huntington's disease models. Notably, animals expressing Aβ revealed a reduction in proteasome activity in a distal tissue-manner. These results show that Aβ toxicity is not limited to the cells where it is expressed, suggesting a complex cross-tissue communication in *C. elegans*.

Finally, the analysis of the ultrastructure of Q_{40} aggregates revealed a non-membrane enclosed amyloid structure. The lack of a surrounding membrane may explain the interaction and sequestration of critical cellular components by amyloid aggregates.

The work presented in this thesis advances the understating of the role of distinct proteostasis pathways during aging and disease. It also opens new avenues for further studies, as it will be of high relevance to deeply understand how autophagy and UPS sense the loss of disaggregation capacity. Which protein(s) detects the increase of protein misfolding? Do disaggregating chaperones apart from HSP-70 participate in proteolytic events by targeting proteins to degradation? Moreover, the regulation of the proteolytic pathways during aging should be further explored in additional organismal models by taking advantage of *in vivo* tools. Lastly, there is a need to understand in deep detail how amyloid proteins affect proteostasis and how the sequestration of cellular components by amyloid aggregates perturbs the cellular and organismal physiology.

6 Material and Methods

6.1 Material

6.1.1 Chemicals

Standard chemicals were purchased from Sigma Aldrich (St. Louis, USA), Carl Roth (Karlsruhe, Germany) and Merck (Darmstadt, Germany).

Chemical	Company
Acetone	Sigma Aldrich, St. Louis, USA
Acetonitrile (ACN)	Carl Roth, Karlsruhe, Germany
Agar-Agar Kobe 1	Carl Roth, Karlsruhe, Germany
Agarose	Bio+Sell, Nürnberg, Germany
Ambion™ TRIzol™ reagent	Thermo Fisher Scientific, Waltham, USA
Ampicillin	Carl Roth, Karlsruhe, Germany
APS	Carl Roth, Karlsruhe, Germany
Beta-mercaptoethanol	Carl Roth, Karlsruhe, Germany
Bromphenol blue	Carl Roth, Karlsruhe, Germany
BSA	Carl Roth, Karlsruhe, Germany
Chloroform	Fisher Scientific, Schwerte Germany
Chloroquine	Cell signaling, Massachusetts, United States
Cholesterol	Sigma Aldrich, St. Louis, USA
cOmplete™ Protease inhibitor cocktail	Roche Diagnostics, Mannheim, Germany
Coomassie Brillant Blue R-250	Carl Roth, Karlsruhe, Germany
DAPI	Carl Roth, Karlsruhe, Germany
Digitonin	Sigma Aldrich, St. Louis, USA
DMEM (Fluorobite)	Thermo Fisher Scientific, Waltham, USA
DMEM (Gibco)	Thermo Fisher Scientific, Waltham, USA
DMSO	Carl Roth, Karlsruhe, Germany

dNTP Mix 10 mM	Thermo Fisher Scientific, Waltham, USA
DTT	Carl Roth, Karlsruhe, Germany
Epoxy	Sigma Aldrich, St. Louis, USA
Fetal calf serum	Sigma Aldrich, St. Louis, USA
Formaldehyde (37%)	Carl Roth, Karlsruhe, Germany
Glycerol	Sigma Aldrich, St. Louis, USA
Glutamine (Gibco)	Thermo Fisher Scientific, Waltham, USA
Glutaraldheyde	Sigma Aldrich, St. Louis, USA
Gold powder 0,3-3 micron/99,9 %	Chempur, Karlsruhe, Germany
HEPES	Carl Roth, Karlsruhe, Germany
HM20	Polysciences, Eppelheim, Germany
IPTG	Thermo Fisher Scientific, Waltham, USA
LB agar	Serva, Heidelberg, Germany
LB medium	Carl Roth, Karlsruhe, Germany
Lead citrate	Sigma Aldrich, St. Louis, USA
Levamisole	AppliChem GmbH, Darmstadt, Germany
L-lysine	Sigma Aldrich, St. Louis, USA
Lysotracker-Red DND-99	Thermo Fisher Scientific, Waltham, USA
Magnesium acetate	Carl Roth, Karlsruhe, Germany
Methanol	Fisher Scientific, Schwerte Germany
3-methyladenine	Sigma Aldrich, St. Louis, USA
MG132	Sigma Aldrich, St. Louis, USA
Milk powder	Carl Roth, Karlsruhe, Germany
NP-40 Surfactant Amps®	Thermo Fisher Scientific, Waltham, USA
Nuclease free water	Carl Roth, Karlsruhe, Germany
Osmium	Sigma Aldrich, St. Louis, USA
Penicillin (Gibco)	Thermo Fisher Scientific, Waltham, USA

PMSF	Sigma Aldrich, St. Louis, USA
Potassium acetate	Carl Roth, Karlsruhe, Germany
Rapamycin	Sigma Aldrich, St. Louis, USA
RNAse away	Carl Roth, Karlsruhe, Germany
Rotiphorese® Gel 30 (37.5:1)	Carl Roth, Karlsruhe, Germany
Roti-Quant	Carl Roth, Karlsruhe, Germany
SDS	Carl Roth, Karlsruhe, Germany
Sodium azide	Carl Roth, Karlsruhe, Germany
Sodium hypochloride solution	Fisher Scientific, Schwerte Germany
Streptomycin (Gibco)	Thermo Fisher Scientific, Waltham, USA
Suc-LLVY-AMC	Enzo, New York, United States
Tannic acid	Sigma Aldrich, St. Louis, USA
TEMED	Carl Roth, Karlsruhe, Germany
Triton X-100	Carl Roth, Karlsruhe, Germany
Trypsin-EDTA 10x (Gibco)	Sigma Aldrich, St. Louis, USA
Tween 20	Carl Roth, Karlsruhe, Germany
Uranyl acetate	Sigma Aldrich, St. Louis, USA

6.1.2 Markers and loading dyes

Product	Company
DNA loading dye (6x)	Thermo Fisher Scientific, Waltham, USA
GeneRuler (1kb, 50 bp)	Thermo Fisher Scientific, Waltham, USA
PageRuler Plus Prestained Protein Ladder	Thermo Fisher Scientific, Waltham, USA

6.1.3 Antibodies

Primary antibodies

Antibody	Source	Dilution	Source/ Company

Anti-LGG-1	Rabbit	1:1000	Kirstein lab/ Pineda Antikörper-Service, Berlin, Germany
Anti-SQST-1/p62	Rabbit	1:1000	Kirstein lab/ Pineda Antikörper-Service, Berlin, Germany
Anti-DNJ-12	Rabbit	1:2500	Kirstein lab/ Charles Rivers Laboratories, St. Germain-Nuelles, France
Anti-DNJ-13	Rabbit	1:2500	Kirstein lab/ Charles Rivers Laboratories, St. Germain-Nuelles, France
Anti-DNJ-19	Rabbit	1:5000	Kirstein lab/ Charles Rivers Laboratories, St. Germain-Nuelles, France
Anti-HSP-1	Rabbit	1:5000	Kirstein lab/ Charles Rivers Laboratories, St. Germain-Nuelles, France
Anti-HSP-110	Rabbit	1:2500	Kirstein lab/ Charles Rivers Laboratories, St. Germain-Nuelles, France
Anti-HSP-17	Rabbit	1:4000	Kirstein lab/ Pineda Antikörper-Service
Anti-LC3	Rabbit	1:1000	Abcam, Cambridge, UK
Anti-DNAJB1	Rabbit	1:1000	Proteintech, Manchester, UK
Anti-20S α-subunits	Mouse	1:1000	Enzo New York, United States
Anti-α-tubulin	Mouse	1:2500	Sigma Aldrich, St.

Louis, USA

Secondary antibodies

Antibody	Source	Dilution	Company
Goat-Anti-Mouse IR 680	Goat	1:10 000	LI-COR, Lincoln, USA
Pierce®-Goat-Anti-Mouse IgG + IgM (H+L) Peroxidase Conjugated	Goat	1:10 000	Thermo Fisher Scientific, Waltham, USA
Pierce®-Goat-Anti-Rabbit IgG (H+L) Peroxidase Conjugated	Goat	1:15 000	Thermo Fisher Scientific, Waltham, USA

6.1.4 Buffer, solutions and plates

Buffer	Composition
LB agar-amp plates (sterile)	35 g/l LB Agar 1 mM Ampicillin
LB-amp medium (sterile)	25 g/l LB 1 mM Ampicillin
Liquid culture solution (sterile)	1x S-Basal 1 mM $MgSO_4$ 1 mM $CaCl_2$ 5 µg/ml Cholesterol
Lysis buffer (*C. elegans*)	20 mM HEPES 110 mM KAc

2 mM MgAc$_2$

100 µM Digitionin

Lysis buffer (HEK293 cells)	50 mM Tris/HCl pH 7.4
	150 mM NaCl
	1 mM EDTA
	1 % Triton-X100
	2x complete protease inhibitor
M9 solution (sterile)	58 g/l Na$_2$HPO$_4$
	30 g/l KH$_2$PO$_4$
	5 g/l NaCl
	10 g/l NH$_4$Cl$_2$
NGM agar (sterile)	51.33 mM NaCl
	2.5 g/l Bacto^{TM} Peptone
	17 g/l Agar-Agar Kobe 1
	5 µg/ml cholesterol
	1 mM CaCl$_2$
	1 mM MgSO$_4$
	25 mM KH$_2$PO$_4$ pH 6.0
PBS (10x)	1.37 M NaCl
	27 mM KCl
	100 mM Na$_2$HPO$_4$
	18 mM KH$_2$PO4

PBST (1x)	1x PBS
	0.05% Tween 20
RNAi NGM agar (sterile)	NGM agar
	1 mM IPTG
	1 mM Ampicillin
Sample loading buffer (*C. elegans*, 2x)	50 mM Tris-HCl pH 6.8
	2 % SDS
	15 % glycerol
	0.1 % bromphenol-blue
	100 mM DTT
Sample loading buffer (HEK293 cells, 6x)	350mM Tris-HC pH 6.8
	10% SDS
	30% glycerol
	6% β-Mercaptoethanol
	0.3% bromphenol-blue
SDS PAGE distaining solution	40% methanol
	10% acetic acid
SDS PAGE staining solution	2.5 g/l Coomassie brilliant blue
	40% methanol
	10 % acidic acid
SDS-PAGE running buffer (10x)	1% (w/v) SDS

	250 mM Tris
	1.92 M Glycin
Separation gel buffer	1.5 M Tris-HCl pH 8.8
	0.4 % SDS
Stacking gel buffer	0.5 M Tris-HCl pH 6.8
	0.4% SDS
TAE buffer (50x)	242 g/l Tris,
	57.1 ml/l Glacial Acidic Acid
	100 ml/l 0.5 M EDTA pH 8.0
TBS (10x)	200 mM Tris
	1.5 M NaCl
TBST (10x)	200 mM Tris
	1.5 M NaCl
	1% Tween 20
WB transfer	Bio-Rad Trans-blot Buffer

6.1.5 Kits

Product	Name	Company
cDNA synthesis	Maxima First Strand cDNA Synthesis Kit for RT-qPCR	Thermo Fisher Scientific, Waltham, USA
ECL Detection kit	Pierce ECL Western Blot Substrate	Thermo Fisher Scientific, Waltham, USA

Luciferase activity	Steady-Glo Luciferase mix	Promega, Wisconsin, United States
qRT-PCR	Luminaris Color HiGreen qPCR Mast Mix, high ROX	Thermo Fisher Scientific, Waltham, USA
RNA isolation	NucleoSpin RNA	Macherey-Nagel, Düren, Germany
Tranfection reagent (cells)	jetPRIME	Polyplus transfection, New York, USA

6.1.6 Primer

Primer for qRT-PCR

Primer	Sequence	Concentration (µM)
cdc-42_F	AAACTTGTCTCCTGATCAGCT	0.3
cdc-42_R	TACTGTGACGGCGTAATTGT	0.3
lgg-1_F	GTCCAGAAGATGCTCTGTTCT	0.3
lgg-1_R	GGAACAAGTCTTCCTCGTGA	0.3

6.1.7 Equipment

Device	Name	Company
Agarose gel electrophoresis system		Carl Roth, Karlsruhe, Germany
Balances	440-49N and PCB	Kern, Balingen, Germany
Cell culture flow hood	BDK®	Weiss Technik, Lindenstruth, Germany
Centrifuge	Heraeus Fresco 17	Thermo Fisher Scientific, Waltham, USA
Centrifuge (15 ml/50 ml tubes)	3K12	SIGMA, Osterode am Harz, Germany
Centrifuge (4x 8-PCR tubes)	Ministar	VWR, Radnor, USA
Centrifuge (6x 1.5ml)		Carl Roth, Karlsruhe, Germany

Centrifuge (6x 1l)	Sorvall LYNX 6000 Rotor: F9-6x1000 LEX	Thermo Fisher Scientific, Waltham, USA
Centrifuge (Rotor F45-30-11 05844)	5417C	Eppendorf, Hamburg, Germany
Centrifuge 4°C (Rotor F45-30-11 01599)	5417C	Eppendorf, Hamburg, Germany
Electron Microscope	Zeiss 900	Zeiss, Oberkochen, Germany
Fluorescence microscope	EPI-TIRF	Nikon, Tokio, Japan
Fluorescence microscope	M165FC	Leica, Wetzlar, Germany
Freeze substitution processor with UV light (EM)	AFS	Leica, Wetzlar, Germany
Freezer (-80)	KM-DU73Y1E	Panasonic, Kadoma, Japan
Gamma irradiator	OB29	STS, Braunschweig, Germany
Gel documentation (agarose gel)	G:Box	Syngene, Cambridge, UK
Grids (EM)		Sigma Aldrich, St. Louis, USA
Heating block incubator	HLC	Ditabis, Pforzheim, Germany
High pressure freezer	HPM100	Leica, Wetzlar, Germany
Homogenizer	Precellys®24	Bertin instruments, Montigny-le-Bretonneux, France
Incubator (37°C)	CO2 incubator	Binder GmbH, Tuttlingen, Germany
Incubator (30°C & 37°C)	Heraeus Kelvitron	Thermo Fisher Scientific, Waltham, USA
Incubator (35°C)	HerA Therm	Thermo Fisher Scientific, Waltham, USA
Incubator 15°C	TC255	Lovibond
Incubator 20°C		Thermo Fisher Scientific, Waltham, USA
Laser scanning microscope	LSM710	Zeiss, Oberkochen, Germany

Laser scanning microscope	LSM800	Zeiss, Oberkochen, Germany
Magnetic stirrer	RET basic	IKA, Staufen, Germany
Nanodrop	NanoVue Plus	Ge Healthcare Buckinghamshire, UK
PCR cycler	Mastercycler Gradient	Eppendorf, Hambung, Germany
pH meter		Mettler Toledo, Ohio, USA
Pipettes		Brand, Wertheim, Germany
Pipettor	Pipetboy	Integra Bioscience, Bibertal, Germany
Plate Reader	F200 Pro	Tecan, Männedorf, Switzerland
Power suppliers	PowerPac HC / Basic	Bio-Rad, Hercules, USA
qRT-PCR 48 well	Stepone Realtime PRC System	Applied Biosystems / Thermo Fisher Scientific, Waltham, USA
qRT-PCR 96 well	Stepone Plus Realtime PCR System	Applied Biosystems / Thermo Fisher Scientific, Waltham, USA
SDS PAGE System	Mini-PROTEAN cell chambers	Bio-Rad, Hercules, USA
Shaker (4°C)	SM-30 control	Edmund Bühler GmbH, Hechingen, Germany
Shaker/Incubator	Innova 4230	New Brunswick Scientific/Eppendorf, Hamburg, Germany
Shaker/Incubator	Multitron Pro	Infors HT, Bottmingen, Switzerland
Sonicator	Sonoplis HD 2070/ VW 2070	Bandelin, Berlin, Germany
Speedvac	SPD1010 Savant	Thermo Fisher Scientific, Waltham, USA
Stereomicroscope	SMZ 745	Nikon, Tokio, Japan
Tube roller	RS-TR-5	Phoenix Instrument, Garbsen, Germany
Trimmer (EM sections)	Leica Microtome	Leica, Wetzlar, Germany
Vacuum pump		KNF Lab, New Jersey, USA

Vortexer	Vortex-Genie® 2	Scientific Industries, Bohemia, USA
Water bath		GFL, Burgwedel, Germany
WB Detection System	Lumi-Imager F1™	Boehringer Mannheim GmbH
WB Detection System	Odyssey® Imgage System FC	LI-COR, Lincoln, USA
WB transfer	Trans-blot Turbo	Bio-Rad, Hercules, USA

6.1.8 Consumables

Product	Company
Culture plates (8-well)	Ibidi, Martinsried, Germany
Culture plates (6/24/96-well plate)	Sigma Aldrich, St. Louis, USA
Culture plates (35/60/100 mm)	Sarstedt, Nümbrecht, Germany
Falcon tubes 15 and 50	Sarstedt, Nümbrecht, Germany
Filter tips	Sarstedt, Nümbrecht, Germany
Glass cover slips	Carl Roth, Karlsruhe, Germany
Glass slide 76x26 mm	Carl Roth, Karlsruhe, Germany
Lysing Kit 0.5 ml and 2 ml tubes	Bertin instruments, Montigny-le-Bretonneux, France
MicroAmp™ Fast optical 96-well reaction plate	Applied Biosystem by life technologies
MicroAmp™ Fast optical adhesive film	Applied Biosystem by life technologies
Parafilm	Bemis, Neenah, USA
Pasteur pipettes (glass)	Carl Roth, Karlsruhe, Germany
PCR tubes (single)	Sarstedt, Nümbrecht, Germany
PCR tubes (stripes)	Kisker Biotech GmbH & Co. KG
Plates (96 well, transparent) (plate reader)	Sarstedt, Nümbrecht, Germany
Plates (96 well, black) (plate reader)	Corning, New York, United States
Plates (96 well, white) (plate reader)	Corning, New York, United States

Reaction tubes (1.5 ml)	Sarstedt, Nümbrecht, Germany
Platinic wire	Carl Roth, Karlsruhe, Germany
Reaction tubes (low binding, 1.5 ml)	Sarstedt, Nümbrecht, Germany
Serological pipettes	Sarstedt, Nümbrecht, Germany
Table waste bags	Sarstedt, Nümbrecht, Germany
Tips	Sarstedt, Nümbrecht, Germany

6.1.9 C. elegans strains

Strain name	Description	Source
DA2123	adIs2122 (lgg-1p::GFP::lgg-1 + rol-6(su1006)) *(integrated)*	Caenorhabditis genetic center (CGC)
YD3	xzEx3 (Punc-54::UbG76V::Dendra2) *(non integrated)*	C Holmberg (UH, Helsinki, Finland)
YD12	xzEx12 (PF25B3.3::UbG76V::Dendra2) *(non integrated)*	C Holmberg (UH Helsinki, Finland)
CL2006	(dvIs2 (pCL12(unc-54:hu-Aβ 1–42) + pRF4)) *(integrated)*	CGC
AM1066	rmIs350 (unc-54p::Q$_{40}$:: RFP) *(integrated)*	CGC
AM141	rmIs133 (*unc54*p::Q$_{40}$::YFP) *(integrated)*	CGC
CL2355	smg-1ts (cc546); snb-1::Aβ1−42::long 3′-UTR) *(integrated)*	CGC
AM101	*rmIs110 (F25B3.3p::Q40::YFP) (integrated)*	CGC
AM44	rmIs190 (F25B3.3p::Q$_{67}$::CFP) *(integrated)*	CGC
DA2123/CL2006	adIs2122 (lgg-1p::GFP::lgg-1 + rol-6(su1006)) / (dvIs2 (pCL12(unc-54:hu-Aβ 1–42) + pRF4)) *(integrated)*	Kirstein lab
DA2123/AM1066	adIs2122 (lgg-1p::GFP::lgg-1 + rol-6(su1006)) / rmIs350 (unc-54p::Q$_{40}$:: RFP) *(integrated)*	Kirstein lab

YD3/CL2006	xzEx3 (Punc-54::UbG76V::Dendra2) / (dvIs2 (pCL12(unc-54:hu-Aβ 1–42) + pRF4)) *(non integrated)*	Kirstein lab
YD3/CL2355	xzEx3 (Punc-54::UbG76V::Dendra2) / smg-1ts (cc546); snb-1::Aβ1−42::long 3′-UTR) *(non integrated)*	Kirstein lab
YD3/AM44	xzEx3 (Punc-54::UbG76V::Dendra2) / rmIs190 (F25B3.3p::Q_{67}::CFP) *(non integrated)*	Kirstein lab
YD12/CL2006	xzEx12 (PF25B3.3::UbG76V::Dendra2) / (dvIs2 (pCL12(unc-54:hu-Aβ 1–42) + pRF4)) *(non integrated)*	Kirstein lab
YD12/CL2355	xzEx12 (PF25B3.3::UbG76V::Dendra2) / smg-1ts (cc546); snb-1::Aβ1−42::long 3′-UTR) *(non integrated)*	Kirstein lab
MAH240	sqIs17 (hlh-30p::hlh-30::GFP + rol-6(su1006) *(integrated)*	CGC
RT476	wIs170 (vha6p::GFP::rab-7 + Cbr-unc-119(+)) *(integrated)*	CGC
RT258	pwIs50 (lmp-1::GFP + Cbr-unc-119(+)) *(integrated)*	CGC
N2	*Wild type*	CGC

6.1.10 Mammalian cell lines

Strain name	Description	Source
HEK293 cells	Human embryonic kidney cells 293	Claudia Rutz (FMP, Berlin, Germany)
HEK293 cells (FlucDM)	Human embryonic kidney cells 293 stable expressing FlucDM-GFP	FU Hartl (MPI, Martinsried, Germany)

6.1.11 Bacterial strains and RNAi clones

Strain – application	Genotype
E. coli OP50 – food source	*E. coli* (Uracil auxotroph)
E. coli HT115(DE3) – RNAi	*E. coli* [F-, mcrA, mcrB, IN(rrnD-rrnE)1, rnc14::Tn10(DE3 lysogen: lavUV5 promoter -T7 polymerase].

RNAi clones	Library
hsp-1	Ahringer library
hsp-110	Ahringer library
dnj-12	Ahringer library
dnj-13	Ahringer library
dnj-19	Ahringer library
hsp-16.41	Kirstein lab
hsp-17	Kirstein lab
L4440	Ahringer library
lgg-1	Ahringer library
pas-5	Ahringer library
sqst-1/p62	Ahringer library

6.1.12 DNA and siRNA plasmids

DNA	Source
UbG76V-GFP	Katrin Juenemann (FMP, Berlin, Germany)
GFP	Katrin Juenemann (FMP, Berlin, Germany)
HttExon1Q$_{25}$-GFP	Katrin Juenemann (FMP, Berlin, Germany)

HttExon1Q$_{97}$-GFP   Katrin   Juenemann   (FMP,
                            Berlin, Germany)

siRNA	Description	Company
dnaja1	siGENOME SMARTpool	Dharmacon/Horizon, Colorado, United States
dnaja2	siGENOME SMARTpool	Dharmacon/Horizon, Colorado, United States
dnajb1	siGENOME SMARTpool	Dharmacon/Horizon, Colorado, United States
hspa4	siGENOME SMARTpool	Dharmacon/Horizon, Colorado, United States
hspa8	siGENOME SMARTpool	Dharmacon/Horizon, Colorado, United States
Non-targeting	siGENOME SMARTpool (Pool #1)	Dharmacon/Horizon, Colorado, United States
Non-targeting	siGENOME (#3, for FlucDM experiments)	Dharmacon/Horizon, Colorado, United States

6.1.13 Software and online tools

Software	Name	Company
Bradford Detection	Tecan I-control	Tecan, Männedorf, Switzerland
Data analysis	Excel v14.0.7182.5000	Microsoft
DNA/RNA detection	GeneSys v1.3.1	Syngene, Cambridge, UK
Image analysis	Fiji v2.0.0-rc41	Schindelin et al.
Microscopy	Zen 2010B SP1 v6.0	Zeiss, Oberkochen, Germany
Orthologe prediction	Blastp	NCBI, Bethesda, USA

PCR target Tm	DINAMELT (Markham et al. 2005)	The RNA Institute
Primer design	Primer3 v3	Untergasser et al.
Primer specificity	Primer Blast	NCBI, Bethesda, USA
qRT-PCR 48 well	Stepone Software v2.0	Thermo Fisher Scientific, Waltham, USA
qRT-PCR 96 well	Stepone Software v2.3	Thermo Fisher Scientific, Waltham, USA
WB detection	LumiAnalyst 3.0	Boehringer Mannheim
WB detection	Image Studio v4.0.21	LI-COR, Lincoln, USA

6.2 Methods

6.2.1 C. elegans maintenance

Nematode strains were kept at 15°C on NGM 60 mm plates seeded with *E. coli* OP50 strain for maintenance. To avoid starvation, five to ten animals were placed onto new plates weekly. Animals were kept either on 100 mm, 60 mm or 35 mm NGM-plates or RNAi plates seeded with OP50 or HT115 (DE3) strains (RNAi), respectively, which is indicated in the respective section.

To synchronize nematodes for experiments, adult animals were placed on NGM-plates seeded with OP50 to lay eggs. After, adults were washed from the plate with 1x M9, and the eggs were kept on the plate to hatch at 20°C overnight. On the next day, L1 larvae were collected and used for the indicated experiment.

For aging experiments, progeny needs to be separated from the older animals. Thus, animals were transferred onto new plates from day 4 on until their day of harvest. Picking of individual nematodes was performed with a platinum wire fixed onto a glass pipette. Wires were sterilized by heat and equipped with OP50 (glue), prior to picking.

When a high number of animals was required (such as for the proteasome activity assay), nematodes were grown on several 100 mm plates with the indicated food source. To separate the offspring, animals were washed from the plate with 1x M9 and transferred to 15 or 50 ml tubes and separated from larvae by sedimentation from day 4 on. For further growth, animals were transferred to new 100 mm plates.

6.2.1.1 C. elegans male generation and crossing

Young adult hermaphrodites were incubated at 30°C for 8 h on 60 mm OP50 seeded NGM plates. Animals were grown to lay eggs at 20°C and offspring were scored for male nematodes.

To generate the following crosses: DA2123/CL2006, DA2123/AM1066, YD3/CL2006, YD3/CL2355, YD3/AM44, YD12/CL2006, YD12/CL2355 - 9 males of one of the strains and 1 L4 larvae of the other strain were transferred

to a 35mm OP50 seeded NGM plate at 20°C for mating. The correct phenotypes were screened in the next generations.

6.2.1.2 RNA interference in C. elegans

Synchronized animals were placed onto RNAi plates that were seeded with *E. coli* expressing dsRNAi against *hsp-1*, *hsp-110*, *hsp-16.41*, *hsp-17*, *dnj-12*, *dnj-13,* and *dnj-19* or the empty vector L4440 as a control. The *pas-5* knockdown was performed as described (Hamer et al. 2010). Depletion of *pas-5* leads to developmental arrest if animals are treated from the L1 stage on. To overcome this developmental arrest, animals were grown on OP50 seeded NGM plates until the early L4 stage and then transferred to *pas-5* RNAi plates for 72 h.

6.3   Cell culture maintenance

HEK293 cells were grown in 100 mm dishes and maintained in DMEM medium (Gibco) supplemented with 10% fetal calf serum, 1 mM glutamine (Gibco), 100 U/ml penicillin (Gibco), and 100 µg/ml streptomycin (Gibco) at 37°C supplied 5% CO_2. To avoid starvation, cells were dissociated from the plate with 1x trypsin-EDTA (Gibco) and then splitted into new 100 mm plates once a week.

6.3.1   Transfection

For siRNA-mediated knockdown, cells were seeded with an equal cell number in 6-well plate format for 24 h. Then cells were transfected with siGENOME SMARTpool (Dharmacon/Horizon) DNAJB1 siRNA, HSPA4 siRNA, DNAJA1 siRNA, DNAJA2 siRNA and HSPA8 siRNA in a final concentration of 50 nM. Non-targeting siRNA (Dharmacon/Horizon) was used as negative control. Cells were transfected twice with siRNA (24 and 48 h before harvest).

To assess the autophagic flux, cells were treated with 200 nM Bafilomycin A1 (Sigma-Aldrich) 4 h before harvest.

To analyze the degradation rates of UbG76V, cells were transfected with 2 µg plasmid-DNA of UbG76V-GFP cloned into the pEGFP-N1 vector that was previously described (Juenemann et al., 2013) for 24 h. As a positive control, cells were incubated with 20 µM MG-132 (Sigma-Aldrich) 4 h before harvest.

In order to analyze the impact of polyglutamine aggregates on proteasomal function, cells were transfected with 2 µg plasmid-DNA of GFP, HttExon1Q$_{25}$-GFP, and HttExon1Q$_{97}$-GFP 24 h prior cell harvest.

For transfection experiments, cells were transfected with jetPRIME (Polyplus-transfection) according to the manufacturer's instructions.

After 48 h cells were harvested into a 15 mL tube and washed 2x with 1mL of 1x PBS. The samples were analyzed as described in the following sections.

6.3.2 Live cell imaging of luciferase aggregates

Stable HEK293 cells expressing FlucDM-GFP (Raychaudhuri et al. 2014) were seeded in fluorobrite DMEM medium (Gibco) in an 8-well glass bottom plate (Ibidi) coated with poly L-lysine (Sigma). Then cells were transfected with siRNA (as described above), and imaged with a 40x objective for 48 h in a CSU microscope (Nikon) supplied with 5% CO$_2$ at 37°C. As a positive control, cells were treated with 20 µM MG-132 (Sigma-Aldrich) and DMSO was used as a control.

6.3.3 Luciferase activity

For luminescence activity experiments, stable HEK293 cells expressing FlucDM-GFP (Raychaudhuri et al. 2014) were seeded in 24 well-plates for 24 h and then treated with the indicated siRNA. As a positive control, cells were treated with 20 µM MG-132 (Sigma-Aldrich), and DMSO was used as a control.

To measure luciferase activity, the medium was removed from the wells and cells were incubated with 200 µL Steady-Glo Luciferase mix (Promega) in the indicated time point in the dark at room temperature (25°C) for 10 min. Then 50 µL (duplicates) of the reaction mix was transferred to a 96-well plate (white, bottom white) appropriated for luminescence measurements. Luminescence was recorded in a plate reader (Tecan Safire), and the signal was acquired for 1 sec at 25ºC.

6.4 Protein isolation

6.4.1 C. elegans

Briefly, 50 animals were washed three times with 1x M9, and the pellets were frozen in liquid nitrogen. Then 2x Laemmli loading buffer (50 mM Tris-HCl pH 6.8, 2% SDS, 15% glycerol, 100 mM DTT, 0.1% bromphenol-blue) was added to the samples and incubated with shaking for 10 min at 100°C. Prior to SDS-PAGE separation, the samples were centrifuged at 5000 rpm for 5 min.

6.4.2 HEK293 cells

Cells were harvested in lysis buffer (50 mM Tris/HCl pH 7.4, 150 mM NaCl, 1 mM EDTA, 1 % Triton-X100, supplemented with complete mini protease inhibitor cocktail (Roche)) and incubated for 30 min on ice. Prior to SDS-PAGE, 30 μg of protein were boiled for 5 min with 6x Laemmli loading buffer (350mM Tris-HC pH 6.8, 10% SDS, 30% glycerol, 6% β-Mercaptoethanol, 0.3% bromphenol-blue).

6.4.3 Western Blot

A total protein lysate of *C. elegans* or HEK293 cells was separated in an SDS-PAGE and transferred to a PVDF membrane (Trans-blot Turbo system, Bio-Rad). After blocking the PVDF membrane with 5% milk in TBST, the blots were incubated with the following primary antibodies: anti-α-tubulin (1:2000 in 3% milk/TBST, Sigma), anti-HSP-1 / HSP-110 / DNJ-12 / DNJ-13 / DNJ-19 (1:5000 in 3% milk/TBST, Kirstein lab), anti-DNAJB1 1:1000 in 3% milk/TBST), anti-20S α-subunits (1:1000 in 1% BSA/TBST, Enzo), anti-LGG-1 / SQST-1/p62 (1:1000 in 3% milk/TBST, Kirstein lab) and anti-LC3 (1:1000 in 3% milk/TBST, Abcam). The secondary antibodies used were: anti-mouse / rabbit HRP (1:10000 / 1:15000 in 3% milk/TBST, Thermo Fisher) or anti-mouse-Cy3 antibody (1:10000 in 3%milk/TBST, Licor). The western blot images were acquired in a Lumi-Imager F1 (Boehringer) for HRP detection and in an Odyssey Imaging System (Licor) for Cy3 detection.

The adjustments of brightness and contrast were done in Adobe Photoshop

(equal modifications were done for the same experiment), and the relative protein amounts (normalized to α-Tubulin) were quantified with Fiji ImageJ software.

6.4.4 Antibody generation

The HSP-17 antibody was generated by immunizing rabbits with the purified protein, and the LGG-1 and SQST-1/p62 antibodies were generated by immunizing rabbits with a correspondent synthetic peptide (Pineda, Germany). For LGG-1 the peptide: PKSKLHDLDKKKYL was used and for SQST-1/p62 the peptide: AVPKPAQEPRIPPSPTSALPPPQFFN.

6.5 Compound treatment in *C. elegans*

The nematodes were treated with 0.2% DMSO (Carl Roth), 200 µM of rapamycin (Sigma), 10 mM chloroquine (Cell Signaling) and 10 mM of 3-methyladenine (Sigma) in 1xM9 buffer supplemented with OP50 for 18 h in a 96-well plate at 20°C. To stain the lysosome pool, animals were incubated with 2 µM LysoTracker-Red DND-99 (Thermo Fisher) using the same conditions as described above.

6.6 Microscope imaging

To image the animals, glass slides with 2% agarose (Bio & Sell) and 0.1% NaN$_3$ (Carl Roth) in 1x M9 were freshly prepared. The nematodes were mounted onto the agarose pads and then imaged. The strains RT258, MAH240 and the LysoTracker-Red stained animals were imaged in an EPI-TIRF microscope (Nikon) with a 4x objective. The RT476, DA2123 (mounted on 2% agarose with 2 mM levamisole (Sigma)) and YD3/YD12 (the experimental set-up is described below) strains were imaged using a confocal microscope LSM710 (Zeiss) with 10x or 20x objectives.

Brightness and contrast of images were adjusted equally between the different conditions. Due to high fluorescence intensity, some images were edited separately: in figure 3.3 A - *hsp-1* RNAi images were edited less for brightness

adjustments due to the high fluorescence intensity; in figure 3.8 A – day 10 images were edited less for brightness adjustments compared to day 4, due to the high fluorescence intensity, in addition day 10 *hsp-1* RNAi image were edited less for brightness adjustment compared to the other knockdowns due to the high fluorescence intensity. Fluorescent intensities of RT258, RT476, and LysoTracker-Red stained animals were determined for each animal (fluorescence was normalized to the area of animal) with Fiji ImageJ software.

6.7 Proteasome capacity

6.7.1 UbG76V levels - C. elegans and HEK293 cells

The YD3 and YD12 strains were used to measure the degradation rates of UbG76V::Dendra2. The photoconversion was performed as described previously (Hamer et al. 2010). Briefly, day 4/7 animals were mounted on 3% agarose pads with 0.5 mM levamisole. Photoconversion and imaging were performed using a LSM710 microscope. After imaging, nematodes were recovered on the respective feeding plate and imaged 3 (YD12) or 24 (YD3) hours later. The UbG76V::Dendra2 fluorescence was quantified with Fiji ImageJ software.

A similar approach was used for HEK293 cells. As described above, HEK293 cells were transfected with UbG76V-GFP, and the UbG76V-GFP levels were measured by western blot.

6.7.2 Chymotrypsin-like activity – C. elegans and HEK293 cells

Proteasome activity assay was performed as previously described (Kisselev et al. 2005, Vilchez et al. 2012). Animals were lysed using a Precellys 24 homogenizer (Bertin Technologies) in lysis buffer (20 mM HEPES, 110 mM KAc, 2 mM $MgAc_2$, 100 µM Digitonin). Protein concentration was determined by Bradford assay (Roti-Quant, Carl Roth) and 25 µg of protein was incubated with 100 µM of Suc-LLVY-AMC (Enzo) in a 96-well plate (Corning). As a positive control, 50 µM of MG-132 (Sigma) was incubated with 25 µg of lysate for 30 min on ice before the addition of Suc-LLVY-AMC. A plate reader (Tecan Safire) was used to monitor the fluorescence (380ex/460em) with measurements every 5

min for 2 h at 25°C. Each measurement for each condition was performed in duplicates.

A similar experimental procedure was applied for HEK293 cells. Some adjustments were done, 10 µg of protein were used in the experiments and the measurements were performed at 37°C. For proteasome inhibition, 20 µM of MG-132 was incubated with 10 µg of protein.

The slope (in the linear phase) was used to calculate the relative activities and then normalized to the control condition.

6.8   Electron microscopy and correlative-light electron microscopy

Nematodes were cryofixed by high pressure freezing using the HPM100 instrument in bacteria (OP50) for cryoprotection. For CLEM, nematodes were freeze substituted (FS) in acetone plus 0,1% uranyl acetate, 0,1% tannic acid, 0,05% glutaraldehyde, 0,5% H_2O (at -90 C). Following FS, animals were washed in pure acetone and infiltrated with HM20 resin/acetone mixes (1:2; 1:1; 2:1) and pure HM20 changes 2 h each plus pure HM20 last change overnight (all steps were carried out at -45°C). UV induced polymerization was done for 72 h (-45 to -5°C).

FS program: 5 h -90°C; 9 h increase from -90 to -45 (5°C per h); 24 h -45°C; 48 h -45 plus UV light; 8,5 h increase from -45 to -5 plus UV light; -5°C 16 h plus UV light.

Polymerized blocks where trimmed and ultrathin sectioned onto the Finder grids (Plano). After DAPI staining, grids were positioned into the imaging chamber in PBS/glycerol (10%) solution. Sections were imaged with LSM800 equipped with an AIRYscan detector. Retrieved grids were contrasted with uranyl acetate and lead citrate and imaged at Zeiss 900 microscope. DAPI specific (nuclei, bacteria) and cytoplasmic background staining were used to correlate LSM images with EM images.

For regular Epoxy embedding, nematodes were freeze substituted in acetone, 1% osmium, 0,1% uranyl acetate, 0,1% glutaraldehyde (FS program from -90°C to 0°C in 36 h). After FS, nematodes were washed in 100% acetone and infiltrated with Epoxy resin/acetone (1:2; 1:1; 2:1) followed by changes of pure Epoxy resin and polymerization at 60°C.

6.9   Relative mRNA quantification

6.9.1   RNA isolation

Total RNA was extracted with TRIzol reagent (Invitrogen). Adult animals (day 4 and older) were dissolved in 250 µl TRIzol, vortexed for 1 min and 20 min at room temperature and 4°C, respectively, and incubated for 12 min on ice. After the addition of 50 µl chloroform, the samples were inverted for 15 sec and incubated for 3 min at room temperature. For further phase separation, samples were centrifuged at 12 000 rpm for 15 min at 4°C. RNA from the aqueous phase was mixed with 300 µl of 70% ethanol and was purified using NucleoSpin®RNA kit (Macherey-Nagel) according to manufacturer's instructions. The quality of the isolated RNA was evaluated by agarose gel electrophoresis and measurements of the 260/280 nm as well as 260/230 nm absorption ratios (Desjardins et al. 2010).

6.9.2   cDNA synthesis

500 ng of RNA were reverse transcribed using Maxima First Strand cDNA Synthesis Kit for qRT-PCR (Thermo Scientific). For control, samples without the reverse transcriptase enzyme, 250 ng RNA were used in 10 µl aliquots.

6.9.3   Primer design and validation

Primers for qRT-PCR were designed using the Primer3 software and tested for specificity and amplicon secondary structures using NCBI primer blast, DINAMelt Web Server, melting curves and agarose gel electrophoresis of PCR products (Markham et al. 2005, Thornton et al. 2011). In order to use the 2-ΔΔCt method, amplification efficiencies of the gene of interest (GOI) and the reference gene (RG) have to be equal. Suitable primer concentrations for the 2-ΔΔCt method were validated by dilution series of different cDNA amounts (undiluted to 1:1000-fold) of mixed cDNA samples (Livak et al. 2001). Primer concentrations were defined as suitable if the slope of ΔCt (CTgoi-CTref) vs. log (cDNA) was less than 0.1 (absolute value) (QIAGEN 2010).

6.9.4 qRT-PCR

Quantitative RT-PCR was performed using Luminaris Color HiGreen High ROX qPCR Master Mix (Thermo Scientific) in 20 µl reactions. 2 µl of a 1:10 diluted cDNA solution were analyzed in a two-step cycling protocol according to manufacturer's instruction of the Master Mix with a StepOneTM Real-Time PCR System and StepOneTM Software version 2.0 as well as StepOnePlusTM Real-Time PCR System and StepOneTM Software version 2.3 (Applied Biosystem, life technologies). Relative expression of GOI mRNA expression was calculated with the 2-ΔΔCt-method (Livak et al. 2001). Ct-value duplicates were measured in three independent batches and averages of the duplicates were referred to the internal control *cdc-42* to obtain ΔCt. Averaged ΔCt values (3 batches) were normalized to average ΔCt of control samples to obtain ΔΔCt. Standard deviations were calculated from the ΔCt values of the three different batches. Fold changes were obtained by the formula: relative mRNA level = 2-(ΔΔCt SDΔC). In case of high expressional variation within the same sample in three independent batches, relative mRNA levels of the individual batches were averaged.

6.10 Statistical analysis

The data was analyzed with ANOVA to test for statistical significance. p values <0.05 were considered significant: p<0,05 (*), <0,01(**), <0,001 (***).

7   References

Desjardins, P. and D. Conklin (2010). NanoDrop microvolume quantitation of nucleic acids. J Vis Exp(45).

Hamer, G., O. Matilainen and C. I. Holmberg (2010). A photoconvertible reporter of the ubiquitin-proteasome system in vivo. Nat Methods **7**(6): 473-478.

Kisselev, A. F. and A. L. Goldberg (2005). Monitoring activity and inhibition of 26S proteasomes with fluorogenic peptide substrates. Methods Enzymol **398**: 364-378.

Livak, K. J. and T. D. Schmittgen (2001). Analysis of relative gene expression data using real-time quantitative PCR and the 2(-Delta Delta C(T)) Method. Methods **25**(4): 402-408.

Raychaudhuri, S., C. Loew, R. Korner, S. Pinkert, M. Theis, M. Hayer-Hartl, F. Buchholz and F. U. Hartl (2014). Interplay of acetyltransferase EP300 and the proteasome system in regulating heat shock transcription factor 1. Cell **156**(5): 975-985.

Thornton, B. and C. Basu (2011). Real-time PCR (qPCR) primer design using free online software. Biochem Mol Biol Educ **39**(2): 145-154.

Vilchez, D., I. Morantte, Z. Liu, P. M. Douglas, C. Merkwirth, A. P. Rodrigues, G. Manning and A. Dillin (2012). RPN-6 determines C. elegans longevity under proteotoxic stress conditions. Nature **489**(7415): 263-268.

Agarraberes, F. A. and J. F. Dice (2001). A molecular chaperone complex at the lysosomal membrane is required for protein translocation. J Cell Sci **114**(Pt 13): 2491-2499.

Altun, M., H. C. Besche, H. S. Overkleeft, R. Piccirillo, M. J. Edelmann, B. M. Kessler, A. L. Goldberg and B. Ulfhake (2010). Muscle wasting in aged, sarcopenic rats is associated with enhanced activity of the ubiquitin proteasome pathway. J Biol Chem **285**(51): 39597-39608.

Altun, Z. F. a. H., D.H (2017). Handbook of C. elegans Anatomy WormAtlas.

Amm, I., T. Sommer and D. H. Wolf (2014). Protein quality control and elimination of protein waste: the role of the ubiquitin-proteasome system. Biochim Biophys Acta **1843**(1): 182-196.

Andrew, S. E., Y. P. Goldberg, B. Kremer, H. Telenius, J. Theilmann, S. Adam, E. Starr, F. Squitieri, B. Lin, M. A. Kalchman and et al. (1993). The relationship

between trinucleotide (CAG) repeat length and clinical features of Huntington's disease. Nat Genet **4**(4): 398-403.

Anfinsen, C. B. (1973). Principles that govern the folding of protein chains. Science **181**(4096): 223-230.

Anfinsen, C. B., E. Haber, M. Sela and F. H. White, Jr. (1961). The kinetics of formation of native ribonuclease during oxidation of the reduced polypeptide chain. Proc Natl Acad Sci U S A **47**: 1309-1314.

Ashkenazi, A., C. F. Bento, T. Ricketts, M. Vicinanza, F. Siddiqi, M. Pavel, F. Squitieri, M. C. Hardenberg, S. Imarisio, F. M. Menzies and D. C. Rubinsztein (2017). Polyglutamine tracts regulate beclin 1-dependent autophagy. Nature **545**(7652): 108-111.

Balchin, D., M. Hayer-Hartl and F. U. Hartl (2016). In vivo aspects of protein folding and quality control. Science **353**(6294): aac4354.

Bauerlein, F. J. B., I. Saha, A. Mishra, M. Kalemanov, A. Martinez-Sanchez, R. Klein, I. Dudanova, M. S. Hipp, F. U. Hartl, W. Baumeister and R. Fernandez-Busnadiego (2017). In Situ Architecture and Cellular Interactions of PolyQ Inclusions. Cell **171**(1): 179-187 e110.

Behrends, C., M. E. Sowa, S. P. Gygi and J. W. Harper (2010). Network organization of the human autophagy system. Nature **466**(7302): 68-76.

Ben-Zvi, A., E. A. Miller and R. I. Morimoto (2009). Collapse of proteostasis represents an early molecular event in Caenorhabditis elegans aging. Proc Natl Acad Sci U S A **106**(35): 14914-14919.

Bence, N. F., R. M. Sampat and R. R. Kopito (2001). Impairment of the ubiquitin-proteasome system by protein aggregation. Science **292**(5521): 1552-1555.

Bennett, E. J., N. F. Bence, R. Jayakumar and R. R. Kopito (2005). Global impairment of the ubiquitin-proteasome system by nuclear or cytoplasmic protein aggregates precedes inclusion body formation. Mol Cell **17**(3): 351-365.

Berg, T. O., M. Fengsrud, P. E. Stromhaug, T. Berg and P. O. Seglen (1998). Isolation and characterization of rat liver amphisomes. Evidence for fusion of autophagosomes with both early and late endosomes. J Biol Chem **273**(34): 21883-21892.

Bernadotte, A., V. M. Mikhelson and I. M. Spivak (2016). Markers of cellular senescence. Telomere shortening as a marker of cellular senescence. Aging (Albany NY) **8**(1): 3-11.

Bhat, K. P., S. Yan, C. E. Wang, S. Li and X. J. Li (2014). Differential ubiquitination and degradation of huntingtin fragments modulated by ubiquitin-protein ligase E3A. Proc Natl Acad Sci U S A **111**(15): 5706-5711.

Bhatia-Dey, N., R. R. Kanherkar, S. E. Stair, E. O. Makarev and A. B. Csoka (2016). Cellular Senescence as the Causal Nexus of Aging. Front Genet **7**: 13.

Bhattacharyya, S., H. Yu, C. Mim and A. Matouschek (2014). Regulated protein turnover: snapshots of the proteasome in action. Nat Rev Mol Cell Biol **15**(2): 122-133.

Bjedov, I., J. M. Toivonen, F. Kerr, C. Slack, J. Jacobson, A. Foley and L. Partridge (2010). Mechanisms of life span extension by rapamycin in the fruit fly Drosophila melanogaster. Cell Metab **11**(1): 35-46.

Bjorkoy, G., T. Lamark, A. Brech, H. Outzen, M. Perander, A. Overvatn, H. Stenmark and T. Johansen (2005). p62/SQSTM1 forms protein aggregates degraded by autophagy and has a protective effect on huntingtin-induced cell death. J Cell Biol **171**(4): 603-614.

Bloom, G. S. (2014). Amyloid-beta and tau: the trigger and bullet in Alzheimer disease pathogenesis. JAMA Neurol **71**(4): 505-508.

Bracher, A. and J. Verghese (2015). The nucleotide exchange factors of Hsp70 molecular chaperones. Front Mol Biosci **2**: 10.

Brenner, S. (1974). The genetics of Caenorhabditis elegans. Genetics **77**(1): 71-94.

Breusing, N., J. Arndt, P. Voss, N. Bresgen, I. Wiswedel, A. Gardemann, W. Siems and T. Grune (2009). Inverse correlation of protein oxidation and proteasome activity in liver and lung. Mech Ageing Dev **130**(11-12): 748-753.

Bulteau, A. L., L. I. Szweda and B. Friguet (2002). Age-dependent declines in proteasome activity in the heart. Arch Biochem Biophys **397**(2): 298-304.

Byerly, L., R. C. Cassada and R. L. Russell (1976). The life cycle of the nematode Caenorhabditis elegans. I. Wild-type growth and reproduction. Dev Biol **51**(1): 23-33.

Caniard, A., K. Ballweg, C. Lukas, A. O. Yildirim, O. Eickelberg and S. Meiners (2015). Proteasome function is not impaired in healthy aging of the lung. Aging (Albany NY) **7**(10): 776-792.

Carnini, A., L. O. Scott, E. Ahrendt, J. Proft, R. J. Winkfein, S. W. Kim, M. A. Colicos and J. E. Braun (2012). Cell line specific modulation of extracellular abeta42 by Hsp40. PLoS One **7**(5): e37755.

Cattaneo, E., C. Zuccato and M. Tartari (2005). Normal huntingtin function: an alternative approach to Huntington's disease. Nat Rev Neurosci **6**(12): 919-930.

Chang, J. T., C. Kumsta, A. B. Hellman, L. M. Adams and M. Hansen (2017). Spatiotemporal regulation of autophagy during Caenorhabditis elegans aging. Elife **6**.

Chapin, H. C., M. Okada, A. J. Merz and D. L. Miller (2015). Tissue-specific autophagy responses to aging and stress in C. elegans. Aging (Albany NY) **7**(6): 419-434.

Chen, X., Y. Bi, T. Wang, P. Li, X. Yan, S. Hou, C. E. Bammert, J. Ju, K. M. Gibson, W. J. Pavan and L. Bi (2015). Lysosomal targeting with stable and sensitive fluorescent probes (Superior LysoProbes): applications for lysosome labeling and tracking during apoptosis. Sci Rep **5**: 9004.

Chiti, F. and C. M. Dobson (2006). Protein misfolding, functional amyloid, and human disease. Annu Rev Biochem **75**: 333-366.

Chondrogianni, N., K. Georgila, N. Kourtis, N. Tavernarakis and E. S. Gonos (2015). 20S proteasome activation promotes life span extension and resistance to proteotoxicity in Caenorhabditis elegans. FASEB J **29**(2): 611-622.

Chudakov, D. M., S. Lukyanov and K. A. Lukyanov (2007). Tracking intracellular protein movements using photoswitchable fluorescent proteins PS-CFP2 and Dendra2. Nat Protoc **2**(8): 2024-2032.

Ciechanover, A. and P. Brundin (2003). The ubiquitin proteasome system in neurodegenerative diseases: sometimes the chicken, sometimes the egg. Neuron **40**(2): 427-446.

Codogno, P. and A. J. Meijer (2005). Autophagy and signaling: their role in cell survival and cell death. Cell Death Differ **12 Suppl 2**: 1509-1518.

Cohen-Kaplan, V., I. Livneh, N. Avni, B. Fabre, T. Ziv, Y. T. Kwon and A. Ciechanover (2016). p62- and ubiquitin-dependent stress-induced autophagy of

the mammalian 26S proteasome. Proc Natl Acad Sci U S A **113**(47): E7490-E7499.

Collins, G. A. and A. L. Goldberg (2017). The Logic of the 26S Proteasome. Cell **169**(5): 792-806.

Consortium, C. e. S. (1998). Genome sequence of the nematode C. elegans: a platform for investigating biology. Science **282**(5396): 2012-2018.

Cook, C., J. Gass, J. Dunmore, J. Tong, J. Taylor, J. Eriksen, E. McGowan, J. Lewis, J. Johnston and L. Petrucelli (2009). Aging is not associated with proteasome impairment in UPS reporter mice. PLoS One **4**(6): e5888.

Craig, E. A. and J. Marszalek (2017). How Do J-Proteins Get Hsp70 to Do So Many Different Things? Trends Biochem Sci **42**(5): 355-368.

Cuervo, A. M. and E. Wong (2014). Chaperone-mediated autophagy: roles in disease and aging. Cell Res **24**(1): 92-104.

Dantuma, N. P., K. Lindsten, R. Glas, M. Jellne and M. G. Masucci (2000). Short-lived green fluorescent proteins for quantifying ubiquitin/proteasome-dependent proteolysis in living cells. Nat Biotechnol **18**(5): 538-543.

David, D. C., N. Ollikainen, J. C. Trinidad, M. P. Cary, A. L. Burlingame and C. Kenyon (2010). Widespread protein aggregation as an inherent part of aging in C. elegans. PLoS Biol **8**(8): e1000450.

De Duve, C., B. C. Pressman, R. Gianetto, R. Wattiaux and F. Appelmans (1955). Tissue fractionation studies. 6. Intracellular distribution patterns of enzymes in rat-liver tissue. Biochem J **60**(4): 604-617.

Demand, J., S. Alberti, C. Patterson and J. Hohfeld (2001). Cooperation of a ubiquitin domain protein and an E3 ubiquitin ligase during chaperone/proteasome coupling. Curr Biol **11**(20): 1569-1577.

Desjardins, P. and D. Conklin (2010). NanoDrop microvolume quantitation of nucleic acids. J Vis Exp(45).

Di Micco, R., A. Cicalese, M. Fumagalli, M. Dobreva, A. Verrecchia, P. G. Pelicci and F. di Fagagna (2008). DNA damage response activation in mouse embryonic fibroblasts undergoing replicative senescence and following spontaneous immortalization. Cell Cycle **7**(22): 3601-3606.

Diaz-Villanueva, J. F., R. Diaz-Molina and V. Garcia-Gonzalez (2015). Protein Folding and Mechanisms of Proteostasis. Int J Mol Sci **16**(8): 17193-17230.

Dorman, J. B., B. Albinder, T. Shroyer and C. Kenyon (1995). The age-1 and daf-2 genes function in a common pathway to control the lifespan of Caenorhabditis elegans. Genetics **141**(4): 1399-1406.

Dunn, W. A., Jr. (1990). Studies on the mechanisms of autophagy: maturation of the autophagic vacuole. J Cell Biol **110**(6): 1935-1945.

Duthey, B. (2013). A Public Health Aproach to Innovation - Alzheimer Disease an other Dementias. WHO.

Ellis, J. (1987). Proteins as molecular chaperones. Nature **328**(6129): 378-379.

Ellis, R. J. (2001). Macromolecular crowding: an important but neglected aspect of the intracellular environment. Curr Opin Struct Biol **11**(1): 114-119.

Ellis, R. J. and A. P. Minton (2006). Protein aggregation in crowded environments. Biol Chem **387**(5): 485-497.

Esser, C., S. Alberti and J. Hohfeld (2004). Cooperation of molecular chaperones with the ubiquitin/proteasome system. Biochim Biophys Acta **1695**(1-3): 171-188.

Faber, P. W., J. R. Alter, M. E. MacDonald and A. C. Hart (1999). Polyglutamine-mediated dysfunction and apoptotic death of a Caenorhabditis elegans sensory neuron. Proc Natl Acad Sci U S A **96**(1): 179-184.

Fader, C. M., D. Sanchez, M. Furlan and M. I. Colombo (2008). Induction of autophagy promotes fusion of multivesicular bodies with autophagic vacuoles in k562 cells. Traffic **9**(2): 230-250.

Fass, E., E. Shvets, I. Degani, K. Hirschberg and Z. Elazar (2006). Microtubules support production of starvation-induced autophagosomes but not their targeting and fusion with lysosomes. J Biol Chem **281**(47): 36303-36316.

Fourie, A. M., J. F. Sambrook and M. J. Gething (1994). Common and divergent peptide binding specificities of hsp70 molecular chaperones. J Biol Chem **269**(48): 30470-30478.

Friedman, D. B. and T. E. Johnson (1988). A mutation in the age-1 gene in Caenorhabditis elegans lengthens life and reduces hermaphrodite fertility. Genetics **118**(1): 75-86.

Gaczynska, M., K. L. Rock and A. L. Goldberg (1993). Role of proteasomes in antigen presentation. Enzyme Protein **47**(4-6): 354-369.

Gao, X., M. Carroni, C. Nussbaum-Krammer, A. Mogk, N. B. Nillegoda, A. Szlachcic, D. L. Guilbride, H. R. Saibil, M. P. Mayer and B. Bukau (2015).

Human Hsp70 Disaggregase Reverses Parkinson's-Linked alpha-Synuclein Amyloid Fibrils. Mol Cell **59**(5): 781-793.

Garsin, D. A., J. M. Villanueva, J. Begun, D. H. Kim, C. D. Sifri, S. B. Calderwood, G. Ruvkun and F. M. Ausubel (2003). Long-lived C. elegans daf-2 mutants are resistant to bacterial pathogens. Science **300**(5627): 1921.

Ghazi, A., S. Henis-Korenblit and C. Kenyon (2007). Regulation of Caenorhabditis elegans lifespan by a proteasomal E3 ligase complex. Proc Natl Acad Sci U S A **104**(14): 5947-5952.

Glover, J. R. and S. Lindquist (1998). Hsp104, Hsp70, and Hsp40: a novel chaperone system that rescues previously aggregated proteins. Cell **94**(1): 73-82.

Goldberg, A. L. (2003). Protein degradation and protection against misfolded or damaged proteins. Nature **426**(6968): 895-899.

Goldberg, Y. P., H. Telenius and M. R. Hayden (1994). The molecular genetics of Huntington's disease. Curr Opin Neurol **7**(4): 325-332.

Greene, M. K., K. Maskos and S. J. Landry (1998). Role of the J-domain in the cooperation of Hsp40 with Hsp70. Proc Natl Acad Sci U S A **95**(11): 6108-6113.

Greer, E. L. and A. Brunet (2008). Signaling networks in aging. J Cell Sci **121**(Pt 4): 407-412.

Gruber, A., D. Hornburg, M. Antonin, N. Krahmer, J. Collado, M. Schaffer, G. Zubaite, C. Luchtenborg, T. Sachsenheimer, B. Brugger, M. Mann, W. Baumeister, F. U. Hartl, M. S. Hipp and R. Fernandez-Busnadiego (2018). Molecular and structural architecture of polyQ aggregates in yeast. Proc Natl Acad Sci U S A.

Guisbert, E., D. M. Czyz, K. Richter, P. D. McMullen and R. I. Morimoto (2013). Identification of a tissue-selective heat shock response regulatory network. PLoS Genet **9**(4): e1003466.

Guo, J. L. and V. M. Lee (2014). Cell-to-cell transmission of pathogenic proteins in neurodegenerative diseases. Nat Med **20**(2): 130-138.

Guo, Q., C. Lehmer, A. Martinez-Sanchez, T. Rudack, F. Beck, H. Hartmann, M. Perez-Berlanga, F. Frottin, M. S. Hipp, F. U. Hartl, D. Edbauer, W. Baumeister and R. Fernandez-Busnadiego (2018). In Situ Structure of Neuronal C9orf72 Poly-GA Aggregates Reveals Proteasome Recruitment. Cell **172**(4): 696-705 e612.

Gupta, R., P. Kasturi, A. Bracher, C. Loew, M. Zheng, A. Villella, D. Garza, F. U. Hartl and S. Raychaudhuri (2011). Firefly luciferase mutants as sensors of proteome stress. Nat Methods **8**(10): 879-884.

Gusella, J. F. and M. E. MacDonald (1998). Huntingtin: a single bait hooks many species. Curr Opin Neurobiol **8**(3): 425-430.

Gutierrez, M. G., D. B. Munafo, W. Beron and M. I. Colombo (2004). Rab7 is required for the normal progression of the autophagic pathway in mammalian cells. J Cell Sci **117**(Pt 13): 2687-2697.

Hageman, J. and H. H. Kampinga (2009). Computational analysis of the human HSPH/HSPA/DNAJ family and cloning of a human HSPH/HSPA/DNAJ expression library. Cell Stress Chaperones **14**(1): 1-21.

Hamer, G., O. Matilainen and C. I. Holmberg (2010). A photoconvertible reporter of the ubiquitin-proteasome system in vivo. Nat Methods **7**(6): 473-478.

Hammack, L. J., K. Firestone, W. Chang and A. R. Kusmierczyk (2017). Molecular chaperones of the Hsp70 family assist in the assembly of 20S proteasomes. Biochem Biophys Res Commun **486**(2): 438-443.

Hansen, M., A. Chandra, L. L. Mitic, B. Onken, M. Driscoll and C. Kenyon (2008). A role for autophagy in the extension of lifespan by dietary restriction in C. elegans. PLoS Genet **4**(2): e24.

Hariharan, I. K. and D. A. Haber (2003). Yeast, flies, worms, and fish in the study of human disease. N Engl J Med **348**(24): 2457-2463.

Harman, D. (1956). Aging: a theory based on free radical and radiation chemistry. J Gerontol **11**(3): 298-300.

Harrison, D. E., R. Strong, Z. D. Sharp, J. F. Nelson, C. M. Astle, K. Flurkey, N. L. Nadon, J. E. Wilkinson, K. Frenkel, C. S. Carter, M. Pahor, M. A. Javors, E. Fernandez and R. A. Miller (2009). Rapamycin fed late in life extends lifespan in genetically heterogeneous mice. Nature **460**(7253): 392-395.

Hartl, F. U. (1996). Molecular chaperones in cellular protein folding. Nature **381**(6583): 571-579.

Hartl, F. U., A. Bracher and M. Hayer-Hartl (2011). Molecular chaperones in protein folding and proteostasis. Nature **475**(7356): 324-332.

Haslbeck, V., J. M. Eckl, C. J. Kaiser, K. Papsdorf, M. Hessling and K. Richter (2013). Chaperone-interacting TPR proteins in Caenorhabditis elegans. J Mol Biol **425**(16): 2922-2939.

Hershko, A., A. Ciechanover, H. Heller, A. L. Haas and I. A. Rose (1980). Proposed role of ATP in protein breakdown: conjugation of protein with multiple chains of the polypeptide of ATP-dependent proteolysis. Proc Natl Acad Sci U S A **77**(4): 1783-1786.

Heschl, M. F. and D. L. Baillie (1989). Characterization of the hsp70 multigene family of Caenorhabditis elegans. DNA **8**(4): 233-243.

Hipp, M. S., S. H. Park and F. U. Hartl (2014). Proteostasis impairment in protein-misfolding and -aggregation diseases. Trends Cell Biol **24**(9): 506-514.

Hipp, M. S., C. N. Patel, K. Bersuker, B. E. Riley, S. E. Kaiser, T. A. Shaler, M. Brandeis and R. R. Kopito (2012). Indirect inhibition of 26S proteasome activity in a cellular model of Huntington's disease. J Cell Biol **196**(5): 573-587.

Hoffmann, A., A. H. Becker, B. Zachmann-Brand, E. Deuerling, B. Bukau and G. Kramer (2012). Concerted action of the ribosome and the associated chaperone trigger factor confines nascent polypeptide folding. Mol Cell **48**(1): 63-74.

Holmberg, C. I., K. E. Staniszewski, K. N. Mensah, A. Matouschek and R. I. Morimoto (2004). Inefficient degradation of truncated polyglutamine proteins by the proteasome. EMBO J **23**(21): 4307-4318.

Honda, Y. and S. Honda (1999). The daf-2 gene network for longevity regulates oxidative stress resistance and Mn-superoxide dismutase gene expression in Caenorhabditis elegans. FASEB J **13**(11): 1385-1393.

Ikeda, H., M. Yamaguchi, S. Sugai, Y. Aze, S. Narumiya and A. Kakizuka (1996). Expanded polyglutamine in the Machado-Joseph disease protein induces cell death in vitro and in vivo. Nat Genet **13**(2): 196-202.

Iwata, A., J. C. Christianson, M. Bucci, L. M. Ellerby, N. Nukina, L. S. Forno and R. R. Kopito (2005). Increased susceptibility of cytoplasmic over nuclear polyglutamine aggregates to autophagic degradation. Proc Natl Acad Sci U S A **102**(37): 13135-13140.

Jiang, P. and N. Mizushima (2014). Autophagy and human diseases. Cell Res **24**(1): 69-79.

Johansen, T. and T. Lamark (2011). Selective autophagy mediated by autophagic adapter proteins. Autophagy **7**(3): 279-296.

Juenemann, K., S. Schipper-Krom, A. Wiemhoefer, A. Kloss, A. Sanz Sanz and E. A. Reits (2013). Expanded polyglutamine-containing N-terminal huntingtin

fragments are entirely degraded by mammalian proteasomes. J Biol Chem **288**(38): 27068-27084.

Kabeya, Y., N. Mizushima, T. Ueno, A. Yamamoto, T. Kirisako, T. Noda, E. Kominami, Y. Ohsumi and T. Yoshimori (2000). LC3, a mammalian homologue of yeast Apg8p, is localized in autophagosome membranes after processing. EMBO J **19**(21): 5720-5728.

Kampinga, H. H. and E. A. Craig (2010). The HSP70 chaperone machinery: J proteins as drivers of functional specificity. Nat Rev Mol Cell Biol **11**(8): 579-592.

Kang, C., Y. J. You and L. Avery (2007). Dual roles of autophagy in the survival of Caenorhabditis elegans during starvation. Genes Dev **21**(17): 2161-2171.

Kaushik, S. and A. M. Cuervo (2015). Proteostasis and aging. Nat Med **21**(12): 1406-1415.

Keller, J. N., F. F. Huang and W. R. Markesbery (2000). Decreased levels of proteasome activity and proteasome expression in aging spinal cord. Neuroscience **98**(1): 149-156.

Kenyon, C., J. Chang, E. Gensch, A. Rudner and R. Tabtiang (1993). A C. elegans mutant that lives twice as long as wild type. Nature **366**(6454): 461-464.

Kenyon, C. J. (2010). The genetics of ageing. Nature **464**(7288): 504-512.

Kim, J., M. Kundu, B. Viollet and K. L. Guan (2011). AMPK and mTOR regulate autophagy through direct phosphorylation of Ulk1. Nat Cell Biol **13**(2): 132-141.

Kim, Y. E., M. S. Hipp, A. Bracher, M. Hayer-Hartl and F. U. Hartl (2013). Molecular chaperone functions in protein folding and proteostasis. Annu Rev Biochem **82**: 323-355.

Kirstein, J., K. Arnsburg, A. Scior, A. Szlachcic, D. L. Guilbride, R. I. Morimoto, B. Bukau and N. B. Nillegoda (2017). In vivo properties of the disaggregase function of J-proteins and Hsc70 in Caenorhabditis elegans stress and aging. Aging Cell **16**(6): 1414-1424.

Kirstein-Miles, J., A. Scior, E. Deuerling and R. I. Morimoto (2013). The nascent polypeptide-associated complex is a key regulator of proteostasis. EMBO J **32**(10): 1451-1468.

Kisselev, A. F. and A. L. Goldberg (2005). Monitoring activity and inhibition of 26S proteasomes with fluorogenic peptide substrates. Methods Enzymol **398**: 364-378.

Kityk, R., M. Vogel, R. Schlecht, B. Bukau and M. P. Mayer (2015). Pathways of allosteric regulation in Hsp70 chaperones. Nat Commun **6**: 8308.

Klein, A. M., N. W. Kowall and R. J. Ferrante (1999). Neurotoxicity and oxidative damage of beta amyloid 1-42 versus beta amyloid 1-40 in the mouse cerebral cortex. Ann N Y Acad Sci **893**: 314-320.

Klionsky, D. J., J. M. Cregg, W. A. Dunn, Jr., S. D. Emr, Y. Sakai, I. V. Sandoval, A. Sibirny, S. Subramani, M. Thumm, M. Veenhuis and Y. Ohsumi (2003). A unified nomenclature for yeast autophagy-related genes. Dev Cell **5**(4): 539-545.

Kriegenburg, F., L. Ellgaard and R. Hartmann-Petersen (2012). Molecular chaperones in targeting misfolded proteins for ubiquitin-dependent degradation. FEBS J **279**(4): 532-542.

Kruegel, U., B. Robison, T. Dange, G. Kahlert, J. R. Delaney, S. Kotireddy, M. Tsuchiya, S. Tsuchiyama, C. J. Murakami, J. Schleit, G. Sutphin, D. Carr, K. Tar, G. Dittmar, M. Kaeberlein, B. K. Kennedy and M. Schmidt (2011). Elevated proteasome capacity extends replicative lifespan in Saccharomyces cerevisiae. PLoS Genet **7**(9): e1002253.

Kumar, D. P., C. Vorvis, E. B. Sarbeng, V. C. Cabra Ledesma, J. E. Willis and Q. Liu (2011). The four hydrophobic residues on the Hsp70 inter-domain linker have two distinct roles. J Mol Biol **411**(5): 1099-1113.

Kumsta, C., J. T. Chang, J. Schmalz and M. Hansen (2017). Hormetic heat stress and HSF-1 induce autophagy to improve survival and proteostasis in C. elegans. Nat Commun **8**: 14337.

Labbadia, J. and R. I. Morimoto (2015). The biology of proteostasis in aging and disease. Annu Rev Biochem **84**: 435-464.

Lai, C. H., C. Y. Chou, L. Y. Ch'ang, C. S. Liu and W. Lin (2000). Identification of novel human genes evolutionarily conserved in Caenorhabditis elegans by comparative proteomics. Genome Res **10**(5): 703-713.

Lapierre, L. R., C. D. De Magalhaes Filho, P. R. McQuary, C. C. Chu, O. Visvikis, J. T. Chang, S. Gelino, B. Ong, A. E. Davis, J. E. Irazoqui, A. Dillin and

M. Hansen (2013). The TFEB orthologue HLH-30 regulates autophagy and modulates longevity in Caenorhabditis elegans. Nat Commun **4**: 2267.

Lapointe, J. and S. Hekimi (2008). Early mitochondrial dysfunction in long-lived Mclk1+/- mice. J Biol Chem **283**(38): 26217-26227.

Lapointe, J., Z. Stepanyan, E. Bigras and S. Hekimi (2009). Reversal of the mitochondrial phenotype and slow development of oxidative biomarkers of aging in long-lived Mclk1+/- mice. J Biol Chem **284**(30): 20364-20374.

Laufen, T., M. P. Mayer, C. Beisel, D. Klostermeier, A. Mogk, J. Reinstein and B. Bukau (1999). Mechanism of regulation of hsp70 chaperones by DnaJ cochaperones. Proc Natl Acad Sci U S A **96**(10): 5452-5457.

Lawrence, B. P. and W. J. Brown (1992). Autophagic vacuoles rapidly fuse with pre-existing lysosomes in cultured hepatocytes. J Cell Sci **102 (Pt 3)**: 515-526.

Lee, D. H. and A. L. Goldberg (1996). Selective inhibitors of the proteasome-dependent and vacuolar pathways of protein degradation in Saccharomyces cerevisiae. J Biol Chem **271**(44): 27280-27284.

Lemmon, M. A. and J. Schlessinger (2010). Cell signaling by receptor tyrosine kinases. Cell **141**(7): 1117-1134.

Levy, M. Z., R. C. Allsopp, A. B. Futcher, C. W. Greider and C. B. Harley (1992). Telomere end-replication problem and cell aging. J Mol Biol **225**(4): 951-960.

Li, L., X. Zhang and W. Le (2008). Altered macroautophagy in the spinal cord of SOD1 mutant mice. Autophagy **4**(3): 290-293.

Li, W. W., J. Li and J. K. Bao (2012). Microautophagy: lesser-known self-eating. Cell Mol Life Sci **69**(7): 1125-1136.

Lin, M. G. and Q. Zhong (2011). Interaction between small GTPase Rab7 and PI3KC3 links autophagy and endocytosis: A new Rab7 effector protein sheds light on membrane trafficking pathways. Small GTPases **2**(2): 85-88.

Lindquist, S. (1986). The heat-shock response. Annu Rev Biochem **55**: 1151-1191.

Lindquist, S. and G. Kim (1996). Heat-shock protein 104 expression is sufficient for thermotolerance in yeast. Proc Natl Acad Sci U S A **93**(11): 5301-5306.

Link, C. D. (1995). Expression of human beta-amyloid peptide in transgenic Caenorhabditis elegans. Proc Natl Acad Sci U S A **92**(20): 9368-9372.

Link, C. D., A. Taft, V. Kapulkin, K. Duke, S. Kim, Q. Fei, D. E. Wood and B. G. Sahagan (2003). Gene expression analysis in a transgenic Caenorhabditis elegans Alzheimer's disease model. Neurobiol Aging **24**(3): 397-413.

Lithgow, G. J., T. M. White, S. Melov and T. E. Johnson (1995). Thermotolerance and extended life-span conferred by single-gene mutations and induced by thermal stress. Proc Natl Acad Sci U S A **92**(16): 7540-7544.

Liu, G., J. Rogers, C. T. Murphy and C. Rongo (2011). EGF signalling activates the ubiquitin proteasome system to modulate C. elegans lifespan. EMBO J **30**(15): 2990-3003.

Liu, X., N. Jiang, B. Hughes, E. Bigras, E. Shoubridge and S. Hekimi (2005). Evolutionary conservation of the clk-1-dependent mechanism of longevity: loss of mclk1 increases cellular fitness and lifespan in mice. Genes Dev **19**(20): 2424-2434.

Livak, K. J. and T. D. Schmittgen (2001). Analysis of relative gene expression data using real-time quantitative PCR and the 2(-Delta Delta C(T)) Method. Methods **25**(4): 402-408.

Longatti, A. and S. A. Tooze (2009). Vesicular trafficking and autophagosome formation. Cell Death Differ **16**(7): 956-965.

Lopez Salon, M., L. Pasquini, M. Besio Moreno, J. M. Pasquini and E. Soto (2003). Relationship between beta-amyloid degradation and the 26S proteasome in neural cells. Exp Neurol **180**(2): 131-143.

Markaki, M. and N. Tavernarakis (2010). Modeling human diseases in Caenorhabditis elegans. Biotechnol J **5**(12): 1261-1276.

Markham, N. R. and M. Zuker (2005). DINAMelt web server for nucleic acid melting prediction. Nucleic Acids Research **33**(Web Server issue): W577-W581.

Marsden, I. T., L. S. Minamide and J. R. Bamburg (2011). Amyloid-beta-induced amyloid-beta secretion: a possible feed-forward mechanism in Alzheimer's Disease. J Alzheimers Dis **24**(4): 681-691.

Marshall, R. S., F. Li, D. C. Gemperline, A. J. Book and R. D. Vierstra (2015). Autophagic Degradation of the 26S Proteasome Is Mediated by the Dual ATG8/Ubiquitin Receptor RPN10 in Arabidopsis. Mol Cell **58**(6): 1053-1066.

Marshall, R. S., F. McLoughlin and R. D. Vierstra (2016). Autophagic Turnover of Inactive 26S Proteasomes in Yeast Is Directed by the Ubiquitin Receptor Cue5 and the Hsp42 Chaperone. Cell Rep **16**(6): 1717-1732.

Matilainen, O., L. Arpalahti, V. Rantanen, S. Hautaniemi and C. I. Holmberg (2013). Insulin/IGF-1 signaling regulates proteasome activity through the deubiquitinating enzyme UBH-4. Cell Rep **3**(6): 1980-1995.

Mayer, M. P. (2013). Hsp70 chaperone dynamics and molecular mechanism. Trends Biochem Sci **38**(10): 507-514.

Mayer, M. P. and B. Bukau (2005). Hsp70 chaperones: cellular functions and molecular mechanism. Cell Mol Life Sci **62**(6): 670-684.

Meijer, W. H., I. J. van der Klei, M. Veenhuis and J. A. Kiel (2007). ATG genes involved in non-selective autophagy are conserved from yeast to man, but the selective Cvt and pexophagy pathways also require organism-specific genes. Autophagy **3**(2): 106-116.

Melendez, A., Z. Talloczy, M. Seaman, E. L. Eskelinen, D. H. Hall and B. Levine (2003). Autophagy genes are essential for dauer development and life-span extension in C. elegans. Science **301**(5638): 1387-1391.

Melentijevic, I., M. L. Toth, M. L. Arnold, R. J. Guasp, G. Harinath, K. C. Nguyen, D. Taub, J. A. Parker, C. Neri, C. V. Gabel, D. H. Hall and M. Driscoll (2017). C. elegans neurons jettison protein aggregates and mitochondria under neurotoxic stress. Nature **542**(7641): 367-371.

Menzies, F. M., A. Fleming and D. C. Rubinsztein (2015). Compromised autophagy and neurodegenerative diseases. Nat Rev Neurosci **16**(6): 345-357.

Milward, E. A., R. Papadopoulos, S. J. Fuller, R. D. Moir, D. Small, K. Beyreuther and C. L. Masters (1992). The amyloid protein precursor of Alzheimer's disease is a mediator of the effects of nerve growth factor on neurite outgrowth. Neuron **9**(1): 129-137.

Miners, J. O. and D. J. Birkett (1998). Cytochrome P4502C9: an enzyme of major importance in human drug metabolism. Br J Clin Pharmacol **45**(6): 525-538.

Mizumura, K., A. M. Choi and S. W. Ryter (2014). Emerging role of selective autophagy in human diseases. Front Pharmacol **5**: 244.

Mizushima, N. and M. Komatsu (2011). Autophagy: renovation of cells and tissues. Cell **147**(4): 728-741.

Mizushima, N., T. Noda, T. Yoshimori, Y. Tanaka, T. Ishii, M. D. George, D. J. Klionsky, M. Ohsumi and Y. Ohsumi (1998). A protein conjugation system essential for autophagy. Nature **395**(6700): 395-398.

Mizushima, N., T. Yoshimori and B. Levine (2010). Methods in mammalian autophagy research. Cell **140**(3): 313-326.

Mogk, A., T. Tomoyasu, P. Goloubinoff, S. Rudiger, D. Roder, H. Langen and B. Bukau (1999). Identification of thermolabile Escherichia coli proteins: prevention and reversion of aggregation by DnaK and ClpB. EMBO J **18**(24): 6934-6949.

Morimoto, R. I. and A. M. Cuervo (2014). Proteostasis and the aging proteome in health and disease. J Gerontol A Biol Sci Med Sci **69 Suppl 1**: S33-38.

Morley, J. F., H. R. Brignull, J. J. Weyers and R. I. Morimoto (2002). The threshold for polyglutamine-expansion protein aggregation and cellular toxicity is dynamic and influenced by aging in Caenorhabditis elegans. Proc Natl Acad Sci U S A **99**(16): 10417-10422.

Mukhopadhyay, A., S. W. Oh and H. A. Tissenbaum (2006). Worming pathways to and from DAF-16/FOXO. Exp Gerontol **41**(10): 928-934.

Naidoo, N., M. Ferber, M. Master, Y. Zhu and A. I. Pack (2008). Aging impairs the unfolded protein response to sleep deprivation and leads to proapoptotic signaling. J Neurosci **28**(26): 6539-6548.

Niccoli, T. and L. Partridge (2012). Ageing as a risk factor for disease. Curr Biol **22**(17): R741-752.

Nillegoda, N. B., J. Kirstein, A. Szlachcic, M. Berynskyy, A. Stank, F. Stengel, K. Arnsburg, X. Gao, A. Scior, R. Aebersold, D. L. Guilbride, R. C. Wade, R. I. Morimoto, M. P. Mayer and B. Bukau (2015). Crucial HSP70 co-chaperone complex unlocks metazoan protein disaggregation. Nature **524**(7564): 247-251.

Nillegoda, N. B., A. Stank, D. Malinverni, N. Alberts, A. Szlachcic, A. Barducci, P. De Los Rios, R. C. Wade and B. Bukau (2017). Evolution of an intricate J-protein network driving protein disaggregation in eukaryotes. Elife **6**.

Nixon, R. A. (2013). The role of autophagy in neurodegenerative disease. Nat Med **19**(8): 983-997.

Noda, T. and Y. Ohsumi (1998). Tor, a phosphatidylinositol kinase homologue, controls autophagy in yeast. J Biol Chem **273**(7): 3963-3966.

Noda, T., K. Suzuki and Y. Ohsumi (2002). Yeast autophagosomes: de novo formation of a membrane structure. Trends Cell Biol **12**(5): 231-235.

Nozaki, K., O. Onodera, H. Takano and S. Tsuji (2001). Amino acid sequences flanking polyglutamine stretches influence their potential for aggregate formation. Neuroreport **12**(15): 3357-3364.

Nussbaum-Krammer, C. I., K. W. Park, L. Li, R. Melki and R. I. Morimoto (2013). Spreading of a prion domain from cell-to-cell by vesicular transport in Caenorhabditis elegans. PLoS Genet **9**(3): e1003351.

O'Brien, D., L. M. Jones, S. Good, J. Miles, M. S. Vijayabaskar, R. Aston, C. E. Smith, D. R. Westhead and P. van Oosten-Hawle (2018). A PQM-1-Mediated Response Triggers Transcellular Chaperone Signaling and Regulates Organismal Proteostasis. Cell Rep **23**(13): 3905-3919.

Ogrodnik, M., S. Miwa, T. Tchkonia, D. Tiniakos, C. L. Wilson, A. Lahat, C. P. Day, A. Burt, A. Palmer, Q. M. Anstee, S. N. Grellscheid, J. H. J. Hoeijmakers, S. Barnhoorn, D. A. Mann, T. G. Bird, W. P. Vermeij, J. L. Kirkland, J. F. Passos, T. von Zglinicki and D. Jurk (2017). Cellular senescence drives age-dependent hepatic steatosis. Nat Commun **8**: 15691.

Otto, H., C. Conz, P. Maier, T. Wolfle, C. K. Suzuki, P. Jeno, P. Rucknagel, J. Stahl and S. Rospert (2005). The chaperones MPP11 and Hsp70L1 form the mammalian ribosome-associated complex. Proc Natl Acad Sci U S A **102**(29): 10064-10069.

Padurariu, M., A. Ciobica, I. Mavroudis, D. Fotiou and S. Baloyannis (2012). Hippocampal neuronal loss in the CA1 and CA3 areas of Alzheimer's disease patients. Psychiatr Danub **24**(2): 152-158.

Park, S. H., Y. Kukushkin, R. Gupta, T. Chen, A. Konagai, M. S. Hipp, M. Hayer-Hartl and F. U. Hartl (2013). PolyQ proteins interfere with nuclear degradation of cytosolic proteins by sequestering the Sis1p chaperone. Cell **154**(1): 134-145.

Park, S. K., P. M. Tedesco and T. E. Johnson (2009). Oxidative stress and longevity in Caenorhabditis elegans as mediated by SKN-1. Aging Cell **8**(3): 258-269.

Parsell, D. A., A. S. Kowal, M. A. Singer and S. Lindquist (1994). Protein disaggregation mediated by heat-shock protein Hsp104. Nature **372**(6505): 475-478.

Paul, S. (2008). Dysfunction of the ubiquitin-proteasome system in multiple disease conditions: therapeutic approaches. Bioessays **30**(11-12): 1172-1184.

QIAGEN (2010). Primer efficiency - https://www.gene-quantification.de/qiagen-qpcr-sample-assay-tech-guide-2010.pdf.

Rampelt, H., J. Kirstein-Miles, N. B. Nillegoda, K. Chi, S. R. Scholz, R. I. Morimoto and B. Bukau (2012). Metazoan Hsp70 machines use Hsp110 to power protein disaggregation. EMBO J **31**(21): 4221-4235.

Ravikumar, B., R. Duden and D. C. Rubinsztein (2002). Aggregate-prone proteins with polyglutamine and polyalanine expansions are degraded by autophagy. Hum Mol Genet **11**(9): 1107-1117.

Raviol, H., H. Sadlish, F. Rodriguez, M. P. Mayer and B. Bukau (2006). Chaperone network in the yeast cytosol: Hsp110 is revealed as an Hsp70 nucleotide exchange factor. EMBO J **25**(11): 2510-2518.

Raychaudhuri, S., C. Loew, R. Korner, S. Pinkert, M. Theis, M. Hayer-Hartl, F. Buchholz and F. U. Hartl (2014). Interplay of acetyltransferase EP300 and the proteasome system in regulating heat shock transcription factor 1. Cell **156**(5): 975-985.

Raynes, R., C. Juarez, L. C. Pomatto, D. Sieburth and K. J. Davies (2017). Aging and SKN-1-dependent Loss of 20S Proteasome Adaptation to Oxidative Stress in C. elegans. J Gerontol A Biol Sci Med Sci **72**(2): 143-151.

Reiner, A., I. Dragatsis, S. Zeitlin and D. Goldowitz (2003). Wild-type huntingtin plays a role in brain development and neuronal survival. Mol Neurobiol **28**(3): 259-276.

Reszka, A. A., R. Seger, C. D. Diltz, E. G. Krebs and E. H. Fischer (1995). Association of mitogen-activated protein kinase with the microtubule cytoskeleton. Proc Natl Acad Sci U S A **92**(19): 8881-8885.

Rogov, V., V. Dotsch, T. Johansen and V. Kirkin (2014). Interactions between autophagy receptors and ubiquitin-like proteins form the molecular basis for selective autophagy. Mol Cell **53**(2): 167-178.

Ross, C. A. and M. A. Poirier (2004). Protein aggregation and neurodegenerative disease. Nat Med **10 Suppl**: S10-17.

Rousseau, A. and A. Bertolotti (2018). Regulation of proteasome assembly and activity in health and disease. Nat Rev Mol Cell Biol.

Rubinsztein, D. C., G. Marino and G. Kroemer (2011). Autophagy and aging. Cell **146**(5): 682-695.

Rudiger, S., A. Buchberger and B. Bukau (1997). Interaction of Hsp70 chaperones with substrates. Nat Struct Biol **4**(5): 342-349.

Sala, A. J., L. C. Bott and R. I. Morimoto (2017). Shaping proteostasis at the cellular, tissue, and organismal level. J Cell Biol **216**(5): 1231-1241.

Sanchez, Y. and S. L. Lindquist (1990). HSP104 required for induced thermotolerance. Science **248**(4959): 1112-1115.

Schipper-Krom, S., K. Juenemann, A. H. Jansen, A. Wiemhoefer, R. van den Nieuwendijk, D. L. Smith, M. A. Hink, G. P. Bates, H. Overkleeft, H. Ovaa and E. Reits (2014). Dynamic recruitment of active proteasomes into polyglutamine initiated inclusion bodies. FEBS Lett **588**(1): 151-159.

Schlessinger, J. (2000). Cell signaling by receptor tyrosine kinases. Cell **103**(2): 211-225.

Schmidt, M. and D. Finley (2014). Regulation of proteasome activity in health and disease. Biochim Biophys Acta **1843**(1): 13-25.

Schuff, N., N. Woerner, L. Boreta, T. Kornfield, L. M. Shaw, J. Q. Trojanowski, P. M. Thompson, C. R. Jack, Jr., M. W. Weiner and I. Alzheimer's Disease Neuroimaging (2009). MRI of hippocampal volume loss in early Alzheimer's disease in relation to ApoE genotype and biomarkers. Brain **132**(Pt 4): 1067-1077.

Schulte, J. and J. T. Littleton (2011). The biological function of the Huntingtin protein and its relevance to Huntington's Disease pathology. Curr Trends Neurol **5**: 65-78.

Scior, A., A. Buntru, K. Arnsburg, A. Ast, M. Iburg, K. Juenemann, M. L. Pigazzini, B. Mlody, D. Puchkov, J. Priller, E. E. Wanker, A. Prigione and J. Kirstein (2018). Complete suppression of Htt fibrilization and disaggregation of Htt fibrils by a trimeric chaperone complex. EMBO J **37**(2): 282-299.

Seglen, P. O. and P. B. Gordon (1982). 3-Methyladenine: specific inhibitor of autophagic/lysosomal protein degradation in isolated rat hepatocytes. Proc Natl Acad Sci U S A **79**(6): 1889-1892.

Seglen, P. O., B. Grinde and A. E. Solheim (1979). Inhibition of the lysosomal pathway of protein degradation in isolated rat hepatocytes by ammonia, methylamine, chloroquine and leupeptin. Eur J Biochem **95**(2): 215-225.

Seidel, K., S. Siswanto, M. Fredrich, M. Bouzrou, E. R. Brunt, F. W. van Leeuwen, H. H. Kampinga, H. W. Korf, U. Rub and W. F. den Dunnen (2016). Polyglutamine aggregation in Huntington's disease and spinocerebellar ataxia

type 3: similar mechanisms in aggregate formation. Neuropathol Appl Neurobiol **42**(2): 153-166.

Sengupta, P. and A. D. Samuel (2009). Caenorhabditis elegans: a model system for systems neuroscience. Curr Opin Neurobiol **19**(6): 637-643.

Settembre, C., C. Di Malta, V. A. Polito, M. Garcia Arencibia, F. Vetrini, S. Erdin, S. U. Erdin, T. Huynh, D. Medina, P. Colella, M. Sardiello, D. C. Rubinsztein and A. Ballabio (2011). TFEB links autophagy to lysosomal biogenesis. Science **332**(6036): 1429-1433.

Shemesh, N., N. Shai and A. Ben-Zvi (2013). Germline stem cell arrest inhibits the collapse of somatic proteostasis early in Caenorhabditis elegans adulthood. Aging Cell **12**(5): 814-822.

Shibatani, T., M. Nazir and W. F. Ward (1996). Alteration of rat liver 20S proteasome activities by age and food restriction. J Gerontol A Biol Sci Med Sci **51**(5): B316-322.

Shintani, T. and D. J. Klionsky (2004). Autophagy in health and disease: a double-edged sword. Science **306**(5698): 990-995.

Shorter, J. (2011). The mammalian disaggregase machinery: Hsp110 synergizes with Hsp70 and Hsp40 to catalyze protein disaggregation and reactivation in a cell-free system. PLoS One **6**(10): e26319.

Snell, R. G., J. C. MacMillan, J. P. Cheadle, I. Fenton, L. P. Lazarou, P. Davies, M. E. MacDonald, J. F. Gusella, P. S. Harper and D. J. Shaw (1993). Relationship between trinucleotide repeat expansion and phenotypic variation in Huntington's disease. Nat Genet **4**(4): 393-397.

Stack, J. H., M. Whitney, S. M. Rodems and B. A. Pollok (2000). A ubiquitin-based tagging system for controlled modulation of protein stability. Nat Biotechnol **18**(12): 1298-1302.

Stranks, S. D., H. Ecroyd, S. Van Sluyter, E. J. Waters, J. A. Carver and L. von Smekal (2009). Model for amorphous aggregation processes. Phys Rev E Stat Nonlin Soft Matter Phys **80**(5 Pt 1): 051907.

Sulston, J. E. and H. R. Horvitz (1977). Post-embryonic cell lineages of the nematode, Caenorhabditis elegans. Dev Biol **56**(1): 110-156.

Suzuki, Y., K. Nakayama, N. Hashimoto and I. Yazawa (2010). Proteolytic processing regulates pathological accumulation in dentatorubral-pallidoluysian atrophy. FEBS J **277**(23): 4873-4887.

Taipale, M., D. F. Jarosz and S. Lindquist (2010). HSP90 at the hub of protein homeostasis: emerging mechanistic insights. Nat Rev Mol Cell Biol **11**(7): 515-528.

Tanida, I., N. Minematsu-Ikeguchi, T. Ueno and E. Kominami (2005). Lysosomal turnover, but not a cellular level, of endogenous LC3 is a marker for autophagy. Autophagy **1**(2): 84-91.

Tardif, K. D., K. Mori and A. Siddiqui (2002). Hepatitis C virus subgenomic replicons induce endoplasmic reticulum stress activating an intracellular signaling pathway. J Virol **76**(15): 7453-7459.

Thibaudeau, T. A., R. T. Anderson and D. M. Smith (2018). A common mechanism of proteasome impairment by neurodegenerative disease-associated oligomers. Nat Commun **9**(1): 1097.

Thorne, N., J. Inglese and D. S. Auld (2010). Illuminating insights into firefly luciferase and other bioluminescent reporters used in chemical biology. Chem Biol **17**(6): 646-657.

Thornton, B. and C. Basu (2011). Real-time PCR (qPCR) primer design using free online software. Biochem Mol Biol Educ **39**(2): 145-154.

Tonoki, A., E. Kuranaga, T. Tomioka, J. Hamazaki, S. Murata, K. Tanaka and M. Miura (2009). Genetic evidence linking age-dependent attenuation of the 26S proteasome with the aging process. Mol Cell Biol **29**(4): 1095-1106.

Tooze, J., M. Hollinshead, T. Ludwig, K. Howell, B. Hoflack and H. Kern (1990). In exocrine pancreas, the basolateral endocytic pathway converges with the autophagic pathway immediately after the early endosome. J Cell Biol **111**(2): 329-345.

Tooze, S. A., H. B. Jefferies, E. Kalie, A. Longatti, F. E. McAlpine, N. C. McKnight, A. Orsi, H. E. Polson, M. Razi, D. J. Robinson and J. L. Webber (2010). Trafficking and signaling in mammalian autophagy. IUBMB Life **62**(7): 503-508.

Torroja, L., M. Packard, M. Gorczyca, K. White and V. Budnik (1999). The Drosophila beta-amyloid precursor protein homolog promotes synapse differentiation at the neuromuscular junction. J Neurosci **19**(18): 7793-7803.

Treweek, T. M., S. Meehan, H. Ecroyd and J. A. Carver (2015). Small heat-shock proteins: important players in regulating cellular proteostasis. Cell Mol Life Sci **72**(3): 429-451.

Tsai, J. and M. G. Douglas (1996). A conserved HPD sequence of the J-domain is necessary for YDJ1 stimulation of Hsp70 ATPase activity at a site distinct from substrate binding. J Biol Chem **271**(16): 9347-9354.

Tsukada, M. and Y. Ohsumi (1993). Isolation and characterization of autophagy-defective mutants of Saccharomyces cerevisiae. FEBS Lett **333**(1-2): 169-174.

Tyedmers, J., A. Mogk and B. Bukau (2010). Cellular strategies for controlling protein aggregation. Nat Rev Mol Cell Biol **11**(11): 777-788.

United Nations, D. o. E. a. S. A. (2015). World Population Ageing. **ST/ESA/SER.A/39**.

van Oosten-Hawle, P. and R. I. Morimoto (2014). Transcellular chaperone signaling: an organismal strategy for integrated cell stress responses. J Exp Biol **217**(Pt 1): 129-136.

van Oosten-Hawle, P., R. S. Porter and R. I. Morimoto (2013). Regulation of organismal proteostasis by transcellular chaperone signaling. Cell **153**(6): 1366-1378.

Venkatachalam, G., U. Surana and M. V. Clement (2017). Replication stress-induced endogenous DNA damage drives cellular senescence induced by a sub-lethal oxidative stress. Nucleic Acids Res **45**(18): 10564-10582.

Vernace, V. A., L. Arnaud, T. Schmidt-Glenewinkel and M. E. Figueiredo-Pereira (2007). Aging perturbs 26S proteasome assembly in Drosophila melanogaster. FASEB J **21**(11): 2672-2682.

Vilchez, D., I. Morantte, Z. Liu, P. M. Douglas, C. Merkwirth, A. P. Rodrigues, G. Manning and A. Dillin (2012). RPN-6 determines C. elegans longevity under proteotoxic stress conditions. Nature **489**(7415): 263-268.

Vilchez, D., I. Saez and A. Dillin (2014). The role of protein clearance mechanisms in organismal ageing and age-related diseases. Nat Commun **5**: 5659.

Waite, K. A., A. De-La Mota-Peynado, G. Vontz and J. Roelofs (2016). Starvation Induces Proteasome Autophagy with Different Pathways for Core and Regulatory Particles. J Biol Chem **291**(7): 3239-3253.

Walther, D. M., P. Kasturi, M. Zheng, S. Pinkert, G. Vecchi, P. Ciryam, R. I. Morimoto, C. M. Dobson, M. Vendruscolo, M. Mann and F. U. Hartl (2015).

Widespread Proteome Remodeling and Aggregation in Aging C. elegans. Cell **161**(4): 919-932.

Webb, J. L., B. Ravikumar, J. Atkins, J. N. Skepper and D. C. Rubinsztein (2003). Alpha-Synuclein is degraded by both autophagy and the proteasome. J Biol Chem **278**(27): 25009-25013.

Weibezahn, J., P. Tessarz, C. Schlieker, R. Zahn, Z. Maglica, S. Lee, H. Zentgraf, E. U. Weber-Ban, D. A. Dougan, F. T. Tsai, A. Mogk and B. Bukau (2004). Thermotolerance requires refolding of aggregated proteins by substrate translocation through the central pore of ClpB. Cell **119**(5): 653-665.

WHO (2010). World Population Prospects: The 2010 Revision. **Volume I: Comprehensive Tables**.

Willcox, B. J., T. A. Donlon, Q. He, R. Chen, J. S. Grove, K. Yano, K. H. Masaki, D. C. Willcox, B. Rodriguez and J. D. Curb (2008). FOXO3A genotype is strongly associated with human longevity. Proc Natl Acad Sci U S A **105**(37): 13987-13992.

Winslow, A. R., C. W. Chen, S. Corrochano, A. Acevedo-Arozena, D. E. Gordon, A. A. Peden, M. Lichtenberg, F. M. Menzies, B. Ravikumar, S. Imarisio, S. Brown, C. J. O'Kane and D. C. Rubinsztein (2010). alpha-Synuclein impairs macroautophagy: implications for Parkinson's disease. J Cell Biol **190**(6): 1023-1037.

Wolff, S., J. S. Weissman and A. Dillin (2014). Differential scales of protein quality control. Cell **157**(1): 52-64.

Wong, A., P. Boutis and S. Hekimi (1995). Mutations in the clk-1 gene of Caenorhabditis elegans affect developmental and behavioral timing. Genetics **139**(3): 1247-1259.

Wong, E. and A. M. Cuervo (2010). Autophagy gone awry in neurodegenerative diseases. Nat Neurosci **13**(7): 805-811.

Yang, H. and H. Y. Hu (2016). Sequestration of cellular interacting partners by protein aggregates: implication in a loss-of-function pathology. FEBS J **283**(20): 3705-3717.

Yu, L., Y. Chen and S. A. Tooze (2018). Autophagy pathway: Cellular and molecular mechanisms. Autophagy **14**(2): 207-215.

Yu, L., C. K. McPhee, L. Zheng, G. A. Mardones, Y. Rong, J. Peng, N. Mi, Y. Zhao, Z. Liu, F. Wan, D. W. Hailey, V. Oorschot, J. Klumperman, E. H.

Baehrecke and M. J. Lenardo (2010). Termination of autophagy and reformation of lysosomes regulated by mTOR. Nature **465**(7300): 942-946.

Yu, W. H., A. Kumar, C. Peterhoff, L. Shapiro Kulnane, Y. Uchiyama, B. T. Lamb, A. M. Cuervo and R. A. Nixon (2004). Autophagic vacuoles are enriched in amyloid precursor protein-secretase activities: implications for beta-amyloid peptide over-production and localization in Alzheimer's disease. Int J Biochem Cell Biol **36**(12): 2531-2540.

Zhang, H., J. T. Chang, B. Guo, M. Hansen, K. Jia, A. L. Kovacs, C. Kumsta, L. R. Lapierre, R. Legouis, L. Lin, Q. Lu, A. Melendez, E. J. O'Rourke, K. Sato, M. Sato, X. Wang and F. Wu (2015). Guidelines for monitoring autophagy in Caenorhabditis elegans. Autophagy **11**(1): 9-27.

Zhang, L., F. Li, E. Dimayuga, J. Craddock and J. N. Keller (2007). Effects of aging and dietary restriction on ubiquitination, sumoylation, and the proteasome in the spleen. FEBS Lett **581**(28): 5543-5547.

Zheng, Q., T. Huang, L. Zhang, Y. Zhou, H. Luo, H. Xu and X. Wang (2016). Dysregulation of Ubiquitin-Proteasome System in Neurodegenerative Diseases. Front Aging Neurosci **8**: 303.

Zhou, H. X. (2008). Protein folding in confined and crowded environments. Arch Biochem Biophys **469**(1): 76-82.

Zhou, Z., J. B. Fan, H. L. Zhu, F. Shewmaker, X. Yan, X. Chen, J. Chen, G. F. Xiao, L. Guo and Y. Liang (2009). Crowded cell-like environment accelerates the nucleation step of amyloidogenic protein misfolding. J Biol Chem **284**(44): 30148-30158.

Zhuravleva, A., E. M. Clerico and L. M. Gierasch (2012). An interdomain energetic tug-of-war creates the allosterically active state in Hsp70 molecular chaperones. Cell **151**(6): 1296-1307.

Zijlstra, M. P., M. A. Rujano, M. A. Van Waarde, E. Vis, E. R. Brunt and H. H. Kampinga (2010). Levels of DNAJB family members (HSP40) correlate with disease onset in patients with spinocerebellar ataxia type 3. Eur J Neurosci **32**(5): 760-770.

8 List of tables and figures

9 List of abbreviations

°C	Degree Celsius
3-MA	3-Methyladenine
aa	Amino acid
Aβ	Amyloid beta
Ac	Acetate
AD	Alzheimer's disease
ADP	Adenosine diphosphate
age-1	Aging alteration (Protein AGE-1)
ALS	Amyotrophic lateral sclerosis
AMC	7-Amino-4-methylcoumarin
AMPK	5' adenosine monophosphate-activated protein kinase
APP	Amyloid precursor protein
ATG	Autophagy
α-syn	alpha-synuclein
ATP	Adenosine triphosphate
ATPase	Adenosinetriphosphatase
BafA1	Bafilomycin A1
BAG	Bcl-2-associated anthanogene
Bcl-2	B-cell lymphoma 2
bp	Base pair
BSA	Bovine serum albumine
C. elegans	*Caenorhabditis elegans*
cdc-42	Cell division cycle related
CQ	Chloroquine
cDNA	Complementary DNA
CGC	*Caenorhabditis* genetic center
CLEM	Correlative light-electron microscopy
CMA	Chaperone mediated autophagy
C-terminal	Carboxy-terminal
daf (-2,-16,-21)	Abnormal dauer formation: -2: receptor tyrosine kinase (protein: DAF-2) -16: forkhead box O transcription factor (protein: DAF-16) -21: Hsp90 (protein: DAF-21)
DAPI	4′,6-Diamidin-2-phenylindol
DINAMelt	DI-Nucleic acid hybridization and melting prediction

DMSO	Dimethyl sulfoxide
DNA	Deoxyribonucleic acid
dnaj	J-protein family member (gene) (protein: DNAJ)
DNase	deoxyribonuclease
dnj	Nematode J-protein member (gene) (protein: DNJ)
DTT	Dithiothreitol
E. coli	*Escherichia coli*
EDTA	Ethylenediaminetetraacetic acid
EM	Electron microscopy
ER	Endoplasmic reticulum
Fluc (DM)	Firefly luciferase (double mutation)
FOXO3A	Forkhead box protein O 3A
g (µg, mg)	Gram (microgram, miligram)
GFP	Green fluorescent protein
GOI	Gene of interest
h	Hour
HD	Huntington's disease
HEK293	Human Embryonic Kidney cell
HLH-30	Helix Loop Helix 30
HEPES	4-(2-hydroxyethyl)-1-piperazineethanesulfonic acid
HPD	Histidine-proline-aspartate
HS	Heat shock
Hsc70	Constitutive expressed Hsp70 member
HSF-1	Heat shock factor 1
hspa	Heat shock protein A (gene) (protein: HSPA)
hsp	Heat shock protein (gene) (protein: HSP)
HSR	Heat shock response
Htt	Huntingtin
kb	Kilobase
kDa	Kilo Dalton
l, (µl, ml)	Liter (microliter, milliliter)
L1-L4	Nematode larval stages 1 to 4
LMP-1	Lysosomal membrane protein 1
LSM	Laser scanning microscope
m	Muscle
M (nM, µM,mM)	Molar (nanomolar, micromolar, millimoloar)
mHtt	Mutant Huntingtin
mm, µm	Millimeter, micrometer
mTOR	Mammalian target of rapamycin

n	Neurons
NCBI	National center for biotechnology information
NEF	Nucleotide exchange factor
NGM	Nematode growth medium
N-terminal	Amino-terminal
PBS (T)	Phosphate buffered saline (with Tween 20)
PCR	Polymerase chain reaction
PMSF	Phenylmethylsulfonyl fluoride
PN	Proteostasis network
PVDF	Polyvinylidene fluoride
Q	Glutamine
qRT-PCR	Quantitative Real-Time-PCR
Rap	Rapamycin
RFP	Red fluorescent protein
RNA	Ribonucleic acid
RNAi	RNA interference
RNase	Ribonuclease
ROS	Reactive oxygen species
rpm	Revolutions per minute
SDS	Sodium dodecyl sulfate
SDS-PAGE	Sodium dodecyl sulfate polyacrylamide gel electrophoresis
sec	Second
siRNA	Small interfering RNA
sHsps	Small heat shock protein
TAE	Tris-acetate-EDTA
TBS (T)	Tris buffered saline (with Tween 20)
TEMED	Tetramethylethylenediamine
TFEB	Transcription factor EB
Tris	Tris(hydroxymethyl)aminomethane
UPS	Ubiquitin-Proteasome System
Ub	Ubiquitin
UV	Ultraviolet
WB	Western Blot
wt	Wild type

10 Acknowledgments

First of all, I would like to thank Janine Kirstein for giving me the opportunity to be part of her lab and allowing me to carry the presented work. I am genuinely grateful for her support, inspiration and encouragement during my time at FMP. I would like to thank Hartmut Oschkinat for accepting to be the second reviewer of my doctoral work.

A big thanks goes to all Kirstein lab members, including my interns, for the camaraderie, support and engaging discussions during the past years. Also, I want to acknowledge Katrin Jünemann for contributing to all cell based experiments

Furthermore, I want to thank the FMP microscopy facility (Martin Lehmann, Jenny Eichhorst, and Burkhard Wiesner) for the valuable assistance to set up the microscopy experiments and for always being available to discuss any scientific matters. Also, I want to recognize the assistance of my collaboration partners: Dmytro Puchkov (CLEM/EM Q_{40} ultrastructure project) and Carina Holmberg (technology transfer for the in vivo UPS project).

Finally, I would like to thank the support of my friends, but especially the patience, cheering, positivity and love from my family (Ilda, Paulino, Ana e Amanda). I am truly grateful for having you during this fantastic journey.

Vielen Dank!

11 List of publications

1. **Feleciano DR**, Juenemann K, Iburg M, Brás IC, Holmeberg C, Kirstein J "Crosstalk between chaperone-mediated protein disaggregation and proteolytic pathways in aging and disease" Frontiers in Aging Neuroscience, 2019

2. **Feleciano DR**, Arnsburg K, Kirstein J "Interplay between redox and proteostasis" Worm, 2016

3. **Feleciano DR**, Kirstein J "Collapse of redox homeostasis during aging and stress" Molecular and Cellular Oncology, 2015

4. Tolmachova T, **Feleciano DA**, Shapton SW, Evans MJ, Futter CE, Seabra MC "AMD-compatible lysosomal changes in Rab38-deficient mouse model" Investigative Ophthalmology & Visual Science, 2014 (Poster abstract, ARVO)

5. **Feleciano DR**, Puchkov D, Pigazzini ML, Gallrein C, Iburg M, Kirstein J "Analysis of neurodegenerative disease-associated aggregates ultrastructure in *C. elegans*" (Manuscript in final preparation)

6. Arnsburg K, **Feleciano DR**, Scior A, Kirstein J "Chaperone regulation in response to stress, aging and disease" (Manuscript in final preparation)

7. Juenemann K, Neidhardt L, **Feleciano DR**, Sap K, Reits E and Kirstein J "HTT Inclusion Bodies: Local Ubiquitination of N-terminal HTT Fragments for Proteasomal Degradation" (Manuscript in final preparation)

8. Gibert A, Rutz C, **Feleciano DR**, Deldycke C, Michel C, Warschkau D, Kirstein J, Schülein R "Effect of HttExon1 aggregation on the signaling and trafficking of GPCRs" (Manuscript in final preparation)

12 Curriculum Vitae

Personal Information

Diogo Alexandre Rodrigues Feleciano

http://www.linkedin.com/in/feleciano

Education

02/2015 – 12/2018	Doctoral Candidate - Biochemistry
	Freie Universität Berlin, Germany
09/2009 – 01/2013	B.Sc. Biochemistry
	University of Coimbra, Portugal
09/2006 – 07/2009	High School - Science and Technologies
	Externato Cooperativo da Benedita, Portugal

Work experience

02/2015 – 12/2018	Research Scientist - Doctoral Thesis
	Leibniz Institute for Molecular Pharmacology, Berlin, Germany
02/2016 – 03/2016	Visiting Research Scientist
	University of Helsinki, Finland
02/2013 – 07/2014	Research Assistant
	Imperial College London, United Kingdom
07/2012 – 08/2012	Summer Internship
	SICGEN and NOVA Medical School, Lisbon, Portugal
02/2012 – 06/2012	Research Internship - B.Sc Thesis
	IBILI, University of Coimbra, Portugal

Additional experience

03/2017 – Present	Mentor, Native Scientist, Berlin, Germany
12/2016 – 09/2017	PhD Retreat MDC/FMP co-organizer, Berlin, Germany
12/2015 – 01/2017	PhD student representative, FMP Berlin, Germany
11/2016 – 11/2016	Mentor at "Bolsas ASSPA+ 2016", ASSPA, Berlin, Germany
09/2010 – 07/2012	Student representative, University of Coimbra, Portugal

Awards

12/2017	Global Biotech "Leader of Tomorrow 2018" (Cambridge, UK)
07/2016	Selected mentor for the ASPPA scholarship programme (plus a travel grant)
12/2015	EU-COST/STSM Fellowship (financial coverage for a short-term scientific visit)
10/2012	Leonardo da Vinci Fellowship (highly competitive fellowship to work abroad)
2004-2009	Merit award at "Externato Cooperativo da Benedita" High School (yearly top-class distinction)

Declaration of Authorship

I hereby certify that this is the first time that this work is being submitted, and is entirely based on my own work, unless stated otherwise. All contributions from other authors are quoted, and all sources of information have been specifically acknowledged and cited.

Diogo Feleciano
Berlin, 26th of September 2018